



**US Army Corps  
of Engineers®**  
Engineer Research and  
Development Center

## **Load Test and Load Rating Report for Bridge 305 over Foster's Creek Located at Naval Weapons Facility, Charleston, SC**

Jeff L. Schulz, Brett C. Commander, Terry R. Stanton,  
Wilmel Varela-Ortiz, Carmen Y. Lugo, and Mihan H. McKenna

June 2007



# **Load Test and Load Rating Report for Bridge 305 over Foster's Creek Located at Naval Weapons Facility, Charleston, SC**

Jeff L. Schulz and Brett C. Commander

*Bridge Diagnostics, Inc.*  
5398 Manhattan Circle, Suite 100  
Boulder, CO 80303-4239

Terry R. Stanton, Wilmel Varela-Ortiz, Carmen Y. Lugo, and Mihan H. McKenna

*Geotechnical and Structures Laboratory*  
U.S. Army Engineer Research and Development Center  
3909 Halls Ferry Road  
Vicksburg, MS 39180-6199

Final report

Approved for public release; distribution is unlimited.

**Abstract:** This study focuses on the load rating analysis of a prestressed concrete channel-beam located at the Naval Weapons Facility in Charleston, SC, subjected to military moving loads through load testing and analytical models. The superstructure of the bridge was instrumented with 56 reusable strain transducers to accurately characterize the structure's live load response. A load test was initially performed with a 67-kip dump truck across the bridge along three lateral paths. The load test results were used to calibrate a finite element model in order to verify if the structure could safely handle larger loads imposed by the heavy equipment transporter system carrying an M1A1 Abrams tank and the Rough Terrain Container Handler DV43 handler vehicles. Once it was confirmed by the model that these larger vehicles could cross, controlled load tests were performed with both vehicles, and data were recorded during multiple passes of both vehicles. These data were used to verify the predicted responses and to verify that the loads were not inducing damage to the structure.

When the testing phase was completed, the data were examined thoroughly, and the model was revised to best represent the actual structural responses. Load ratings were computed for the standard design and rating vehicles along with several heavy military loads. The main conclusions obtained from the load ratings are that all of the design vehicles and military vehicles can cross the bridge within the Operating (maximum) load limits. All of the vehicles, with the exception of the four-wheeled cargo handlers, can cross the bridge within the Inventory (design) load limits. Two of the most important parameters that can be determined when a load testing analysis is performed are the dynamic allowance (impact factor) and the live load distribution.

**DISCLAIMER:** The contents of this report are not to be used for advertising, publication, or promotional purposes. Citation of trade names does not constitute an official endorsement or approval of the use of such commercial products. All product names and trademarks cited are the property of their respective owners. The findings of this report are not to be construed as an official Department of the Army position unless so designated by other authorized documents.

**DESTROY THIS REPORT WHEN NO LONGER NEEDED. DO NOT RETURN IT TO THE ORIGINATOR.**

# Contents

<b>Figures and Tables</b> .....	<b>iv</b>
<b>Preface</b> .....	<b>vii</b>
<b>Unit Conversion Factors</b> .....	<b>viii</b>
<b>1 Introduction and General Overview</b> .....	<b>1</b>
Structure description .....	2
Instrumentation and testing procedure .....	3
<b>2 Preliminary Investigation of Test Results–Initial Test Data</b> .....	<b>9</b>
<b>3 Preliminary Investigation–Heavy Vehicle Tests</b> .....	<b>16</b>
<b>4 Modeling, Analysis, and Data Correlation</b> .....	<b>24</b>
<b>5 Load Rating Procedures and Results</b> .....	<b>30</b>
<b>6 Conclusions and Recommendations</b> .....	<b>37</b>
<b>7 Measured and Computed Strain Comparisons</b> .....	<b>40</b>
Preliminary test results .....	40
RTCH DV43 cargo hauler test results.....	50
HETS-M1A1 test results .....	56
<b>Appendix A: Field-Testing Procedures</b> .....	<b>60</b>
<b>Appendix B: Modeling and Analysis–The Integrated Approach</b> .....	<b>66</b>
<b>Appendix C: Load Rating Procedure</b> .....	<b>74</b>
<b>Report Documentation Page</b>	

# Figures and Tables

## Figures

Figure 1. Foster Creek Bridge–posted weight limits. ....	2
Figure 2. Longitudinal and transverse cracks in asphalt. ....	3
Figure 3. Reusable strain transducers. ....	4
Figure 4. Instrumentation plan. ....	5
Figure 5. Instrumentation access with boat. ....	5
Figure 6. Foster Creek Bridge–preliminary load test truck configuration (ft-kips). ....	6
Figure 7. Reproducibility of test results–gages directly below wheel line–Path Y2. ....	11
Figure 8. Reproducibility of test results–gages distant from wheel line–Path Y2. ....	12
Figure 9. Midspan strains across the bridge at maximum moment–Path Y2. ....	12
Figure 10. Strain histories at midspan of Beam 2 from Truck Paths Y1, Y2, and Y3. ....	13
Figure 11. Asymmetric strain histories from both sides of Beam 2–Path Y1. ....	13
Figure 12. Slow-speed and high-speed truck crossings–Truck Path Y2. ....	14
Figure 13. Load test with HETS vehicle. ....	16
Figure 14. RTCH DV43 loading vehicle. ....	17
Figure 15. Reproducible and linear-elastic behavior from RTCH DV43. ....	19
Figure 16. Reproducible and linear-elastic behavior from HETS-M1A1. ....	20
Figure 17. Comparison of Spans 3 and 4 measurements along Beam 3W-RTCH DV43. ....	20
Figure 18. Unexpected response at Beam 6E-RTCH DV43. ....	21
Figure 19. Midspan responses at Span 3 cross section-RTCH DV43. ....	21
Figure 20. Wheel path of RTCH DV43. ....	22
Figure 21. Dynamic response from RTCH DV43. ....	22
Figure 22. Finite element Model 3 bridge spans (Spans 2, 3, and 4). ....	25
Figure 23. Beam cross-section properties. ....	26
Figure 24. Midspan strain comparison for RTCH DV43. ....	28
Figure 25. Midspan strain comparison for HETS/M1A1. ....	29
Figure 26. Midspan strain comparisons-three truck passes-Beam 1W. ....	40
Figure 27. Midspan strain comparisons-three truck passes-Beam 2E. ....	41
Figure 28. Midspan strain comparisons-three truck passes-Beam 2W. ....	41
Figure 29. Midspan strain comparisons-three truck passes-Beam 3E. ....	42
Figure 30. Midspan strain comparisons-three truck passes-Beam 3W. ....	42
Figure 31. Midspan strain comparisons-three truck passes-Beam 4E. ....	43
Figure 32. Midspan strain comparisons-three truck passes-Beam 4W. ....	43
Figure 33. Midspan strain comparisons-three truck passes-Beam 5E. ....	44
Figure 34. Midspan strain comparisons-three truck passes-Beam 5W. ....	44
Figure 35. Midspan strain comparisons-three truck passes-Beam 6E. ....	45

Figure 36. Midspan strain comparisons-three truck passes-Beam 6W. ....	45
Figure 37. Midspan strain comparisons-three truck passes-Beam 7E. ....	46
Figure 38. Midspan strain comparisons-three truck passes-Beam 7W. ....	46
Figure 39. Midspan strain comparisons-three truck passes-Beam 8E. ....	47
Figure 40. L/4 span strain comparisons-three truck passes-Beam 2W. ....	47
Figure 41. 3L/4 span strain comparisons-three truck passes-Beam 2W. ....	48
Figure 42. L/4 span strain comparisons-three truck passes-Beam 3E. ....	48
Figure 43. 3L/4 span strain comparisons-three truck passes-Beam 3E. ....	49
Figure 44. Midspan Span 4 strain comparisons-three truck passes-Beam 2W. ....	49
Figure 45. Midspan Span 4 strain comparisons-three truck passes-Beam 3E. ....	50
Figure 46. Midspan strain comparisons-RTCH DV43 crossing-Beam 2W. ....	50
Figure 47. Midspan strain comparisons-RTCH DV43 crossing-Beam 3E. ....	51
Figure 48. Midspan strain comparisons-RTCH DV43 crossing-Beam 3W. ....	51
Figure 49. Midspan strain comparisons-RTCH DV43 crossing-Beam 4E. ....	52
Figure 50. Midspan strain comparisons-RTCH DV43 crossing-Beam 4W. ....	52
Figure 51. Midspan strain comparisons-RTCH DV43 crossing-Beam 5E. ....	53
Figure 52. Midspan strain comparisons-RTCH DV43 crossing-Beam 5W. ....	53
Figure 53. Midspan strain comparisons-RTCH DV43 crossing-Beam 6E. ....	54
Figure 54. Midspan strain comparisons-RTCH DV43 crossing-Beam 6W. ....	54
Figure 55. Midspan strain comparisons-RTCH DV43 crossing-Beam 3E. ....	55
Figure 56. Midspan Span 4 strain comparisons-RTCH DV43 crossing-Beam 3E. ....	55
Figure 57. Midspan Span 4 strain comparisons-RTCH DV43 crossing-Beam 3W. ....	56
Figure 58. Midspan strain comparisons-HETS-M1A1 crossing-Beam 2W. ....	56
Figure 59. Midspan strain comparisons-HETS-M1A1 crossing-Beam 3E. ....	57
Figure 60. Midspan strain comparisons-HETS-M1A1 crossing-Beam 3W. ....	57
Figure 61. Midspan strain comparisons-HETS-M1A1 crossing-Beam 4E. ....	58
Figure 62. Midspan strain comparisons-HETS-M1A1 crossing-Beam 4W. ....	58
Figure 63. Midspan Span 4 strain comparisons-HETS-M1A1 crossing-Beam 3E. ....	59
Figure 64. Midspan Span 4 strain comparisons-HETS-M1A1 crossing-Beam 3W. ....	59

## Tables

Table 1. Description of structure. ....	3
Table 2. Preliminary test procedures with dump truck. ....	7
Table 3. Military vehicle test procedures. ....	7
Table 4. Maximum strain values from initial test truck. ....	14
Table 5. Peak measured strain from RTCH DV43 and HETS crossings. ....	23
Table 6. Model calibration and accuracy results. ....	27
Table 7. Statistical accuracy terms with heavy military vehicles. ....	29
Table 8. Foster Creek Bridge 305 evaluation for CEG-A heavy vehicle loading (13 July 2005) ....	30

---

Table 9. CEG-A heavy vehicle loading axle configurations. ....	32
Table 10. Live-load moment and shear capacity.....	34
Table 11. Foster's Creek load rating results (moment).....	35
Table 12. Foster's Creek load rating results (shear). ....	35
Table 13. Foster's Creek serviceability load rating results (cracking moment).....	36

## Preface

This study was conducted by personnel of U.S. Army Engineer Research and Development Center (ERDC), Geotechnical and Structures Laboratory (GSL), Vicksburg, MS. The sponsor of the study was the Installation Management Command (IMCOM), Arlington, VA. The experiments were funded by MIPR 6GWESB1026. The IMCOM project officer for this study was Yun Heo.

The research was accomplished under the general supervision of Dr. David W. Pittman, Director, GSL; Dr. William P. Grogan, Deputy Director, GSL; and Dr. Robert L. Hall, Chief, Geosciences and Structures Division (GSD), GSL. Direct supervision was provided by James S. Shore, Chief, Structural Engineering Branch (StEB), GSL. The principal investigator for this project was Wilmel Varela-Ortiz; the program manager was Terry R. Stanton; and the financial manager was Gerardo I. Velázquez, StEB.

Partial support for the load testing portion of this research was provided by Jeffrey L. Schulz, Brett Commander, and Scott Aschermann, Bridge Diagnostics, Inc., under contract W912EE-04-D-0006 with the U.S. Army Engineer District, Vicksburg, in Vicksburg, MS. The contracting officer's representative was Ray S. Tisdale.

The authors wish to acknowledge the outstanding contributions of Pano Kordonis, Kenneth Glover, Laura R. Hyde, and Angela White. Corine E. Pugh, Graphics Specialist, Bowhead Information Technology Services, Inc., also assisted the authors in the preparation of this report.

COL Richard B. Jenkins was Commander and Executive Director of ERDC. Dr. James R. Houston was Director.



## Unit Conversion Factors

Multiply	By	To Obtain
cubic feet	0.02831685	cubic meters
feet	0.3048	meters
inches	0.0254	meters
kips (mass)	453.5924	kilograms
miles per hour	0.44704	meters per second
ounces (mass)	0.02834952	kilograms
pounds (force) per square inch	6.894757	kilopascals
pounds (mass)	0.45359237	kilograms
square inches	6.4516 E-04	square meters
tons (force)	8,896.443	newtons
tons (2,000 pounds, mass)	907.1847	kilograms

# 1 Introduction and General Overview

The Foster Creek Bridge is a critical structure along the southern access road at the Naval Weapons Facility in Charleston, SC. It is a prestressed concrete (PS/C) channel-beam structure originally constructed in 1959 and rebuilt in 1969 to handle a Lockheed Missiles and Space Co. A/871056 Missile Carrier. Since some of the current load configurations have significantly heavier single axle weights than those associated with the Missile Carrier, a load testing program was implemented in order to accurately characterize the structure's live load response.

The structure was instrumented in October 2005 and initially tested with a three-axle dump truck that weighed approximately 67 kips. Immediately after this series of tests, a preliminary evaluation of the data and analysis of the structure was performed. It was determined that the structure could safely handle the larger loads of the Rough Terrain Container Handler (RTCH) DV43 Cargo Handler and the heavy equipment transporter system (HETS) carrying the M1A1 Abrams tank. Once it was confirmed that these larger vehicles could cross, during the second day of testing, controlled load tests were performed with both the RTCH DV43 and the HETS, and data were recorded during multiple passes of both vehicles. These data were used to verify the predicted responses and verify that the loads were not inducing damage to the structure. The overall field time required for instrumenting with 56 strain channels, running tests with the three different loading vehicles, making preliminary analysis comparisons, and then instrumentation removal was less than 2 days.

When the testing phase was completed, the data were examined thoroughly and the model revised to best represent the actual structural responses. Load ratings were then computed for the standard design and rating vehicles along with several heavy military loads specified by Combat Equipment Group-Afloat (CEG-A).

This report contains an overview of the load test procedures and evaluation methods along with a summary of load rating results. In addition, detailed information on the testing procedures, analysis techniques, and load ratings are provided in the appendixes at the end of the report.

## Structure description

This bridge originally consisted of seven 18-ft prestressed concrete channel-beam spans. In 1969, the bridge was modified to handle the heavier Missile Carrier loads in accordance with American Concrete Institute (ACI) ACI 318-63 (1963) and American Association of State Highway and Transportation Officials (AASHTO)<sup>1</sup> design codes. Additional bents were installed at midspan of each span resulting in fourteen 9-ft spans, and the new superstructure was assembled from eight prestressed channel beams per span with shear keys in the top flange. There was no lateral posttensioning or concrete deck added to the top of the channel beams; thus, all lateral loads would have to be transferred through the shear keys.

Based on a previous inspection and load rating that was completed in 2002, the bridge was posted at 19 tons for a two-axle vehicle and 72 tons for vehicles with six or more axles as shown in Figure 1.



Figure 1. Foster Creek Bridge–posted weight limits.

<sup>1</sup> American Association of State Highway and Transportation Officials. 1961. *Standard specification for highway bridges*, 8th ed. Washington, DC: American Association of State Highway and Transportation Officials.

Table 1. Description of structure.

Structure Identification	Bridge 305 Foster's Creek
Location	Naval Weapons Facility, Charleston, SC
Structure Type	PS/C channel-beam bridge
Number of Spans	14
Span Lengths	9 ft center to center (c-c) of piers / 8' c-c of beam bearings
Skew	0 (Perpendicular)
Structure/Roadway Widths	25 ft-6 in. / 23 ft-10 in.
Beams	8-prestressed channel beams at 3 ft-2 in.
Deck	None-2 in. asphalt overlay.
Curbs and Parapets	Cast in place reinforced concrete curb on exterior beams.
Visual Condition	Beams appear to be in good condition, with no visible shear or flexural cracks. Longitudinal cracks were visible in the asphalt between every beam and transverse cracks were visible at the center of each pier (see Figure 2).



Figure 2. Longitudinal and transverse cracks in asphalt.

### Instrumentation and testing procedure

The primary objective of the instrumentation plan was to quantify the live load response behavior of the superstructure under both normal service loads and the specified heavy vehicle loads. Of particular concern was the

lateral load distribution capabilities of the longitudinal joints between beams as these could significantly impact the load ratings. The superstructure of the bridge was instrumented with 56 reusable strain transducers as shown in Figure 3, and the instrumentation plan is shown in Figure 4. Only two spans were instrumented (spans three and four from the south end) because all of the spans were the same length and in approximately the same condition. Selection of the spans to instrument was based primarily on accessibility. Span 3 was instrumented most heavily with transducers at midspan of every beam stem and at quarter points of four of the beams. Only four of the beams in Span 4 were instrumented, all at midspan. By instrumenting two adjacent spans with a large number of transducers, both the lateral and longitudinal load transfer characteristics could be quantified. All instrumentation was performed from a small flat bottom boat (see Figure 5).

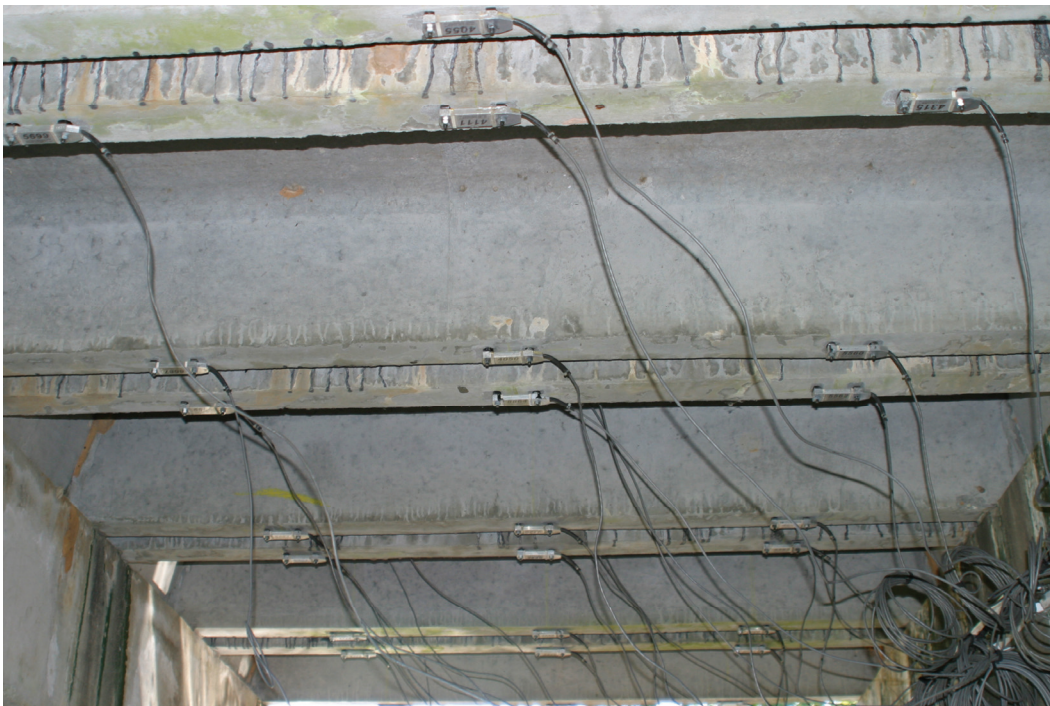


Figure 3. Reusable strain transducers.

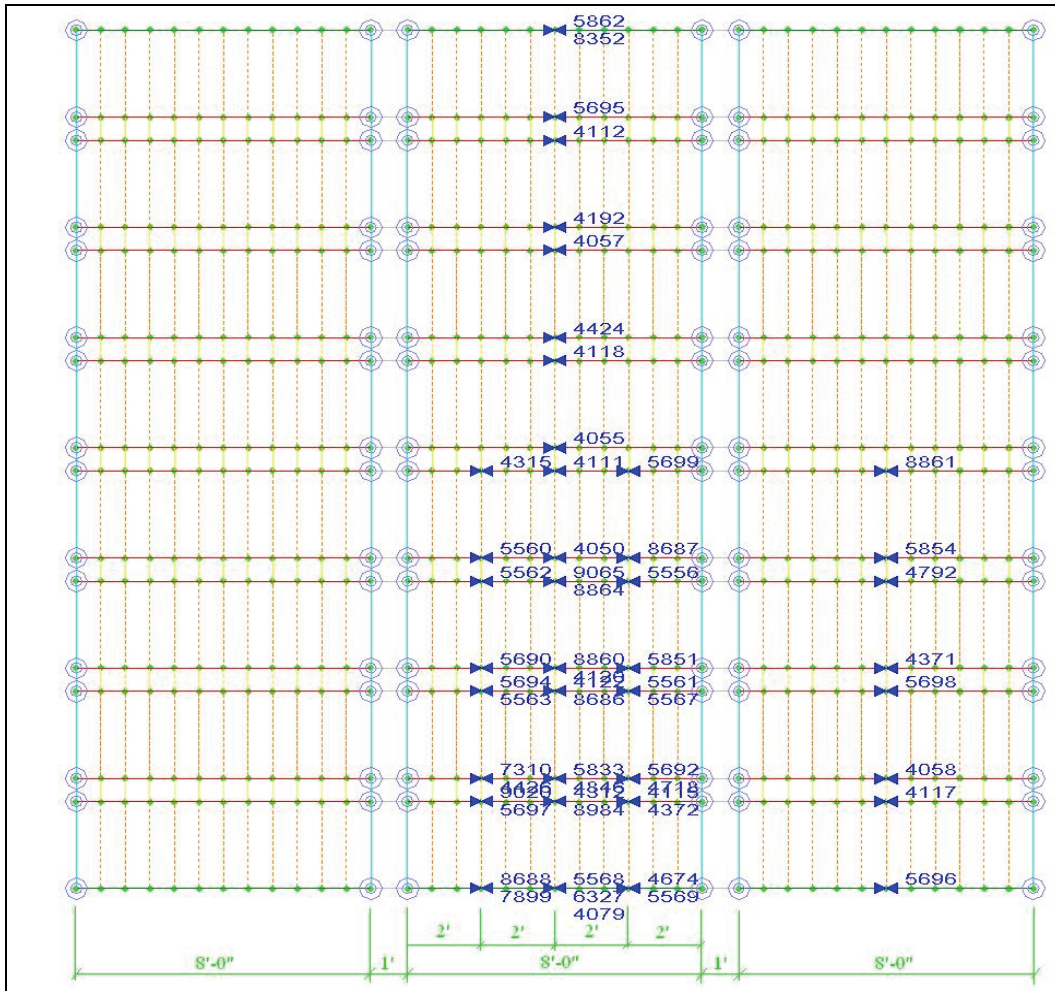


Figure 4. Instrumentation plan.



Figure 5. Instrumentation access with boat.

Preliminary load tests were performed by driving a 67-kip dump truck across the bridge along three lateral paths. The truck paths were located symmetrically on the structure as follows: Driver side wheel line located on the roadway center line, truck centered on bridge, and passenger side wheel line along roadway center line. The tag axle on the dump truck was lifted during the load test to provide a more concentrated load for this series of tests, and it was assumed that this portion of the load was transferred equally to the drive axles. Data were recorded continuously at 40 Hz during each pass, and the truck position was monitored in order to record strain as a function of vehicle position. Typical vehicle speeds were approximately 5 mph to minimize dynamic responses and to facilitate monitoring of the vehicle position. Axle weights and spacing of the test truck are shown in Figure 6.



Figure 6. Foster Creek Bridge—preliminary load test truck configuration (ft-kips).

Tests were repeated for all three truck paths to ensure reproducibility in the procedures and in the structural response. In addition to the semi-static tests, two high-speed truck passes along Path 2 were performed to capture the magnitude of dynamic responses. All instrumentation and test procedures with the dump truck were performed on Tuesday, 18 October 2005. Tests with the heavy military loads were completed, and the instrumentation was removed the following morning. An outline of the test procedures for civil and military vehicles is provided in Table 2 and Table 3. Also, see Appendix A for further details on the basic field-testing procedures.

Table 2. Preliminary test procedures with dump truck.

<b>Date</b>	<b>October 18, 2005</b>
<b>Structural Reference Point</b>	X=0, Y=0 at the south abutment and inside of east curb.
<b>Test Vehicle Direction</b>	North bound for all tests (positive X direction).
<b>Start of Data Recording</b>	Data acquisition began with front axle at X = -15.42 ft (-10 ft - ½ wheel rev.)
<b>AutoClicker Position</b>	Driver side front wheel
<b>Truck Position</b>	AutoClicker recorded truck position at each wheel revolution. Wheel circumference = 10.84 ft
<b>Lateral Truck Path(s)</b>	Three truck paths were defined for the load test. The Y position refers to distance between driver side front wheel and inside of east curb (Y= 0). Y1 = 11.8 ft, Y2 = 15.4 ft, Y3 = 19.75 ft
<b>Measurements</b>	56 removable strain transducers recorded at 40 Hz
<b>Gage Placement</b>	See Figure 4
<b>Number of Test Cycles</b>	Data were recorded while the test truck crossed the bridge at crawl speed (<5 mph). Each truck path was run twice to check reproducibility.
<b>Event</b>	<b>Data Files</b>
Test truck traveling along Y1	FC_1.dat
Test truck traveling along Y1	FC_2.dat
Test truck traveling along Y2	FC_3.dat
Test truck traveling along Y2	FC_5.dat
Test truck traveling along Y3	FC_6.dat
Test truck traveling along Y3	FC_7.dat
Test truck traveling along Y2 @ 50 mph	FC_8.dat
Test truck traveling along Y2 @ 50 mph	FC_9.dat

Table 3. Military vehicle test procedures.

<b>Date</b>	<b>October 19, 2005</b>
<b>Structural Reference Point</b>	X=0, Y=0 at the south abutment and inside of east curb.
<b>Test Vehicle Direction</b>	North bound for all tests (Positive X direction).
<b>Start of Data Recording</b>	Data acquisition began with front axle at X = -10 ft
<b>Truck Position Monitoring</b>	Manual radio clicks at every wheel revolution: RTCH DV43 20.16 ft per revolution HETS 133.46 ft per revolution
<b>Lateral Truck Path</b>	Trucks centered on bridge. Driver side front wheel: RTCH DV43 at Y4 = 16.3 ft HETS at Y2 = 15.4 ft
<b>Event</b>	<b>Data Files</b>
RTCH DV43 @ Y4	FC_11.dat
RTCH DV43 @ Y4	FC_12.dat
RTCH DV43 @ Y4 (17 mph)	FC_13.dat
HETS @ Y2	FC_14.dat
HETS @ Y2	FC_15.dat



After the preliminary load tests, the instrumentation was left in place overnight so that controlled load tests could be performed the following day with the heavy military loads. Two military vehicles were supplied for the testing—a 108K RTCH DV43 Cargo Handler and a 230K HETS carrying an M1A1 Abrams tank. Load tests similar to those completed with the test truck were completed with the military vehicles. Due to the width and weight of the vehicles, the tests were only performed with the trucks centered on the bridge.

## 2 Preliminary Investigation of Test Results— Initial Test Data

Due to the critical load ratings that had been assigned to this structure in 2002, an important part of the field procedures was to immediately compare the results of the first set of tests to the analytical predictions in order to determine if the HETS and DV43 should be allowed to cross.

Therefore, the field data were first examined graphically to determine data quality and to provide a qualitative assessment of the structure's live-load response. Some of the indicators of data quality included reproducibility between identical truck crossings, elastic behavior (strains returning to zero after truck crossing), and any unusually shaped responses that might have indicated nonlinear behavior or possible gage malfunctions.

In addition to a data "quality check," information obtained during the preliminary investigation was used to determine appropriate modeling procedures for effective beam properties and support conditions. For example, the shape of the strain histories of the gages near the ends of the span dictated how the boundary conditions should be modeled. Also, the neutral axis locations on the beams were examined to verify theoretical beam cross-section properties.

Conclusions made directly from the field data were:

- Responses from identical truck paths were reasonably reproducible as shown in Figure 7. However, it was found that gages directly under the wheel lines had a greater than normal variation because the beam strains were very sensitive to the lateral truck position. Because there was no deck and lateral load transfer was provided by the shear keys only, differences as small as 1 in. in the lateral wheel alignment had measurable effects on the strain responses. The data plot shows the upper and lower strain histories at midspan of a beam directly under a wheel line. Strain histories obtained from gages further away from the wheel loads generally had better reproducibility as shown in Figure 8. Note that because these gages were further away and the loads were not being distributed very well, the strain magnitudes were relatively

- small. At these low levels, the resolution of the strain measurement system can be seen.
- From the inspection of upper and lower strain values, it was apparent that the upper gages experienced very little strain due to normal beam flexure. The average neutral axis location was 12.25 in. from the bottom of the beam webs which corresponded closely to the theoretical neutral axis locations (near the bottom of the channel-beam flanges). Upper gages that were directly under the wheel lines all experienced tension spikes due to local cupping of the beam flange as the vertical wheel loads traveled across the gage location.
  - There was essentially no continuity of moment across the piers. Very little negative moment was indicated from any of the gages when the adjacent span was loaded.
  - From examination of midspan strains across the bridge, it was apparent that there was relatively little lateral load distribution. Figure 9 contains the midspan strains from the bottom of each beam stem due to the maximum midspan moment. A relatively sharp change in load is seen from beam to beam—such that the influence of each wheel line is very apparent. The majority of load is carried by the beam stems directly under the wheel lines. The load distribution to beams more than one channel beam away from the wheel lines is relatively insignificant. In the case of a typical beam-slab bridge, a smooth distribution of load across the bridge cross section would be observed.
  - Another good conceptual measure of lateral load distribution was the examination of the strain histories recorded from a single beam due to different lateral truck positions. Figure 10 shows the bottom strain for three truck paths: one with a wheel line directly over the gage location, one with the truck 3.5 ft away, and one path with the nearest wheel line at approximately 7 ft away from the gage location. Examination of the relative strain magnitudes shows that when the wheel-line is 3.5 ft away (just over one channel beam width away) the load applied to a beam stem is reduced to approximately 10% of the direct load condition. When the wheel line is 7 ft away (more than two channel beam widths), the distribution of load to the instrumented beam is practically zero. This level of distribution is significantly less than what is typically seen from a beam-slab type bridge.
  - Responses from the left and right stems of each channel beam were generally non-symmetric as shown in Figure 11. Because the channel beams were relatively wide, they could be loaded unevenly by the tires, resulting in uneven deflections and stresses. Therefore, when analyzing

- and rating the beams, it would not be sufficient to assume loads are applied symmetrically to an entire beam cross section composed of the two stems and the flange. Either torsional effects must be considered on the entire beam cross section or the stems of the beams must be modeled as individual units. Because of the complexity of the beam responses and the irregular load distribution, a simple beam analysis would not be representative of this structure.
- There was very little apparent dynamic effect from the high-speed truck crossings as shown in Figure 12. There were minor variations in strain magnitudes due to the slight variation in the lateral truck position (Path 2), but the maximum strain values due to the high-speed test were approximately equal to those from the crawl speed test.
  - Maximum measured strain on the bottom of a beam was  $84 \mu\epsilon$  (micro-strain) at midspan of Beam 7 and translates to a live load stress value of 0.42 ksi (assuming a concrete modulus of 5,000 ksi). The maximum measured response from each transducer is listed in Table 4.

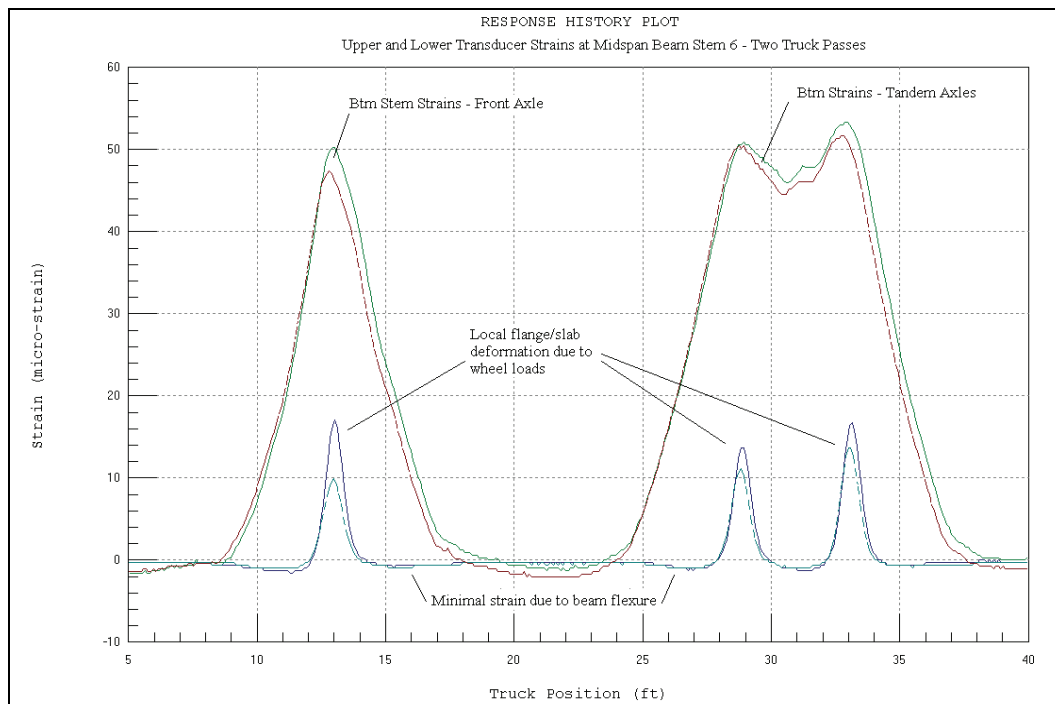


Figure 7. Reproducibility of test results—gages directly below wheel line—Path Y2.

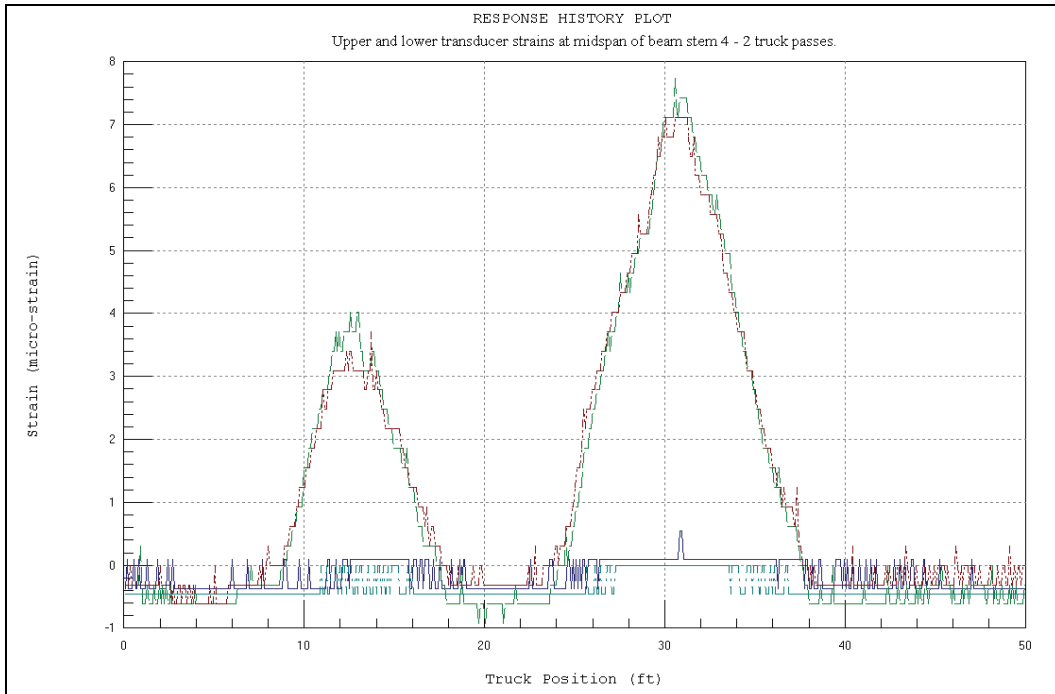


Figure 8. Reproducibility of test results—gages distant from wheel line—Path Y2.

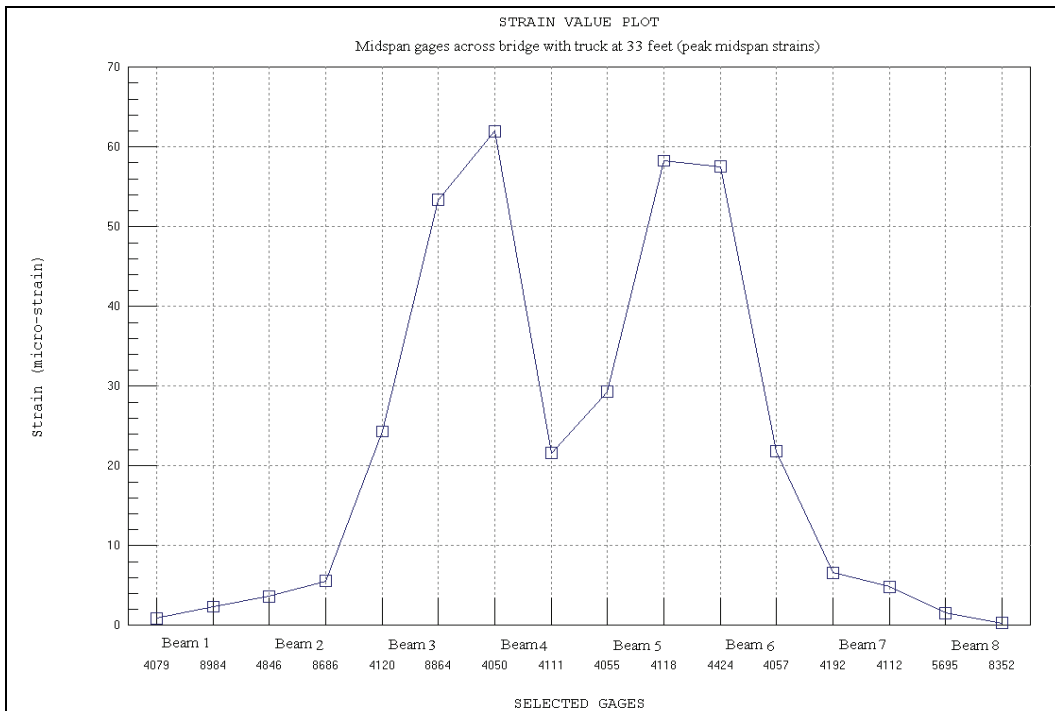


Figure 9. Midspan strains across the bridge at maximum moment—Path Y2.

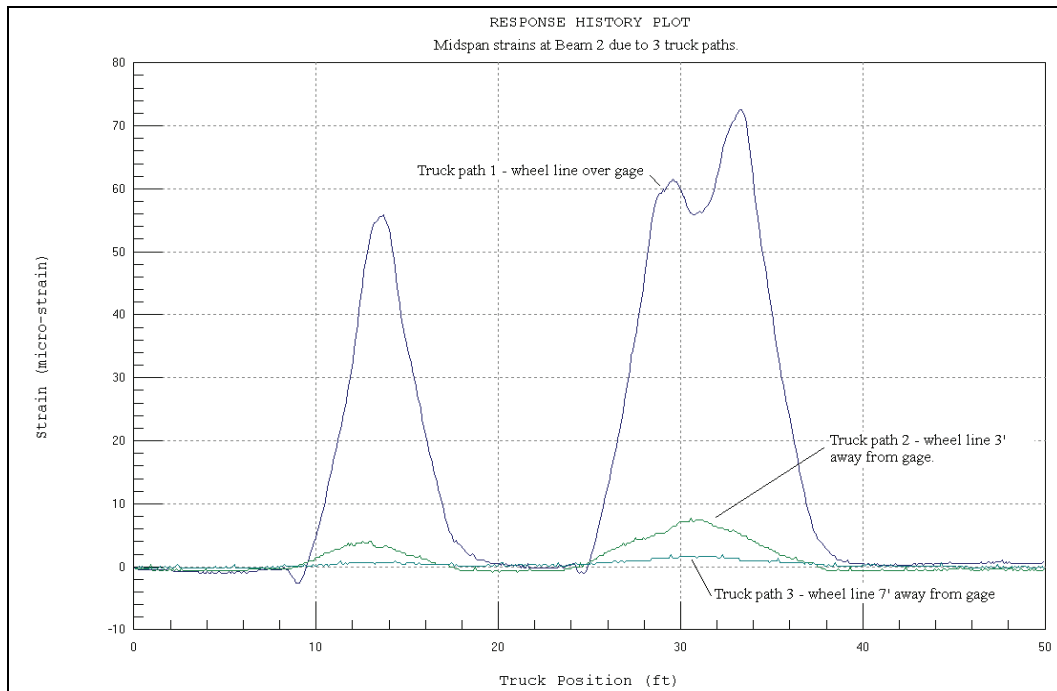


Figure 10. Strain histories at midspan of Beam 2 from Truck Paths Y1, Y2, and Y3.

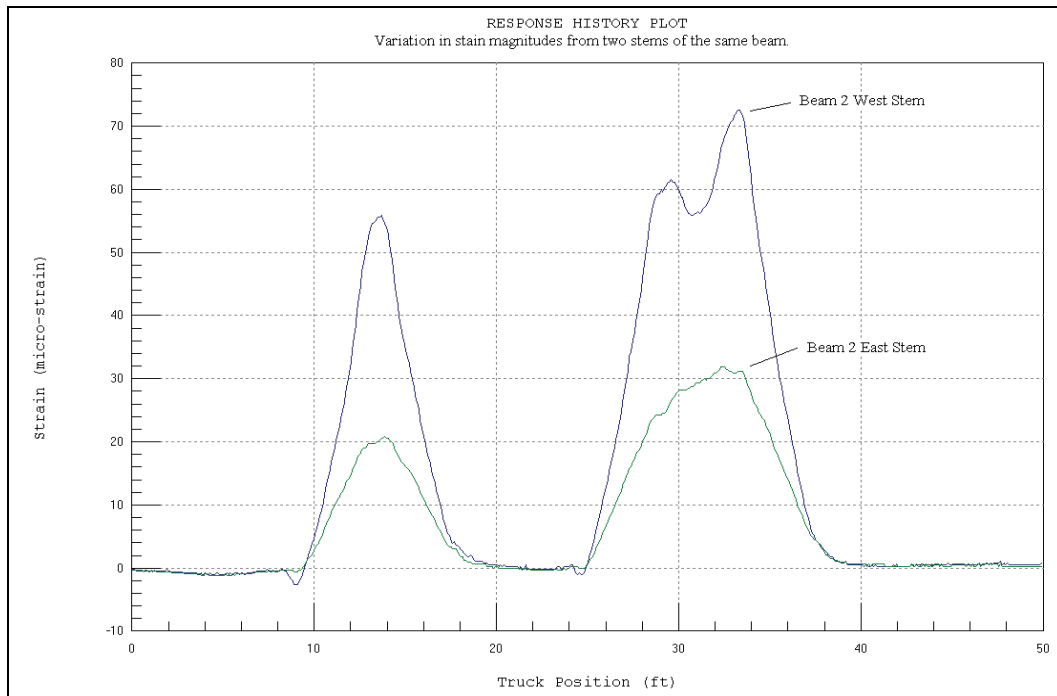


Figure 11. Asymmetric strain histories from both sides of Beam 2-Path Y1.

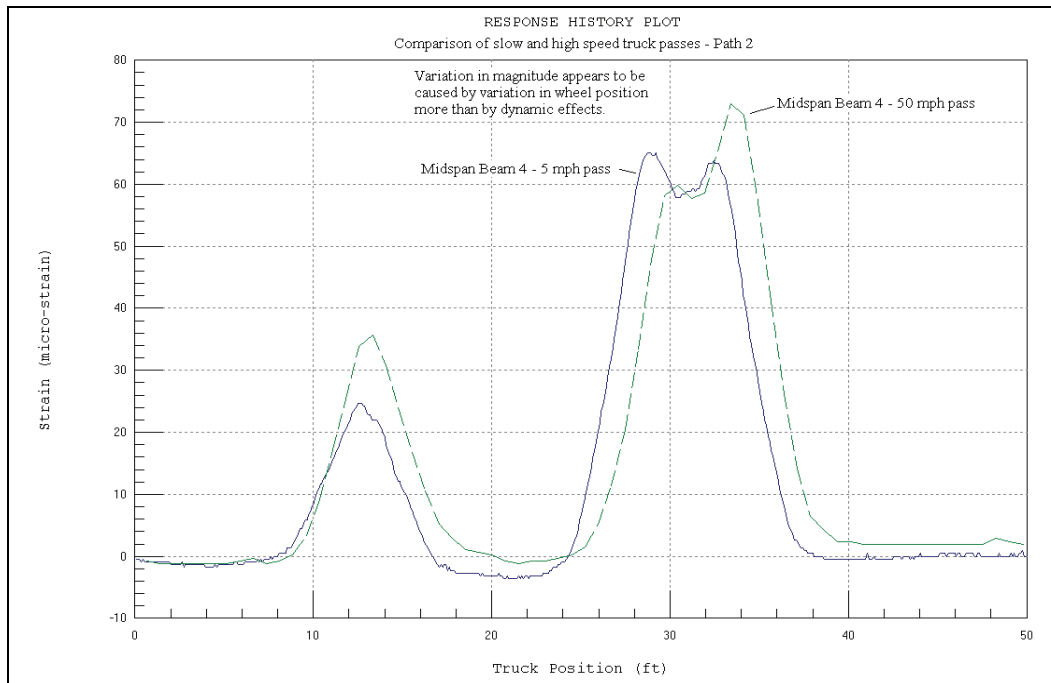


Figure 12. Slow-speed and high-speed truck crossings–Truck Path Y2.

Table 4. Maximum strain values from initial test truck.

Location	Channel	Gage ID	Path 1, $\mu\epsilon$	Path 2, $\mu\epsilon$	Path 3, $\mu\epsilon$	Path 2 (50 mph)
Span 3 - 1/4 Point Beam 1E	20	7899	2	2	1	1
Span 3 - 1/4 Point Beam 1W	38	5697	8	3	1	1
Span 3 - 1/4 Point Beam 2E	37	4426	25	4	1	2
Span 3 - 1/4 Point Beam 2W	6	5563	53	5	2	3
Span 3 - 1/4 Point Beam 3E	5	5690	49	19	3	7
Span 3 - 1/4 Point Beam 3W	30	5562	22	49	8	23
Span 3 - 1/4 Point Beam 4E	29	5560	32	56	15	49
Span 3 - 1/4 Point Beam 4w	49	4315	66	24	47	47
Span 3 - 3/4 Point Beam 1E	54	5569	2	1	1	0
Span 3 - 3/4 Point Beam 1W	40	4372	12	3	1	2
Span 3 - 3/4 Point Beam 2E	39	4718	26	5	2	3
Span 3 - 3/4 Point Beam 2W	2	5567	45	7	2	5
Span 3 - 3/4 Point Beam 3E	1	5851	53	17	4	8
Span 3 - 3/4 Point Beam 3W	42	5556	20	44	7	20
Span 3 - 3/4 Point Beam 4E	41	8687	36	55	13	59
Span 3 - 3/4 Point Beam 4W	52	5699	63	24	43	61
Span 3 - Midspan Beam 1E	53	4079	3	1	1	0
Span 3 - Midspan Beam 1W	26	8984	8	3	1	1
Span 3 - Midspan Beam 2E	25	4846	32	4	1	2
Span 3 - Midspan Beam 2W	8	8686	73	7	2	4
Span 3 - Midspan Beam 3E	7	4120	62	24	4	9

Location	Channel	Gage ID	Path 1, $\mu\epsilon$	Path 2, $\mu\epsilon$	Path 3, $\mu\epsilon$	Path 2 (50 mph)
Span 3 - Midspan Beam 3W	32	8864	27	52	7	26
Span 3 - Midspan Beam 4E	31	4050	43	65	18	73
Span 3 - Midspan Beam 4W	51	4111	63	29	47	56
Span 3 - Midspan Beam 5E	50	4055	47	34	69	47
Span 3 - Midspan Beam 5W	35	4118	15	54	35	39
Span 3 - Midspan Beam 6E	36	4424	8	59	33	54
Span 3 - Midspan Beam 6W	34	4057	5	28	65	69
Span 3 - Midspan Beam 7E	33	4192	2	9	84	31
Span 3 - Midspan Beam 7W	48	4112	1	6	37	14
Span 3 - Midspan Beam 8E	47	5695	1	2	9	6
Span 3 - Midspan Beam 8W	45	8352	1	1	5	3
Span 4 - Midspan Beam 1E	12	5696	2	1	1	0
Span 4 - Midspan Beam 1W	11	4117	7	2	1	1
Span 4 - Midspan Beam 2E	10	4058	34	3	1	2
Span 4 - Midspan Beam 2W	9	5698	66	6	2	3
Span 4 - Midspan Beam 3E	15	4792	22	53	3	19
Span 4 - Midspan Beam 3W	16	4371	59	27	3	8
Span 4 - Midspan Beam 4E	14	5854	44	63	17	65
Span 4 - Midspan Beam 4W	13	8861	77	30	50	74
Maximum Value			77	65	84	74



### 3 Preliminary Investigation–Heavy Vehicle Tests

On the day after the preliminary tests and analyses comparisons were completed for the dump truck, controlled load tests were performed with the RTCH DV43 and the HETS loaded with an M1A1 Abrams tank. Both vehicles were significantly heavier than the bridge's posted weight limits and are shown in Figure 13 and Figure 14.



Figure 13. Load test with HETS vehicle.



Figure 14. RTCH DV43 loading vehicle.

Following is an outline of observations made from data collected during the heavy vehicle passages.

- The data from the RTCH DV43 and HETS crossings indicated that the structure was behaving linearly-elastic, because in all cases the strains returned to zero after the vehicle crossings. Figure 15 and Figure 16 show typical strain responses from both heavy vehicles.
- While most of the responses appeared to be normal, there were some unexpected values recorded as well. For example, one of the sensors was located directly below the wheel line of the RTCH DV43 and should have experienced the greatest strain values, but actually measured smaller values than those at quarter-span on the same beam. Transducer 8864 produced strains significantly less than expected and less than those on the neighboring beams which were not loaded as heavily. This is shown in Figure 17, where the midspan of Span 3 experienced strains that were approximately 60% of the strains measured along the same beam line on Span 4. The large differences in magnitude are of concern because this indicates that either the measurement is incorrect, or that the Span 3 beam is behaving differently from the Span 4 beam.

- The other unexpected response was from Transducer 4424 at midspan of Beam 6E, which corresponds to the beam line directly below the other RTCH DV43 wheel line. This transducer not only experienced less-than-expected strains, but the shape of the response was different than all the other strain histories (see Figure 18). After much examination of the strain data, the cause of the low strain magnitudes and unusually shaped responses directly under wheel lines was unclear. The strains all returned to zero after the load test, so there is no indication of a transducer malfunction. However, it is possible that the transducer attachment was beginning to fail. The low strains and unusual shape could be a result of the transducers being located very close to, but not crossing a flexural crack. The opening of a crack in prestressed concrete would cause the surface strains in the vicinity of the crack to level out as was indicated on Transducer 4424. Both the shape and magnitude of the strain histories could be influenced in a manner similar to what was observed; however, it would be expected that this would occur at much higher strain levels.
- Another illustration of the unusual responses and how they compare with the rest of the strain data is shown in Figure 19, where the maximum midspan strains are plotted for all beams across the bridge. This view of the data provides a good visual indication of the lateral load distribution. In the case of this structure, the reduction in strain magnitudes or “dips” in the strain histories occur directly under the wheel lines, exactly where they should actually be the highest. Figure 20 illustrates the location of the RTCH DV43 wheel lines with respect to the beams and instrumentation. Additionally, the lateral distribution appears to be significantly greater with the RTCH DV43 than with the dump truck. This is primarily due to the wider wheel base (11 ft total width compared to 8 ft total width). An additional factor was that as the beam underwent larger displacements, this in turn increased the amount of load transfer through the channel beam shear keys.
- Similar to the responses measured during high-speed passes of the dump truck, there was little to no apparent dynamic response from the structure when the RTCH DV43 crossed at approximately 17 mph. Figure 21 presents a comparison of the slower and higher speed crossings of the RTCH DV43. While there were some minor

variations, they appeared to be more a function of wheel line location than any impact or dynamic responses. One observation made during the crossing of the RTCH DV43 vehicle was that the vehicle was bouncing significantly, and since the spans were quite short, a “bounce” could either happen directly over a span or possibly even miss the span entirely.

- Maximum measured strain from the RTCH DV43 was  $152 \mu\epsilon$  (0.76 ksi) and the maximum measured strain from the HETS crossing was  $60 \mu\epsilon$  (0.30 ksi). Both of these values were lower than the strain values predicted based on the previous day’s tests and analyses. Another unexpected result was that the maximum strain from the RTCH DV43 occurred at quarter point on Beam 3 (the same beam where low midspan strains were measured). One possible explanation for this supports the theory that the RTCH DV43 loading was great enough to open existing cracks. If a crack opened up at quarter span as the RTCH DV43 crossed the span, the beam would deflect significantly and distribute load to the adjacent beams. This may explain why the midspan and  $3L/4$  point strains were lower than expected and lower than at the adjacent beams. The maximum strain values from each transducer for both military vehicles are shown in Table 5.

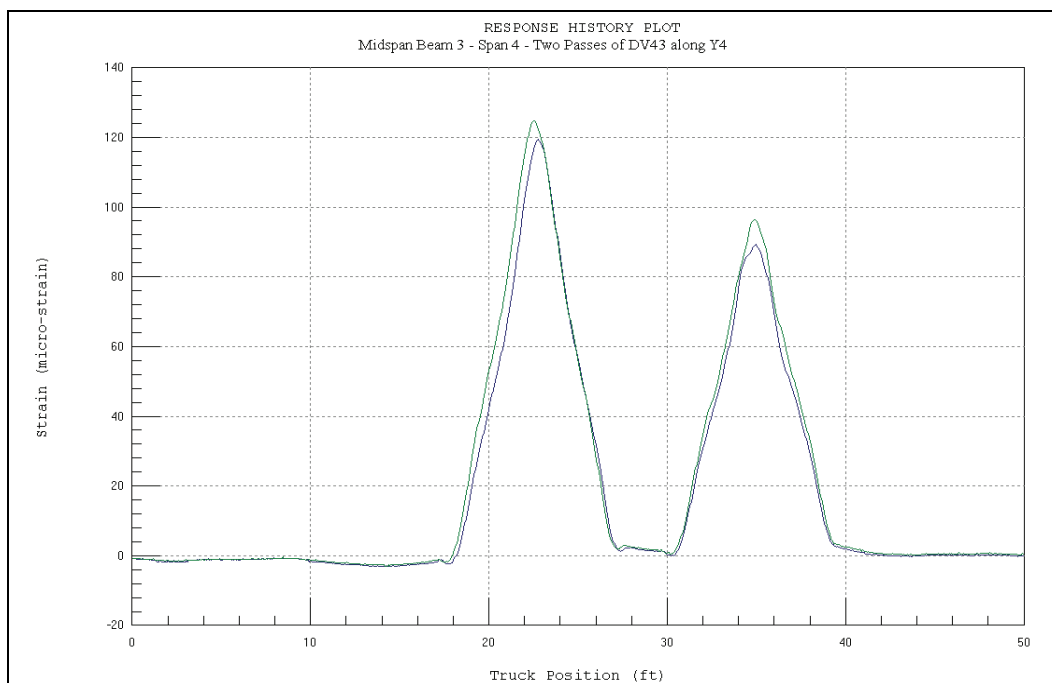


Figure 15. Reproducible and linear-elastic behavior from RTCH DV43.

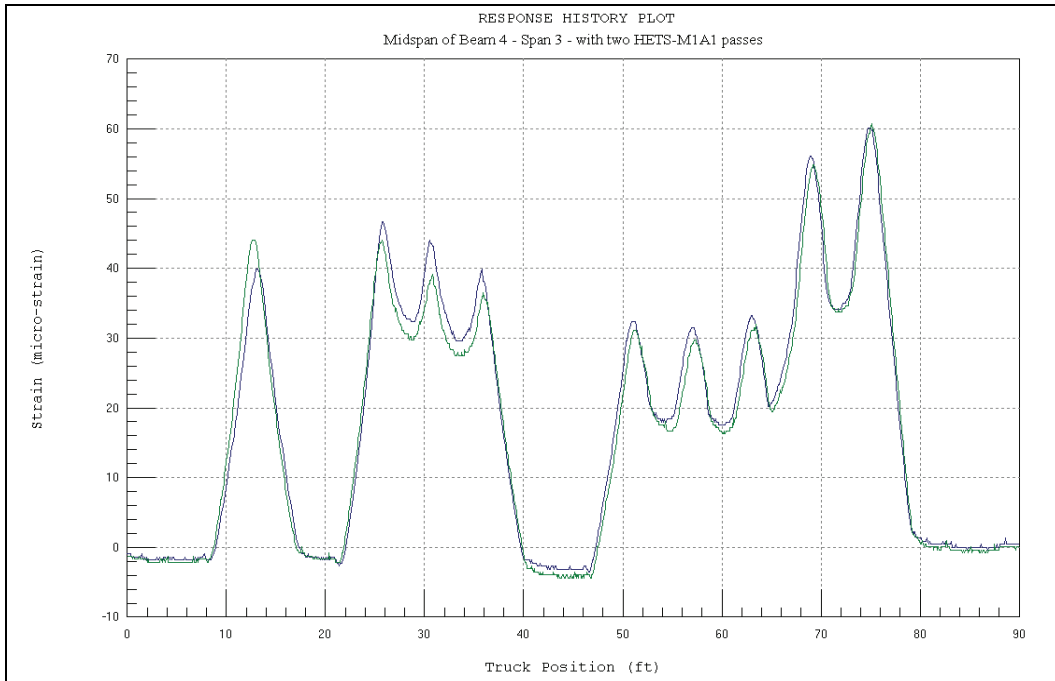


Figure 16. Reproducible and linear-elastic behavior from HETS-M1A1.

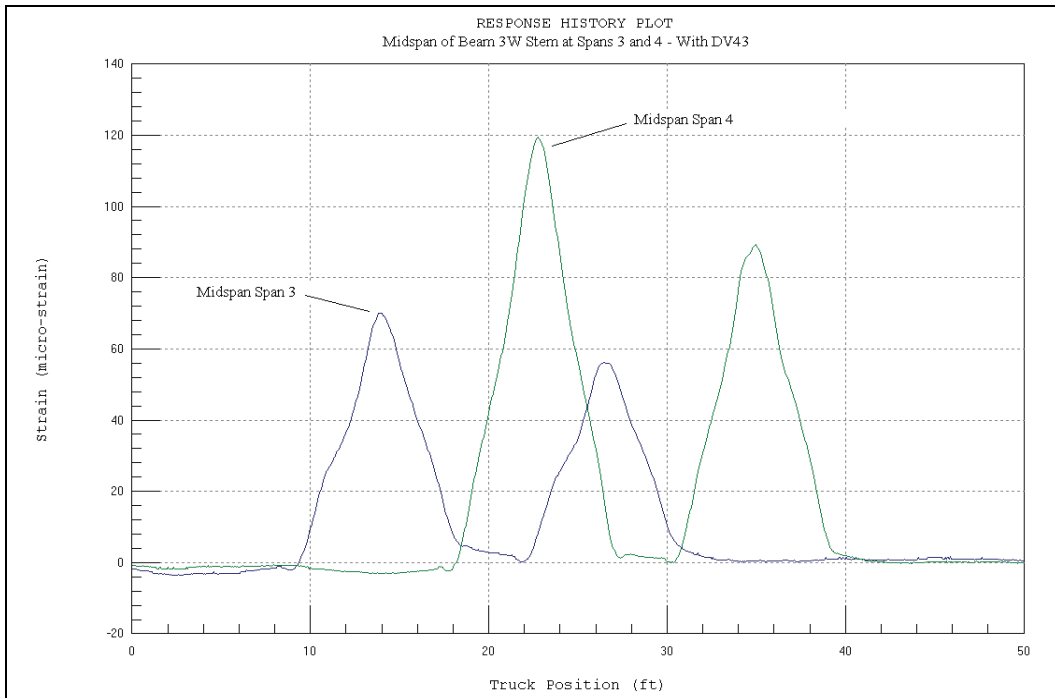


Figure 17. Comparison of Spans 3 and 4 measurements along Beam 3W-RTCH DV43.

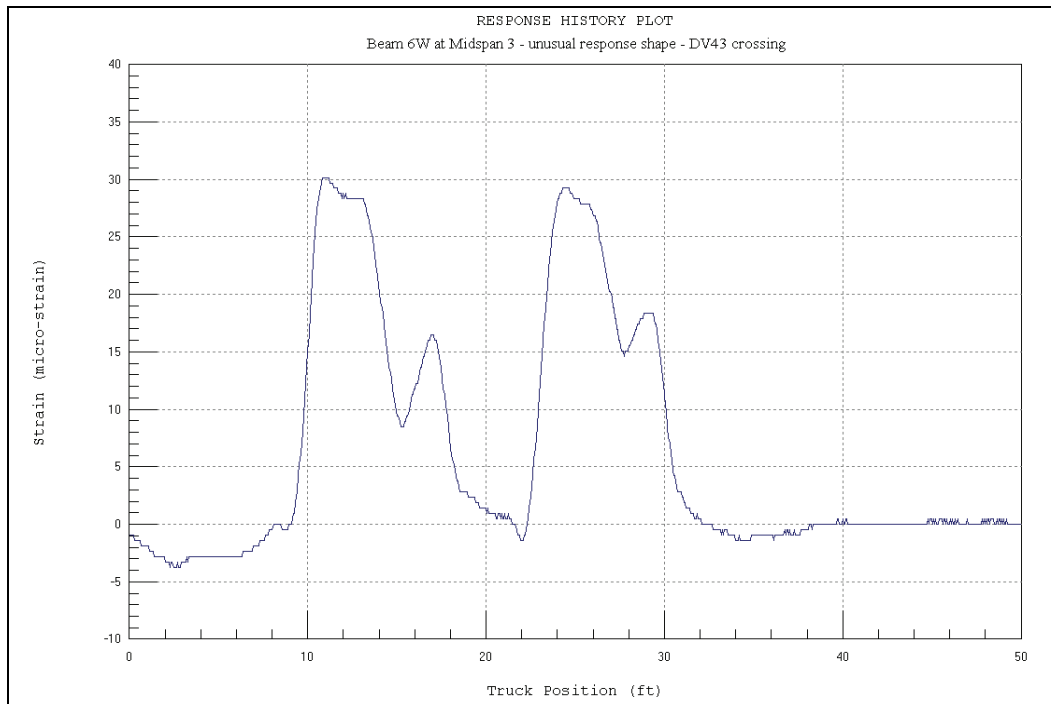


Figure 18. Unexpected response at Beam 6E-RTCH DV43.

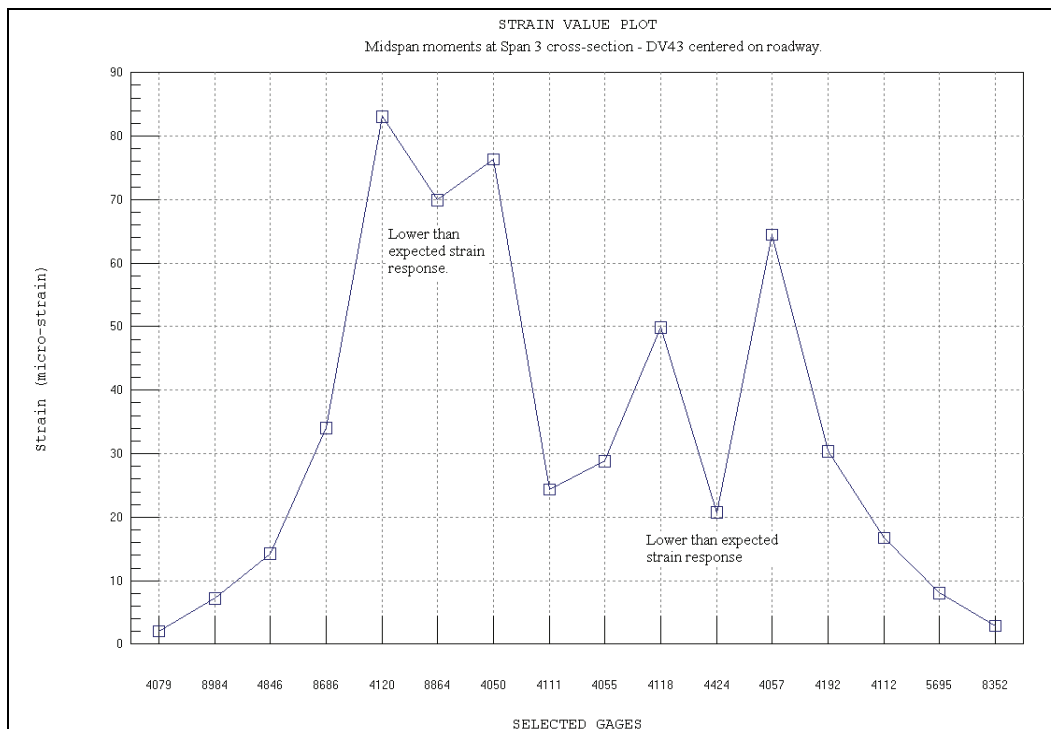


Figure 19. Midspan responses at Span 3 cross section-RTCH DV43.

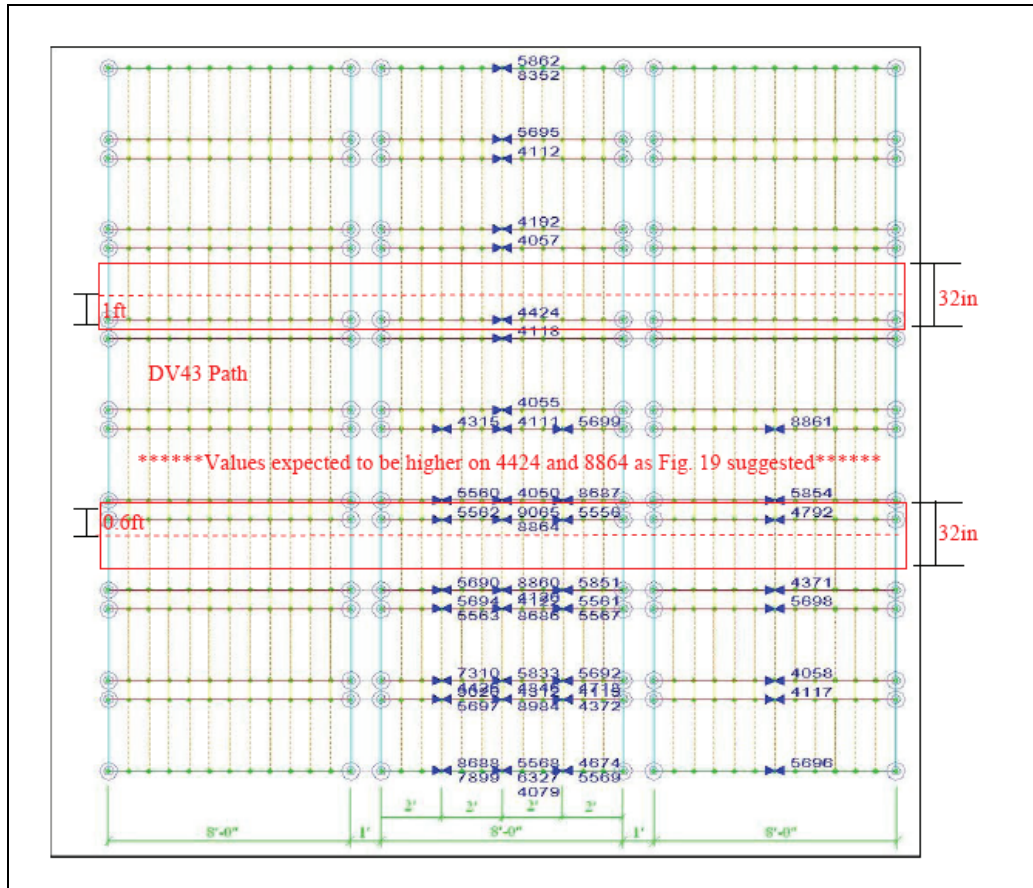


Figure 20. Wheel path of RTCH DV43.

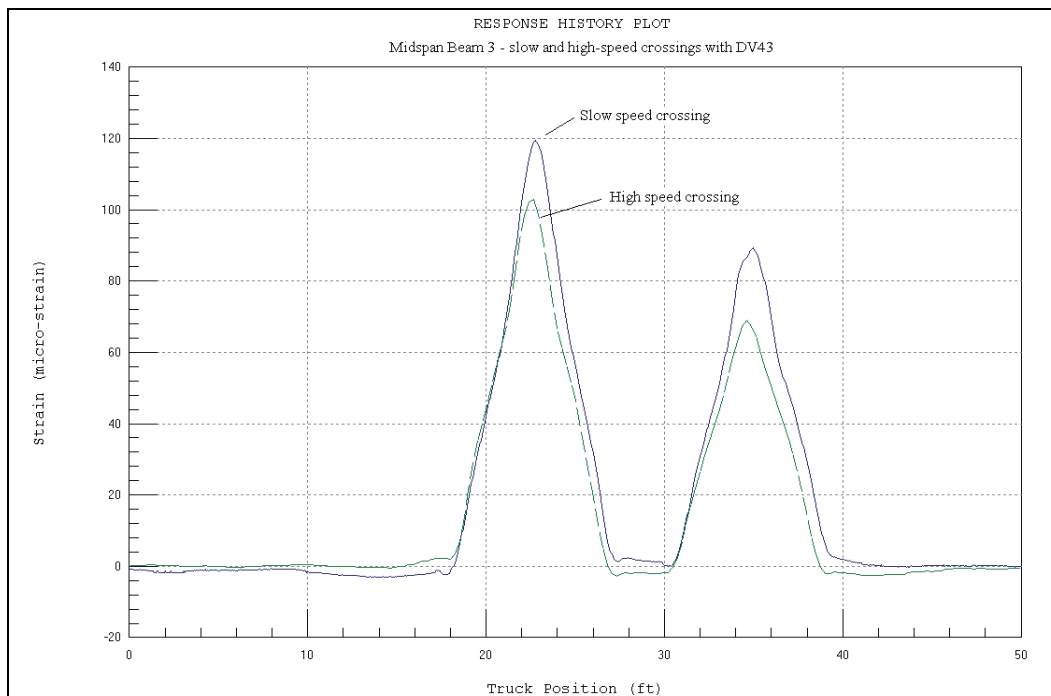


Figure 21. Dynamic response from RTCH DV43.

Table 5. Peak measured strain from RTCH DV43 and HETS crossings.

Location	Channel	Gage ID	RTCH DV43	HETS
Span 3 - 1/4 Point Beam 1E	20	7899	2	1
Span 3 - 1/4 Point Beam 1W	38	5697	8	3
Span 3 - 1/4 Point Beam 2E	37	4426	14	4
Span 3 - 1/4 Point Beam 2W	6	5563	25	6
Span 3 - 1/4 Point Beam 3E	5	5690	121	44
Span 3 - 1/4 Point Beam 3W	30	5562	<b>152</b>	39
Span 3 - 1/4 Point Beam 4E	29	5560	65	50
Span 3 - 1/4 Point Beam 4w	49	4315	26	32
Span 3 - 3/4 Point Beam 1E	54	5569	2	1
Span 3 - 3/4 Point Beam 1W	40	4372	10	4
Span 3 - 3/4 Point Beam 2E	39	4718	14	5
Span 3 - 3/4 Point Beam 2W	2	5567	25	6
Span 3 - 3/4 Point Beam 3E	1	5851	90	37
Span 3 - 3/4 Point Beam 3W	42	5556	101	35
Span 3 - 3/4 Point Beam 4E	41	8687	63	45
Span 3 - 3/4 Point Beam 4W	52	5699	22	30
Span 3 - Midspan Beam 1E	53	4079	2	1
Span 3 - Midspan Beam 1W	26	8984	7	3
Span 3 - Midspan Beam 2E	25	4846	14	4
Span 3 - Midspan Beam 2W	8	8686	35	8
Span 3 - Midspan Beam 3E	7	4120	85	51
Span 3 - Midspan Beam 3W	32	8864	70	35
Span 3 - Midspan Beam 4E	31	4050	78	<b>60</b>
Span 3 - Midspan Beam 4W	51	4111	25	34
Span 3 - Midspan Beam 5E	50	4055	29	32
Span 3 - Midspan Beam 5W	35	4118	50	51
Span 3 - Midspan Beam 6E	36	4424	30	36
Span 3 - Midspan Beam 6W	34	4057	65	55
Span 3 - Midspan Beam 7E	33	4192	32	15
Span 3 - Midspan Beam 7W	48	4112	17	6
Span 3 - Midspan Beam 8E	47	5695	8	3
Span 3 - Midspan Beam 8W	45	8352	3	1
Span 4 - Midspan Beam 1E	12	5696	2	1
Span 4 - Midspan Beam 1W	11	4117	6	2
Span 4 - Midspan Beam 2E	10	4058	12	3
Span 4 - Midspan Beam 2W	9	5698	38	8
Span 4 - Midspan Beam 3E	15	4792	120	47
Span 4 - Midspan Beam 3W	16	4371	101	48
Span 4 - Midspan Beam 4E	14	5854	41	45
Span 4 - Midspan Beam 4W	13	8861	27	37
Maximum Strains			<b>152</b>	<b>60</b>



## 4 Modeling, Analysis, and Data Correlation

Up to this point, all discussion of the bridge behavior had been limited to examination of the load test data. The next phase of the investigation was to verify the measured responses using structural analysis techniques. This was done by developing a two-dimensional model of the structure and making direct comparisons between the analytical results and the measured responses. The differences between the measured and computed data were then used as a means for model modification and improvement until a satisfactory correlation was made. The initial model calibration process was performed based on load test data with the legal load dump truck. Once an acceptable model was obtained, the other heavy vehicle loadings were analyzed and compared with their respective load test data sets. This process was also used to verify linear behavior of the structure and verify that the model could be used to predict the structure's response to other load configurations. Analyses were performed using WinSAC<sup>2</sup>, a finite element analysis and correlation program that is part of the Bridge Diagnostics, Inc. (BNI), modeling analysis and data processing software package.

The finite element model was initially developed as a two-dimensional (2-D) grid consisting of beam lines at each channel beam web and shell elements that represented the flanges and the shear interaction between beams. Rotational springs were used at the supports to simulate any possible end-restraints and continuity of moment over the piers, and the stiffnesses of the elements representing the shear keys were set to practically zero. It was also assumed that the beam bearings were simple supports (no continuity over piers), and a Young's modulus value of 4,400 ksi was assumed for the prestressed concrete.

Figure 22 shows the computer-generated display of the grid model. In order to make this 2-D model more representative of the actual bridge behavior, the beam stems were modeled as trapezoidal cross sections, and an eccentricity of 8.56 in. was provided to separate the beams from the upper deck/flange. In this manner, the stiffness of the beam cross sections

---

<sup>2</sup> WinSAC. 2006. Integrated Approach to Load Testing Instruction Manual. Boulder, CO: Bridge Diagnostics, Inc.

was based both on the flexural stiffness of the individual components (frame elements and shell elements) and the moment couples generated by the eccentricity between the components. This “quasi-3-D” modeling technique provided a simple way to model the stiffness provided by the channel beam stems, which was a requirement based on the initial test data examination. Figure 23 shows the cross-section properties of the channel beam-stems.

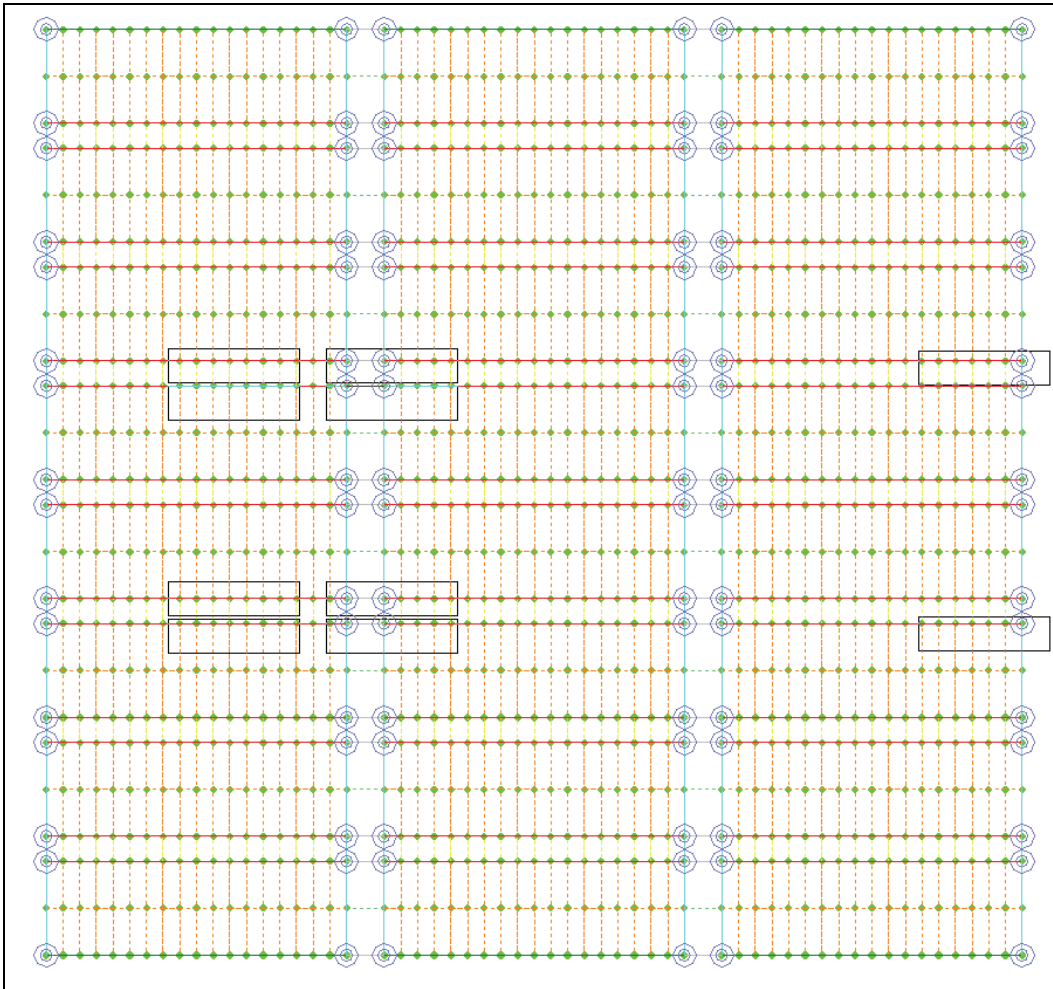


Figure 22. Finite element Model 3 bridge spans (Spans 2, 3, and 4).

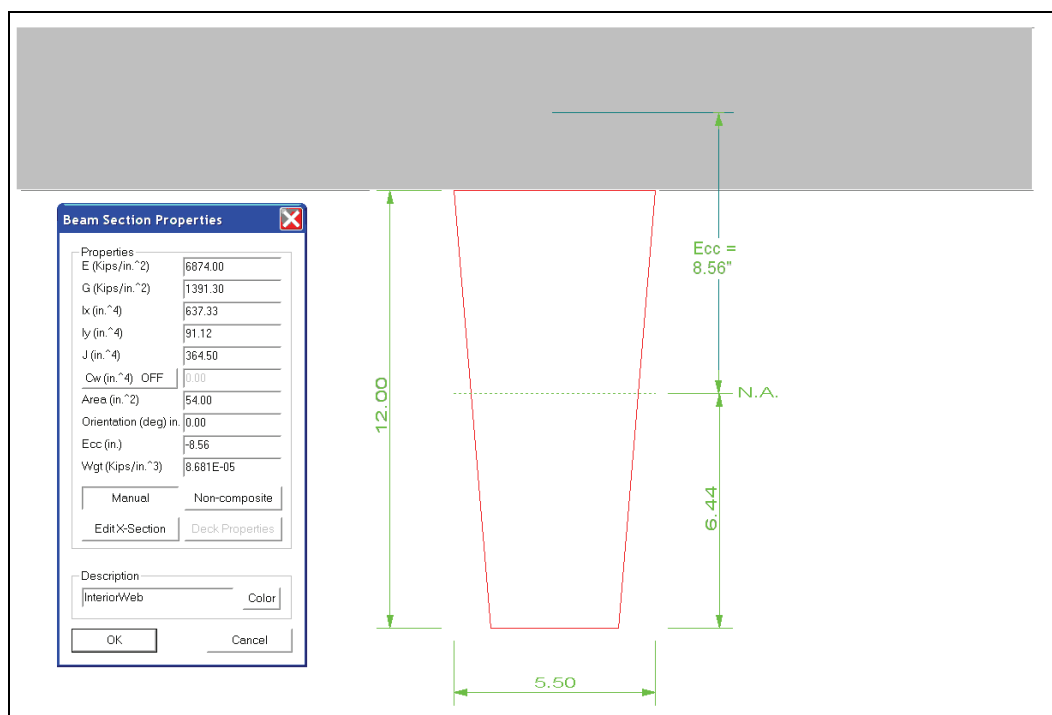


Figure 23. Beam cross-section properties.

Once the model was developed, the field load testing procedures could be reproduced with the BDI WinSAC (2006) software. This process included placing gage locations on the model (using the same transducer IDs), generating a 2-D "footprint" of the test truck, and defining truck paths that were identical to those in the field. The analysis was run and strains were computed at each gage location for each load case consisting of the truck being moved at 1-ft intervals the length of the bridge.

The primary differences in the calculated results indicated that the model did not have sufficient load transfer across the beams, the beams were too flexible, and the lateral position of the truck paths needed to be adjusted slightly. The first several iterations of model calibration consisted of making slight shifts in the truck paths. Because of the discontinuities along shear keys, the measured and calculated responses were very sensitive to the wheel placement. Movements as small as an inch had significant effects on the data comparison. Accuracy of the actual truck positions in the field are assumed to be within a foot.

The fine tuning of the truck position was done by graphical comparison of the midspan cross-section strain plots. Once the shape of lateral distribution was in good agreement, the stiffness variables were modified via the automated optimization process built into the WinSAC (2006)

program. Results from the overall calibration process are shown in Table 6 where the initial and final variables and error values are listed. Additional discussion of the calibration process and definition of the error terms are provided in Appendix B.

**Table 6. Model calibration and accuracy results.**

Stiffness Parameter	Original Value	Final Value
Effective Concrete Modulus ( $E_c$ -ksi)	4,400	6,874
Effective Stiffness of Shear Keys ( $E_j$ -ksi)	0	46
End-restraint via Axial Springs ( $F_x$ - kips/in)	0	0
Continuity Over Piers – ( $E_c$ – ksi)	0	100
Error / Accuracy Term	Initial Model	Final Model
Absolute Error	34,004 $\mu\epsilon$	10,415 $\mu\epsilon$
Percent Error	129%	4.6%
Scale Error	13.4%	6.7%
Correlation Coefficient	0.90	0.98

General conclusions that were made during the calibration process included:

- The “effective” concrete modulus was relatively high compared to the design concrete strength and associated modulus. It is important to note that this effective value is not a true concrete modulus because it includes the effect of the prestressed and conventional reinforcement plus it will compensate for any variation between the design and actual member dimensions (i.e., additional fillets, contribution of asphalt, etc.). This effective modulus was sufficiently high to indicate a high-strength concrete. A good estimate for  $f'_c$  would be a minimum of 6 ksi and possibly as high as 8 ksi.
- The model calibration process confirmed that there was very little end restraint and there was basically no continuity of moment across the piers.
- While the shear keys were quite flexible, they did transfer some load to adjacent beams.
- The resulting final model based on the dump truck loading data was very accurate, indicating that the structure was behaving linearly elastic.

After the calibration process resulted in a model with an acceptable accuracy, load configurations of the RTCH DV43 and the HETS were

applied to the model and analyzed. As was with the dump truck, it was determined that the location of the heavy vehicles on the model needed to be fine-tuned so that a reasonable correlation could be obtained. Aside from the two previously mentioned sensors where unexpectedly low strain values were obtained, the calibrated model was found to be reasonably accurate for predicting the responses measured with the heavy vehicles. This is illustrated in some typical results for the RTCH DV43 shown in Figure 24, where the solid line is the measured strain and the symbols are calculated strains. Measured and computed responses from the HETS also correlated reasonably well, although it was apparent that the actual distribution of loads among the axles on the HETS was significantly different from what was specified by the CEG-Heavy Vehicle Load Table. Figure 25 shows a measured and computed strain comparison for the HETS. Note the variation in the strain peaks in the field data, indicating that the axle weights are distributed differently than indicated by the load table. The specified axle weights on the trailer are relatively consistent with the last axle being approximately 6% heavier than the average trailer axle. The field data indicate the last two trailer axles may be as much as 25% heavier than the other axles. This ratio varies significantly from beam to beam.

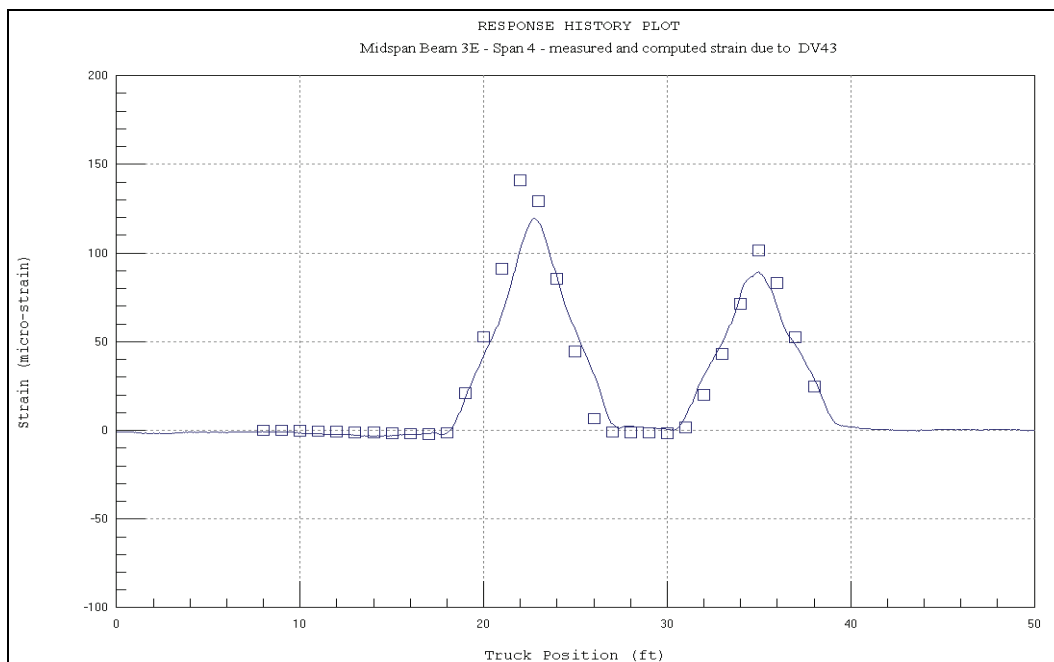


Figure 24. Midspan strain comparison for RTCH DV43.

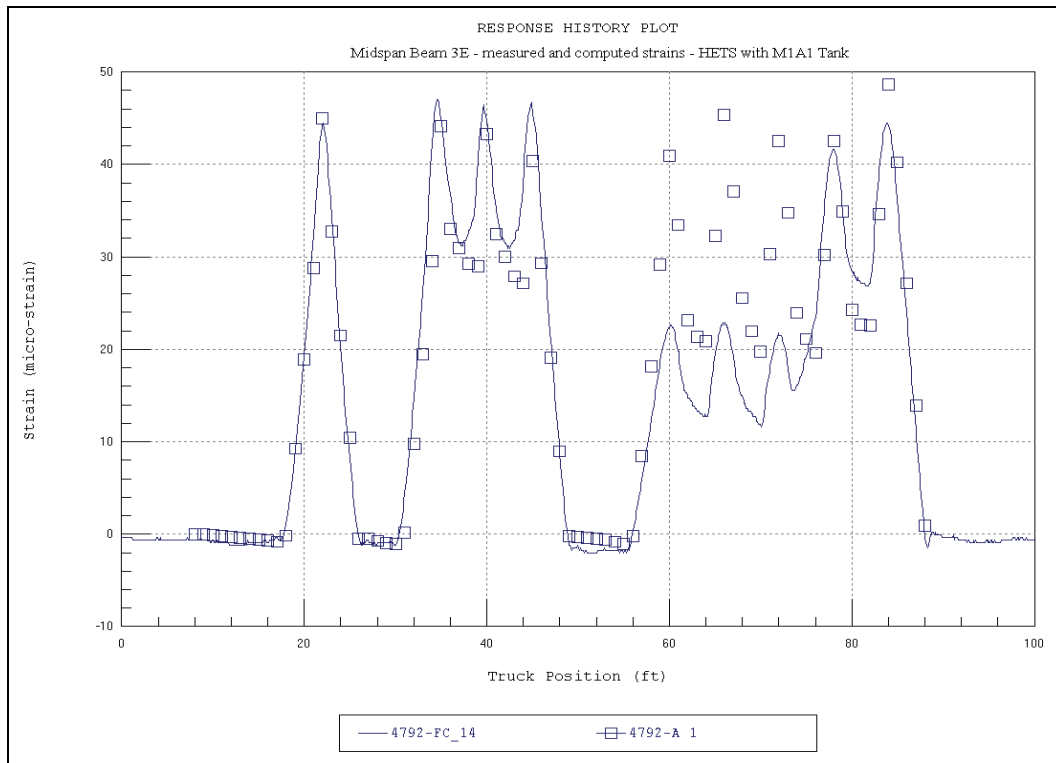


Figure 25. Midspan strain comparison for HETS/M1A1.

Model accuracy values for the RTCH DV43 and the HETS are provided in Table 7. Although these values were not as good as those obtained with the dump truck, they are still within reasonable tolerances. It was noted that for almost every sensor location, the measured strains were less than the predicted strains. This is an indication that lateral wheel load distribution improved with the heavier vehicles and that the analysis which was strictly linear provided slightly conservative results.

Table 7. Statistical accuracy terms with heavy military vehicles.

Error / Accuracy Term	RTCH DV43	HETS-M1A1
Absolute Error	3,526 $\mu\epsilon$	5,691 $\mu\epsilon$
Percent Error	13.5%	13.3%
Scale Error	15.9%	18.9%
Correlation Coefficient	0.93	0.94

## 5 Load Rating Procedures and Results

The goal of producing an accurate model was to predict the structure's actual live load behavior when subjected to the design or any specific permit loads. The primary benefit of a model is that responses from the entire superstructure can be investigated rather than just the instrumented locations. This is important because in most cases, the instrumentation is not located at the critical location on the bridge. Since the load rating is based on an analysis, the approach is practically identical to standard load rating procedures except that a "field verified" model is used instead of a typical beam analysis combined with load distribution factors.

In this case, the goal was to provide rating factors for the standard rating vehicles (HS-20, Type-3, Type 3-3, and Type 3S2) along with the heavy military loads specified in Table 8. Load rating factors were computed using the Load and Resistance Factor Rating (LRFR) methods specified in the AASHTO Condition Evaluation of Highway Bridges Manual<sup>3</sup>. Load ratings were obtained by applying the dead load and the various live-loads to the model and comparing the responses to the available capacity. Shear and moment capacities were computed using current AASHTO LRFD specifications and are listed in Table 10. Because there was a concern that some of the heavier vehicles could potentially crack the beams, the cracking moment capacity is also listed. Serviceability load ratings based on the cracking limit were computed for various vehicles.

**Table 8. Foster Creek Bridge 305 evaluation for CEG-A heavy vehicle loading (13 July 2005).**

Vehicle	Number of Passes in 6-Month Period	Gross Vehicle Weight	Number of Axles	Axle Weights (k-kips, T-Tons)
HETS Hauling M1A1 Tank	7-8 [3-5 per ship, 2-3 ships/year = 15/year max]	230.8 k (115.4 T)	9	Axle 1 - 21.7 k; Axle 2 - 22.3 k; Axle 3 - 21.7 k; Axle 4 - 19.9 k; Axle 5 - 27.0 k; Axle 6 - 29.7 k; Axle 7 - 28.0 k; Axle 8 - 28.0 k;

<sup>3</sup> American Association of State Highway and Transportation Officials. 2003. *Manual for condition evaluation and load and resistance factor rating (LRFR) of highway bridges*. Washington, DC: American Association of State Highway and Transportation Officials.

Vehicle	Number of Passes in 6-Month Period	Gross Vehicle Weight	Number of Axles	Axle Weights (k-kips, T-Tons)
				Axle 9 - 31.4 k
Heavy Lift Mobile Cranes: 275-Ton Capacity	10-18	189.1 k (94.55 T)	9	Axle 1 - 20.8 k; Axle 2 - 20.8 k; Axle 3 - 22.5 k; Axle 4 - 22.5k; Axle 5 - 22.5 k; Axle 6 - 22.5 k; Axle 7 - 19.1 k; Axle 8 - 19.1 k; Axle 9 - 19.1k
90-Ton Capacity		135.5 k (67.8 T)	6	Axle 1 - 20.7 k; Axle 2 - 20.7k; Axle 3 - 29.2 k; Axle 4 - 29.2 k; Axle 5 - 17.9 k; Axle 6 - 17.9 k
HETS Hauling Palletized Load System (PLS) M1075	65	142 k (71 T)	9	Axle 1 - 19.5 k; Axle 2 - 15.7 k; Axle 3 - 15.6 k; Axle 4 - 15.1 k; Axle 5 - 13.6 k; Axle 6 - 13.8 k; Axle 7 - 14.1 k; Axle 8 - 17.2 k; Axle 9 - 17.3 k
HETS Hauling Misc Loading	31	130-140 k (65-70 T)	9	Axle 1 - 19.5 k; Axle 2 - 15.5 k; Axle 3 - 15.4 k; Axle 4 - 15.0 k; Axle 5 - 13.8 k; Axle 6 - 13.6 k; Axle 7 - 13.7 k; Axle 8 - 16.8 k; Axle 9 - 16.6 k
RTCH RT 240	16	119.76 k (60 T)	2	Front axle - 66.4 k Rear axle - 53.36 k
RTCH DV43 Cargo Handler w/Forklift	3	108.2 k (54 T)	2	Front axle - 44.6 k Rear axle - 63.6 k
40-Ton Cranes	4	96 k (48 T)	2	Front axle - 37.5 k Rear axle - 58.5 k
Empty HETS  (HETS Tractor and Semi-Trailer Only)	81  (54/ship, 2-3 ships/year = 162 max/yr)	90.8 k (45.4 T)	9	Axle 1 - 19.5 k; Axle 2 - 0.7 k; Axle 3 - 10.7 k; Axle 4 - 10.1 k; Axle 5 - 6.5 k; Axle 6 - 6.5 k; Axle 7 - 6.3 k; Axle 8 - 10.6 k; Axle 9 - 10.4 k
Tractor with Specialized Lowboy Hauling One M1000s (HETS Semi-Trailer)	68	82.6 k 41.3 T	6	Axle 1 - 19.5 k; Axle 2 - 10.7 k; Axle 3 - 10.7 k; Axle 4 - 10.1 k; Axle 5 - 15.8 k; Axle 6 - 15.8 k;
Tractor Hauling D8 on Lowboy Trailer	3	76.6 k 38.3 T	5	Axle 1- 16.6 k; Axle 2 - 15.5 k; Axle 3 - 15.5 k; Axle 4 - 15.5 k; Axle 5 - 15.5 k
Tractor with Specialized Lowboy Hauling One M1070s (HETS Tractor)	68	72.6 k 36.3 T	6	Axle 1- 19.5 k; Axle 2 - 10.7 k; Axle 3 - 10.7 k; Axle 4 - 10.1 k; Axle 5 - 10.8 k; Axle 6 - 10.8 k
Tractor Hauling D7 on M172A (Trailer)	1	66 k 33 T	5	Axle 1 - 16.6 k; Axle 2 - 15.5 k; Axle 3 - 15.5 k; Axle 4 - 9.2 k; Axle 5 - 9.2 k



Table 9. CEG-A heavy vehicle loading axle configurations.

Vehicle	Axle Configuration
HETS Hauling M1A1 Tank	
Heavy Lift Mobile Cranes: 275-Ton Capacity	
90-Ton Capacity	
HETS Hauling PLS M1075	
HETS Hauling Misc Loading	
RTCH RT 240	

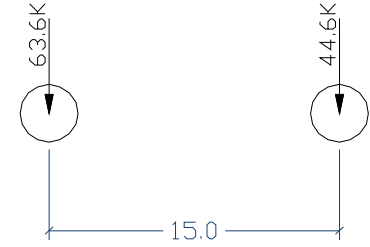
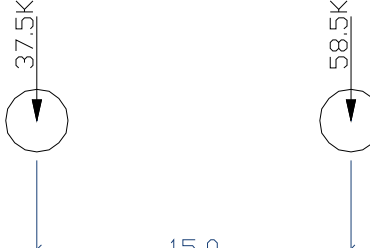
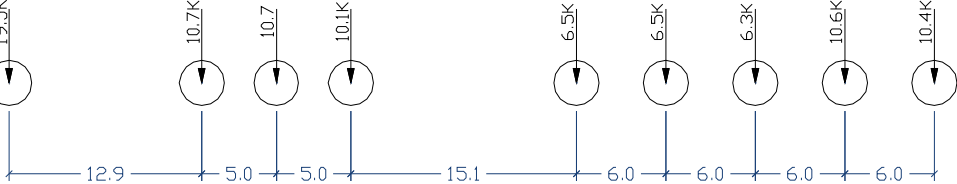

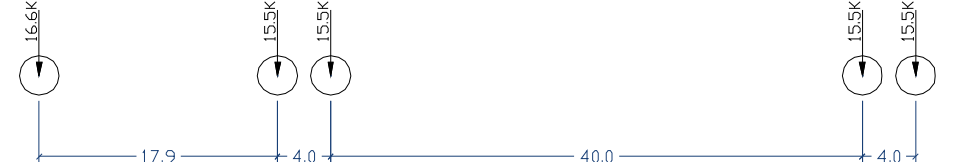


Vehicle	Axle Configuration
RTCH DV43 w/Forklift	
40-Ton Cranes	
Empty HETS (HETS Tractor and Semi-Trailer Only)	
Tractor with Specialized Lowboy Hauling One M1000s (HETS Semi-Trailer)	
Tractor Hauling D8 on Lowboy Trailer	
Tractor with Specialized Lowboy Hauling One M1070s (HETS Tractor)	
Tractor Hauling D7 on M172A (Trailer)	

Table 10. Live-load moment and shear capacity.

Moment Capacity Calculations		LRFR
Concrete Strength	$F'_c$	6 ksi
Width Concrete Flange	$bw$	18.75 in.
Prestressed Steel	$F'_s$	250 ksi
Area Prestressed Steel	$A_s$	0.216 in. <sup>2</sup>
G	Stress Relieved	0.4
Distance	$d$	7.375 in.
Non-Prestressed Steel	$F_y$	40 ksi
Area Non-Prestressed Steel	$A_{s'}$	0.44 in. <sup>2</sup>
Distance	$dt$	15 in.
Average Prestress Stress at Ultimate	$f^*s_u$	238.5 ksi
Ultimate Moment	$M_n$	618.4 kip-in.
Moment of Inertia		3069 in. <sup>4</sup>
Neutral Axis		12.0 in.
Cracking Moment		291.9 kip-in.
Shear Capacity Calculations		LRFR
Web Depth		15 in.
Web Width		4 in.
Area Shear Steel		0.31 in. <sup>2</sup>
Bar Spacing		10 in.
Concrete Shear Capacity	$V_c$	7.9 kips
Steel Shear Capacity	$V_s$	18.6 kips
Total Shear Capacity	$V$	26.5 kips

Load rating factors were obtained by running each of the load configurations across the model. Standard width trucks were rated assuming two-lane loading. The wider vehicles that typically require an escort were rated for single vehicle loading only. Live-load envelopes were generated for each member and compared with the live-load capacity. As per the AASHTO LRFD specifications, a dynamic allowance factor (impact factor) of 33% was used for all cases. Table 11 contains the maximum moment and rating factor for the critical member.

Load rating factors were obtained by running the load configurations across the model. Live-load envelopes were generated for each member

and compared with the live-load capacity. Due to the slow crossing, no impact was applied to the live-load responses. Table 11 contains the maximum moment and rating factor for the critical member. Load ratings based on shear are provided in Table 12. Note that vehicles with axle groups of three or more typically had load ratings that were controlled by shear (i.e., HETS with the M1A1). Serviceability load rating results are listed in Table 13.

**Table 11. Foster's Creek load rating results (moment).**

Truck	Live-load Moment (k-in.)	Inventory Rating Factor/Tons 33% Impact	Operating Rating Factor/Tons 33% Impact	Inventory Rating Factor/Tons No Impact	Operating Rating Factor/Tons No Impact
HS-20 (3-axle 36-ton)	185	1.23 / 44.3	1.60 / 57.6	1.64 / 58.9	2.13 / 76.6
Type 3 (3-axle 25-ton)	113	2.01 / 50.3	2.60 / 65.0	2.67 / 66.9	3.46 / 86.5
Type 3-3 (6-axle 40-ton)	92	2.44 / 97.6	3.20 / 128.0	3.25 / 129.8	4.26 / 170.2
Type 3S2 (5-axle 36-ton)	97	2.37 / 85.3	3.07 / 110.5	3.15 / 113.4	4.08 / 147.0
HETS-M1A1	133	1.71 / 197.3	2.22 / 256.2	2.27 / 262.4	2.95 / 340.7
Heavy Lift Mobile Crane 275-ton	108	2.11 / 199.5	2.74 / 259.1	2.81 / 265.3	3.64 / 344.6
Heavy Lift Mobile Crane 90-ton	120	1.90 / 128.8	2.47 / 167.5	2.53 / 171.3	3.29 / 222.8
HETS - PLS M1075	133	1.71 / 197.3	2.22 / 256.2	2.27 / 262.4	2.95 / 340.7
HETS - Misc 140-kip	133	1.71 / 197.3	2.22 / 256.2	2.27 / 262.4	2.95 / 340.7
RTCH RT 240	266	0.86 / 51.6	1.11 / 66.6	1.14 / 68.6	1.48 / 88.6
RTCH DV43 Cargo Handler	255	0.89 / 48.1	1.16 / 62.6	1.18 / 64.0	1.54 / 83.3
40-ton Cranes	231	0.99 / 47.5	1.28 / 61.4	1.32 / 63.2	1.70 / 81.7
HETS - Empty	133	1.71 / 197.3	2.22 / 256.2	2.27 / 262.4	2.95 / 340.7
Tractor-Lowboy (HETS Semi-Trailer)	92	2.44 / 97.6	3.20 / 128.0	3.25 / 129.8	4.26 / 170.2
Tractor Hauling D8 on Lowboy	97	2.37 / 85.3	3.07 / 110.5	3.15 / 113.4	4.08 / 147.0

**Table 12. Foster's Creek load rating results (shear).**

Truck	Live-load Shear (kips)	Inventory Rating Factor/Tons 33% Impact	Operating Rating Factor/Tons 33% Impact	Inventory Rating Factor/Tons No Impact	Operating Rating Factor/Tons No Impact
HS-20 (3-axle 36-ton)	6.8	1.40 / 50.4	1.82 / 65.5	1.86 / 67.0	2.42 / 87.1
Type 3 (3-axle 25-ton)	4.8	2.01 / 50.3	2.60 / 65.0	2.67 / 66.9	3.46 / 86.5
Type 3-3 (6-axle 40-ton)	3.9	2.44 / 97.6	3.16 / 126.4	3.25 / 129.8	4.20 / 168.1
Type 3S2 (5-axle 36-ton)	4.4	2.20 / 79.2	2.86 / 104.0	2.93 / 105.3	3.80 / 138.3
HETS-M1A1	6.1	1.57 / 181.2	2.03 / 234.3	2.09 / 241.0	2.70 / 311.6
Heavy Lift Mobile Crane 275-ton	4.5	2.13 / 201.4	2.76 / 261.0	2.83 / 267.9	3.67 / 347.1

Truck	Live-load Shear (kips)	Inventory Rating Factor/Tons 33% Impact	Operating Rating Factor/Tons 33% Impact	Inventory Rating Factor/Tons No Impact	Operating Rating Factor/Tons No Impact
Heavy Lift Mobile Crane 90-ton	5.8	1.65 / 111.9	2.14 / 145.1	2.19 / 148.8	2.85 / 193.0
HETS - PLS M1075	6.1	1.57 / 181.2	2.03 / 234.3	2.09 / 241.0	2.70 / 311.6
HETS - Misc 140-kip	6.1	1.57 / 181.2	2.03 / 234.3	2.09 / 241.0	2.70 / 311.6
RTCH RT 240	10.0	0.96 / 57.6	1.25 / 75.0	1.28 / 76.6	1.66 / 99.8
RTCH DV43 Cargo Handler	9.6	1.00 / 54.0	1.30 / 70.2	1.33 / 71.8	1.73 / 93.4
40 ton Cranes	9.5	1.00 / 48.0	1.30 / 62.4	1.33 / 63.8	1.73 / 83.0
HETS - Empty	6.1	1.57 / 181.2	2.03 / 234.3	2.09 / 241.0	2.70 / 311.6
Tractor-Lowboy (HETS Semi-Trailer)	3.9	2.44 / 97.6	3.16 / 126.4	3.25 / 129.8	4.20 / 168.1
Tractor Hauling D8 on Lowboy	4.4	2.20 / 79.2	2.86 / 104.0	2.93 / 105.3	3.80 / 138.3

As defined by the AASHTO Manual for Condition Evaluation of Bridges (2003), Inventory rating level corresponds to the design level of stresses and reflects the existing bridge and material conditions with regard to deterioration and loss of section. Load ratings based on the Inventory Level allow for a determination of a live load which can safely utilize an existing structure for an indefinite period of time. Loadings based on the Operating rating level describe the maximum permissible live load to which the structure may be subjected. Allowing unlimited numbers of vehicles to use the bridge at Operating Level may shorten the life of the bridge. However, infrequent intervals at the Operating Limit would not have adverse effects on a structure's life span.

Table 13. Foster's Creek serviceability load rating results (cracking moment).

Truck	Live-load Moment (k-in)	Serviceability Rating Factor/Tons With 33% Impact	Serviceability Rating Factor/Tons With no Impact
HS-20	185	1.18 / 42.5	1.57 / 56.5
Heavy Lift Mobile Crane 275-ton	108	2.02 / 191.0	2.69 / 254.0
RTCH RT 240	266	0.82 / 49.2	1.09 / 65.4
RTCH DV43	255	0.85 / 45.9	1.13 / 61.0

## 6 Conclusions and Recommendations

Conclusions made directly from the load test data are qualitative in nature and indicate that the structure responded in a linear-elastic mode for both the preliminary tests and the heavy vehicle crossings. Measured neutral axis values were very close to the theoretical values indicating the assumed beam section properties were valid.

During load tests with the heavy military loads, unexpected strain values were recorded at two locations. These locations were directly under the RTCH DV43 wheel loads and should have produced the largest strains. However, the strains were significantly lower than expected. Since these measurements were from the critical locations, the cause of the low strain values was examined thoroughly. One possible cause was the glue holding the sensors in place was beginning to fail. Normally, this occurrence is seen as a sudden slip, and then the sensor no longer provides any output. Therefore, it is apparent that sensors did not completely come loose. During equipment removal it was noted that some of the sensors came off exceptionally easy, although none were completely loose.

The other possibility is that the sensors were located near existing flexural cracks. Strain transducers located near cracks will exhibit normal strain values up to the point where the crack begins to open, and then the strains will level off until the crack closes again. One strain history exhibited this behavior; however, the strain magnitudes at which the leveling off began were considerably less than the peak strains obtained with the dump truck test. Responses from one of the strain transducers did not level off or show any indication of an unusual response other than the low magnitude.

Because of these unexpected responses and the fact that cracking the structure is not desirable (although not an indication of failure), additional analysis and rating limits were examined to see if the heavy loads could crack the bridge or open an existing crack. This result was, of course, entirely based on assumptions regarding prestress losses over the last 36 years (1969-2005) and what level of impact to apply. Assuming prestress losses of about 20% and an impact of 33%, the RTCH DV43 would likely crack the beams directly under the wheel lines. However, during the load test there were no visible cracks, and there was no

apparent dynamic effect during the high-speed crossings. Therefore, the presence of flexural cracks is possible, but not highly likely. If, however, any cracks were already present, then the moment generated by the RTCH DV43 would very likely open the cracks, because the tensile strength of the concrete would not be present, and cause an uneven strain distribution along the bottom surface of the beams, thereby influencing the strain measurements.

The only vehicles that may be of concern with regards to potential flexural cracks are the heavy four-wheeled vehicles (RTCH DV43, RT 240, and the mobile 40-ton crane). The HETS with its heaviest load (M1A1 tank) is not an issue with respect to serviceability or load capacity of this bridge. Although it cannot be determined from the available data whether or not any cracks exist, the consequences of opening existing cracks is relatively minor if the loading is infrequent, such that fatigue in the prestressing strands is not a concern over the remaining life of the structure. The existence of any cracks should be verified before any decisions are made that would limit vehicle crossings.

The general conclusions obtained from the load ratings are that all of the design vehicles and CEG-A specified military vehicles can cross the bridge within the Operating (maximum) load limits. All of the vehicles, with exception to the four-wheeled cargo handlers (RT240, RTCH DV43, and the 40-ton crane), can cross the bridge within the Inventory (Design) load limits. The heavy four-wheeled vehicles are relatively close to the operating limit from a strength limit state. It is important to realize that a dynamic allowance (impact factor) of 33% was used for these calculations, whereas very little dynamic response was observed. Therefore, additional safety can be achieved by limiting the speed of the RTCH DV43, the RT240, and the 40-ton crane to 5 mph when crossing this bridge. Inventory, operating, and serviceability ratings were provided for no impact allowance (allowable by LRFR when speeds are restricted) and critical rating values for all vehicles were above 1.0 at the Inventory level.

While the presence of cracks has no bearing on the strength based load ratings, they may alter the serviceability limits and restrict the frequency of crossing by the worst case vehicles. Therefore, it is recommended that some further investigation be made with regards to the responses with the RTCH DV43. Two options include in situ prestress tests on the concrete to

determine the amount of tension available for live-load and a thorough examination of cracks while the bridge is loaded with a RTCH DV43 or RT240. Cracks would be difficult to detect in the field and may require advanced examination techniques such as photoelasticity or numerous strain measurements along the bottom of a beam.

This bridge was designed for a heavy load compared to the 1969 design loads, and the test results indicate the bridge has a load capacity significantly higher than current legal loads. Under normal highway conditions this bridge would not require any posted weight limits. Since this bridge does carry heavy military and other special loads, some restrictions may be necessary. Posting procedures are generally a function of the inventory and operating limits and are determined by the bridge owner's policy. It is the authors' understanding that the bridge posting policy at the Naval Weapons Facility is based on the inventory load limits. The only vehicles requiring posted limits are the three 4-wheeled vehicles (RTCH DV43, RT240, and the 40-ton crane). Since these vehicles do not carry additional payload, the gross vehicle weights cannot vary significantly. Therefore, the most sensible restriction would be to limit the speed of these vehicles to 5 mph.



## 7 Measured and Computed Strain Comparisons

Although statistical terms provide a means of evaluating the relative accuracy of various modeling procedures and help determine the improvement of a model during a calibration process, the best conceptual measure of a model's accuracy is a visual examination of the response histories. The following graphs contain measured and computed stress histories from each truck path (Figures 26-64). In each graph the continuous lines represent the measured strain at the specified gage location as a function of truck position as it traveled across the bridge. Computed stresses are shown as markers at discrete truck intervals.

### Preliminary test results

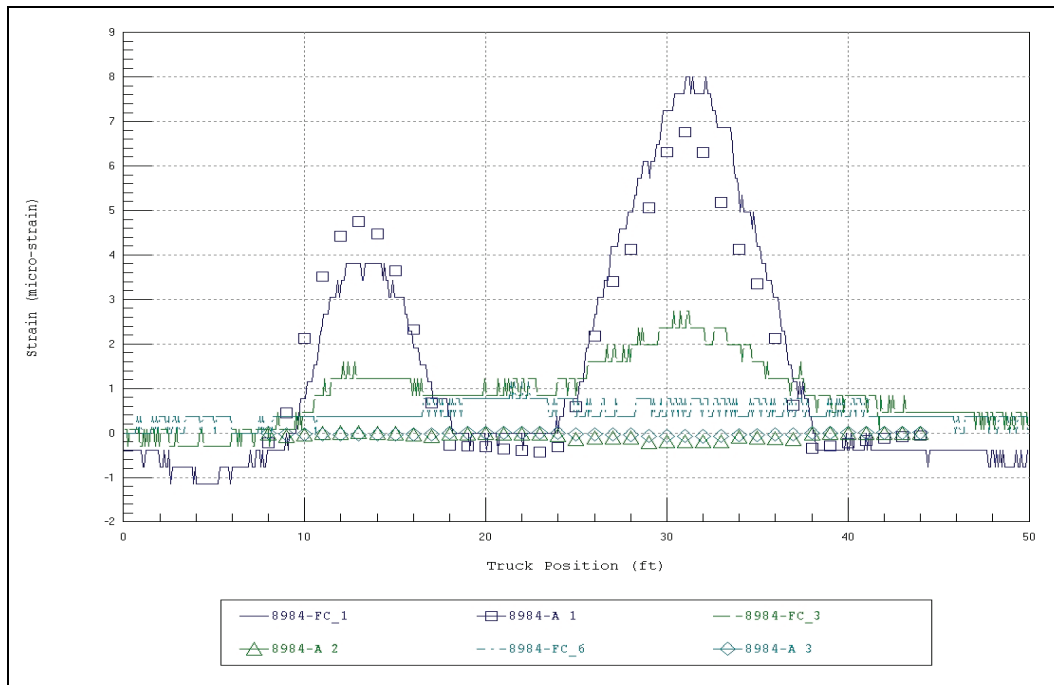


Figure 26. Midspan strain comparisons-three truck passes-Beam 1W.

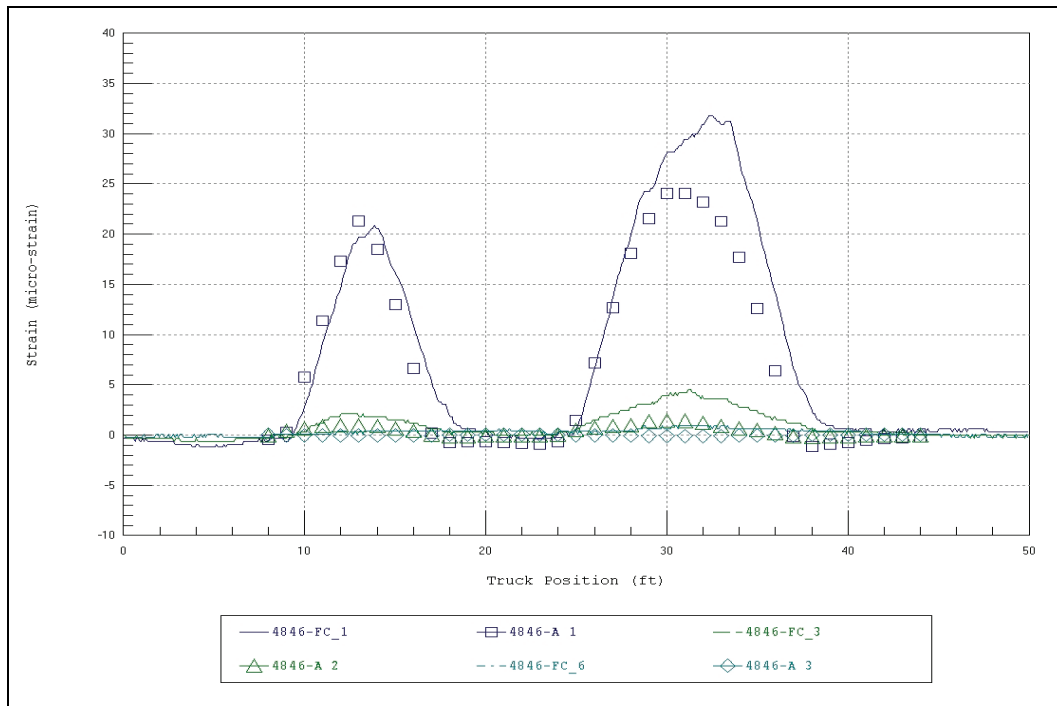


Figure 27. Midspan strain comparisons-three truck passes-Beam 2E.

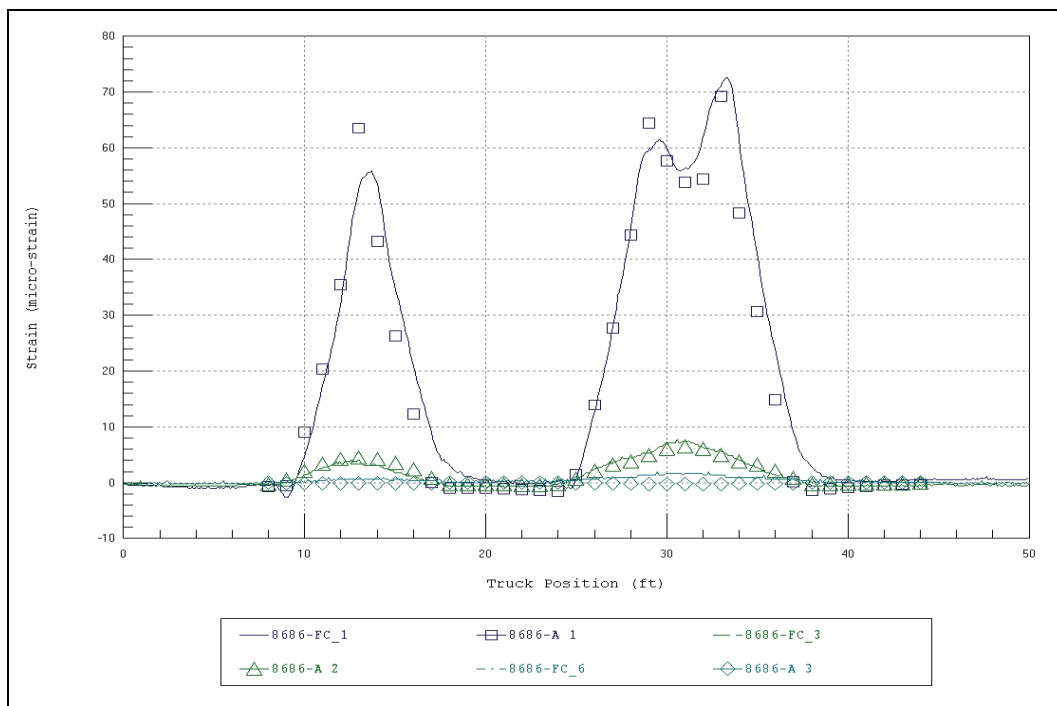


Figure 28. Midspan strain comparisons-three truck passes-Beam 2W.

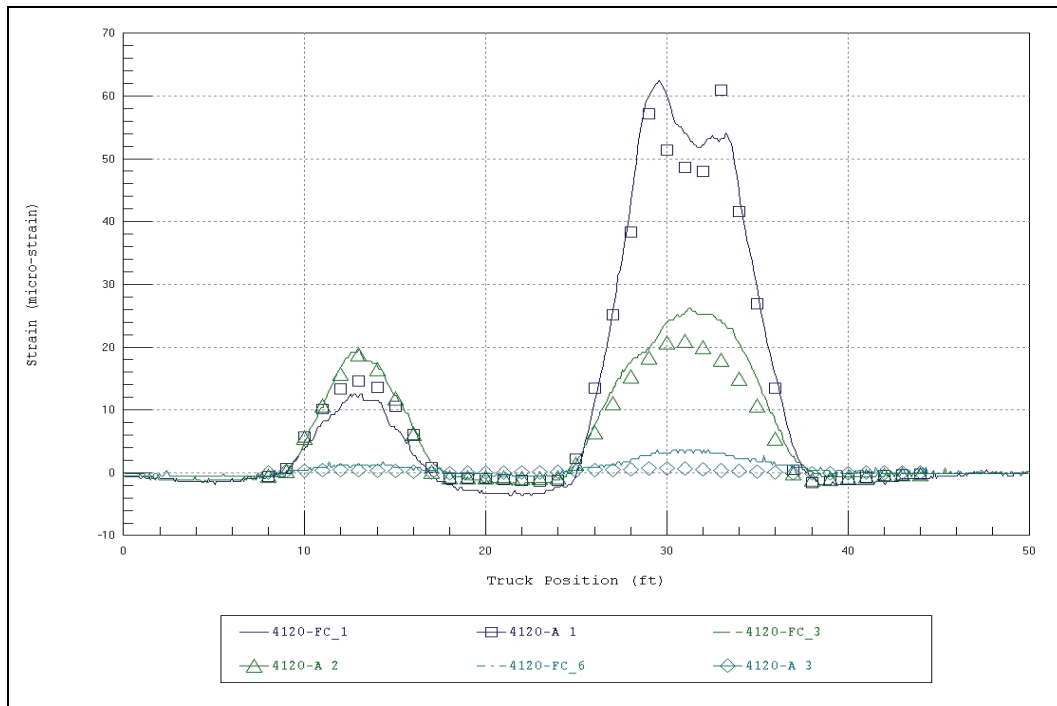


Figure 29. Midspan strain comparisons-three truck passes-Beam 3E.

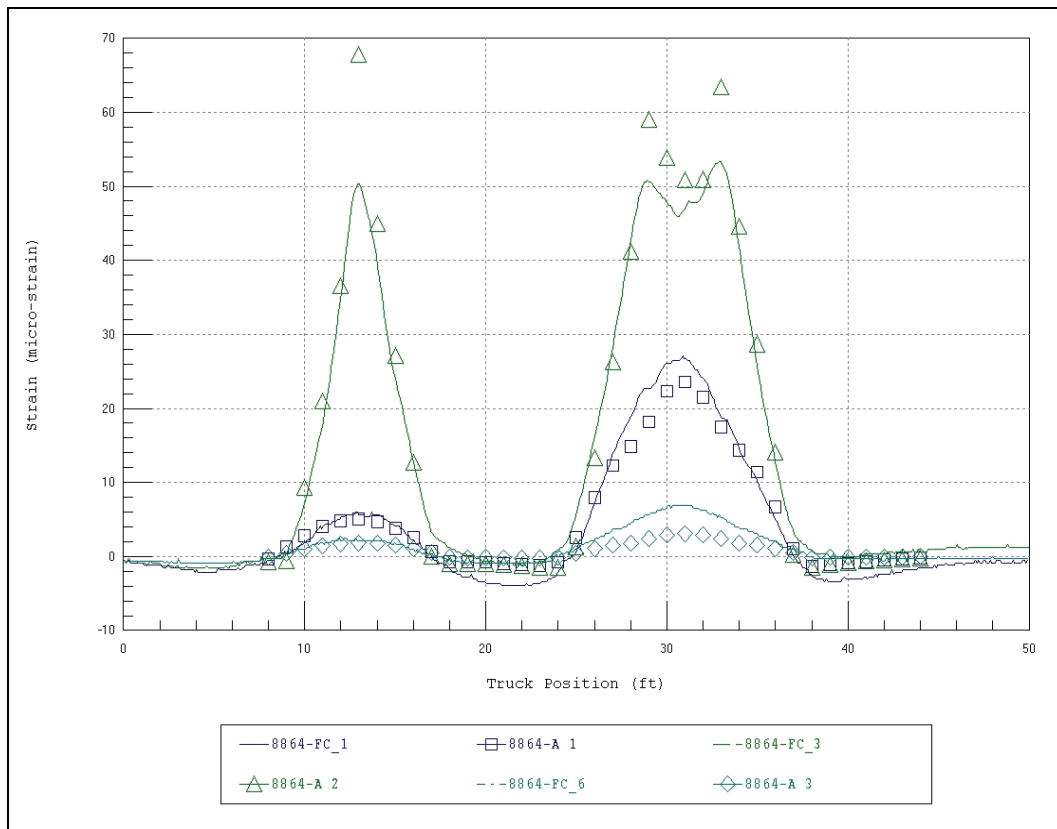


Figure 30. Midspan strain comparisons-three truck passes-Beam 3W.

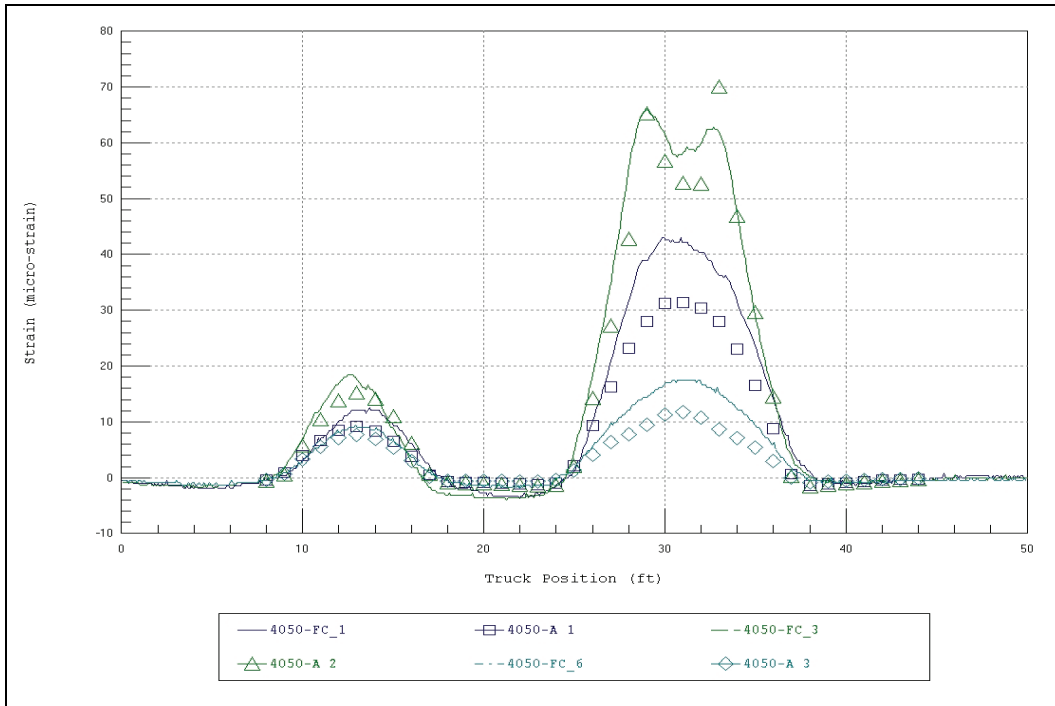


Figure 31. Midspan strain comparisons-three truck passes-Beam 4E.

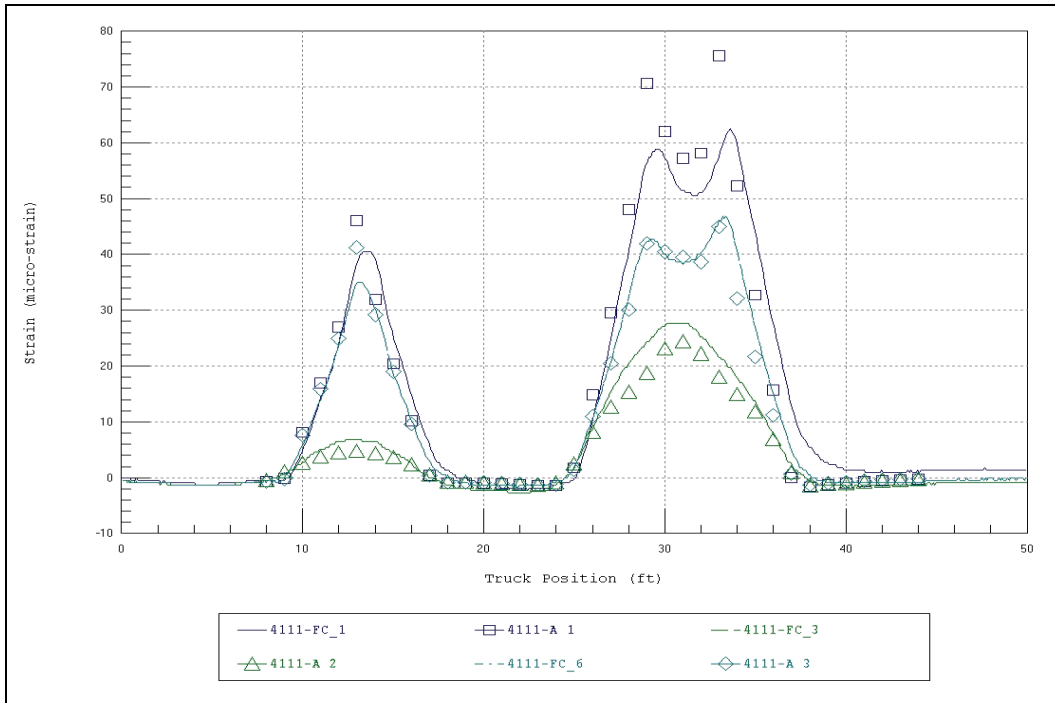


Figure 32. Midspan strain comparisons-three truck passes-Beam 4W.

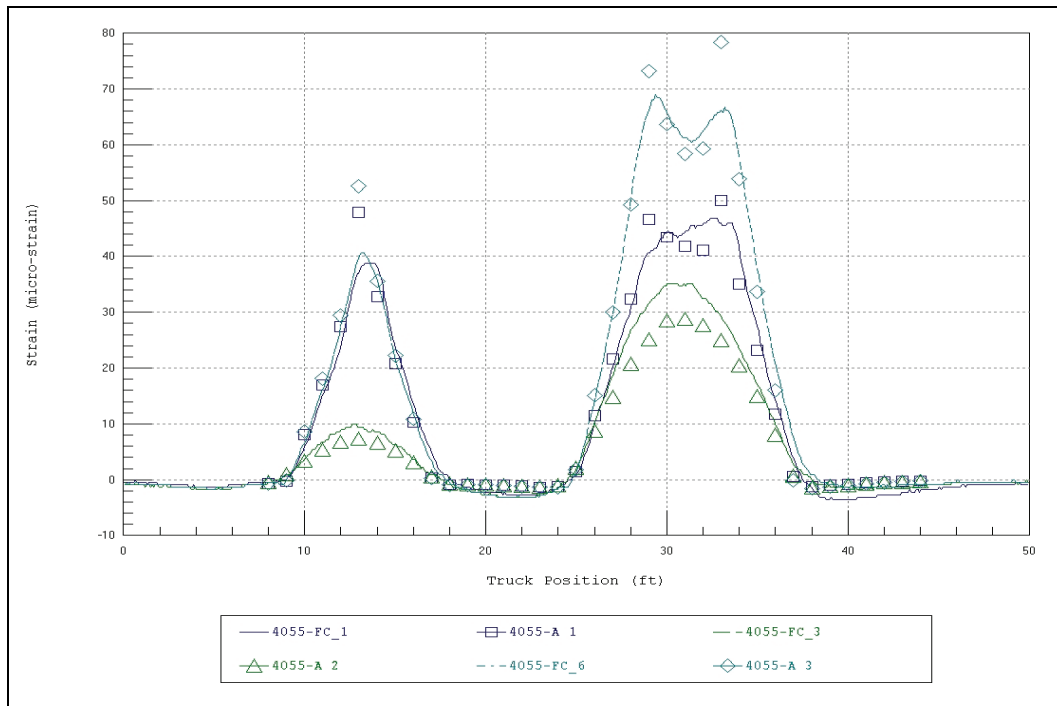


Figure 33. Midspan strain comparisons-three truck passes-Beam 5E.

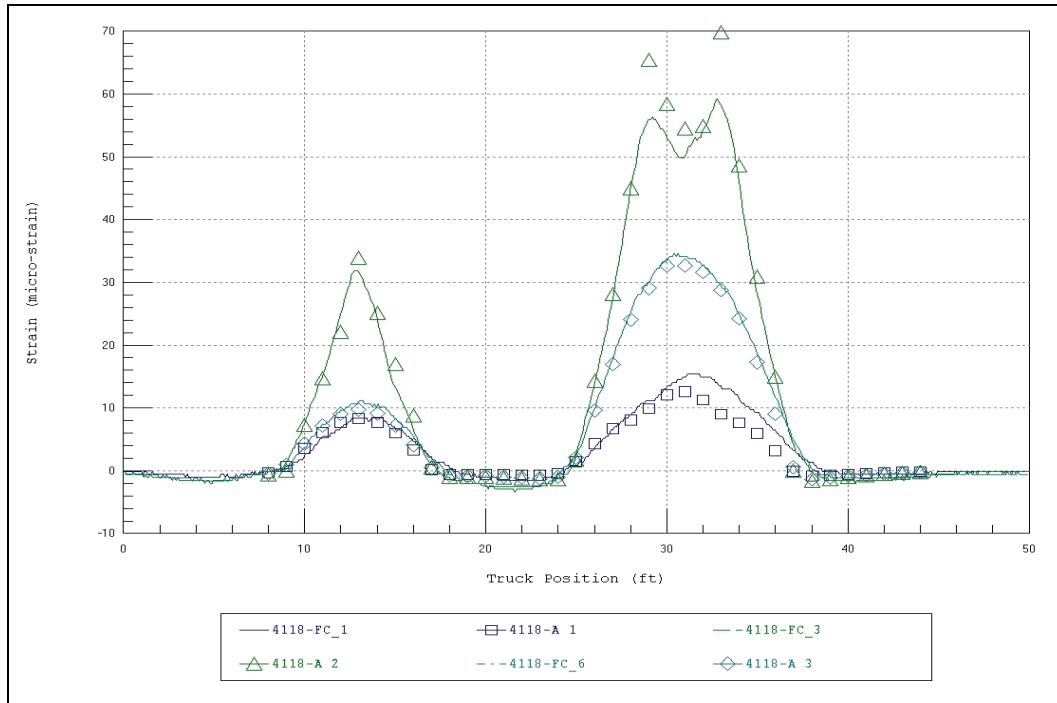


Figure 34. Midspan strain comparisons-three truck passes-Beam 5W.

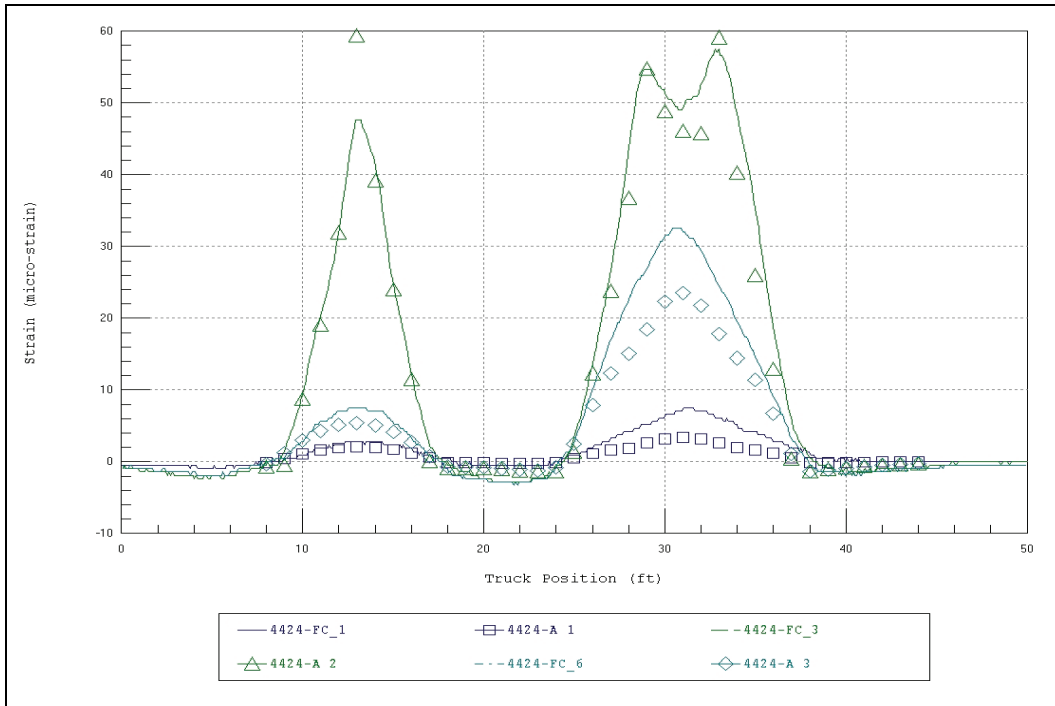


Figure 35. Midspan strain comparisons-three truck passes-Beam 6E.

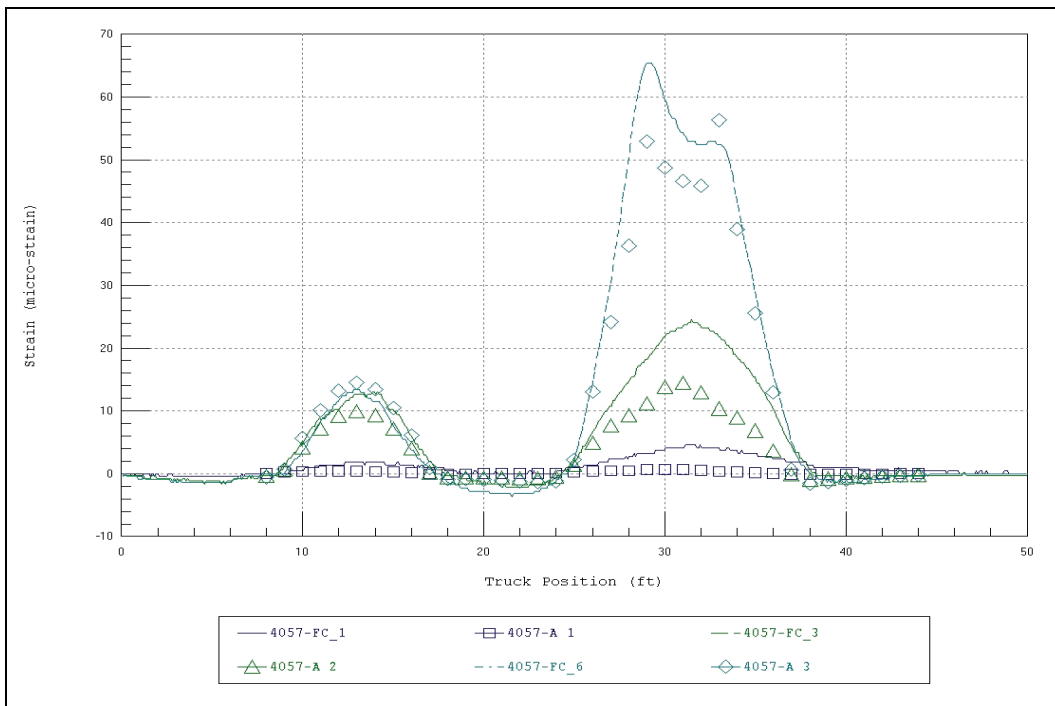


Figure 36. Midspan strain comparisons-three truck passes-Beam 6W.

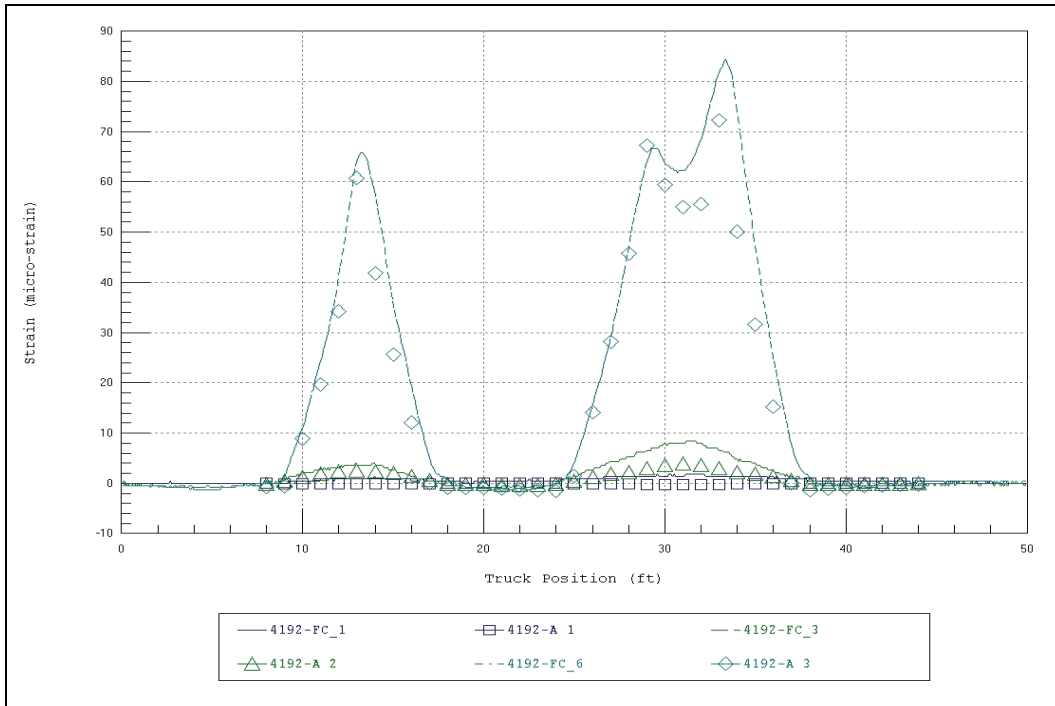


Figure 37. Midspan strain comparisons-three truck passes-Beam 7E.

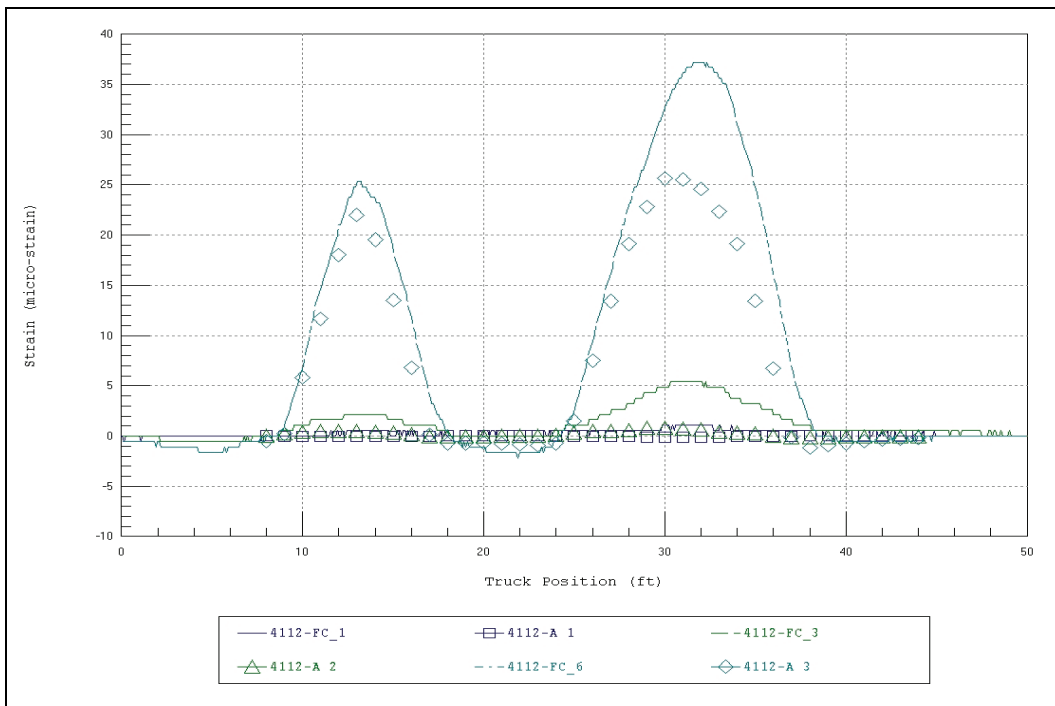


Figure 38. Midspan strain comparisons-three truck passes-Beam 7W.

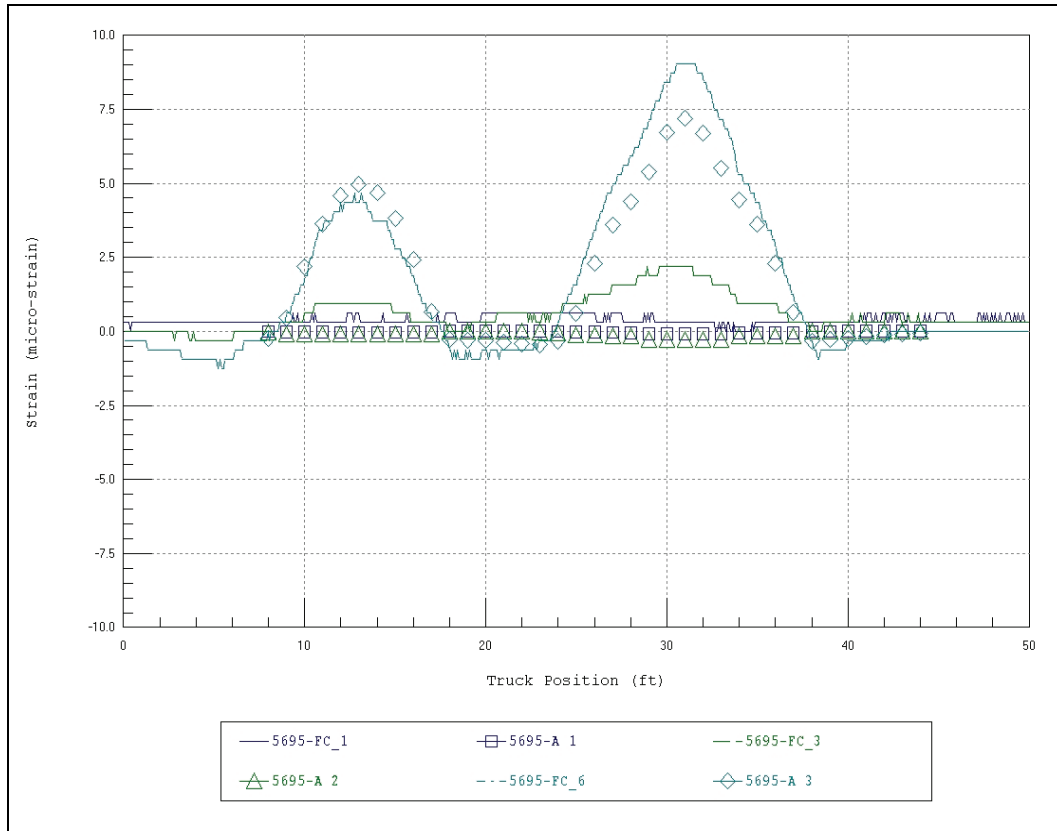


Figure 39. Midspan strain comparisons-three truck passes-Beam 8E.

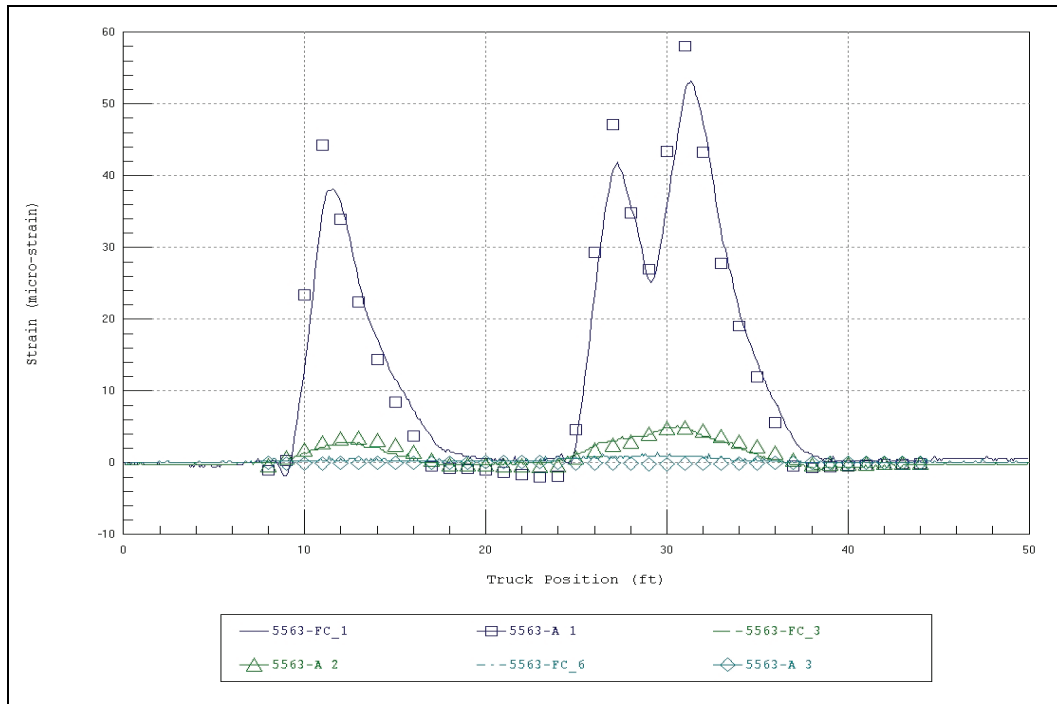


Figure 40. L/4 span strain comparisons-three truck passes-Beam 2W.



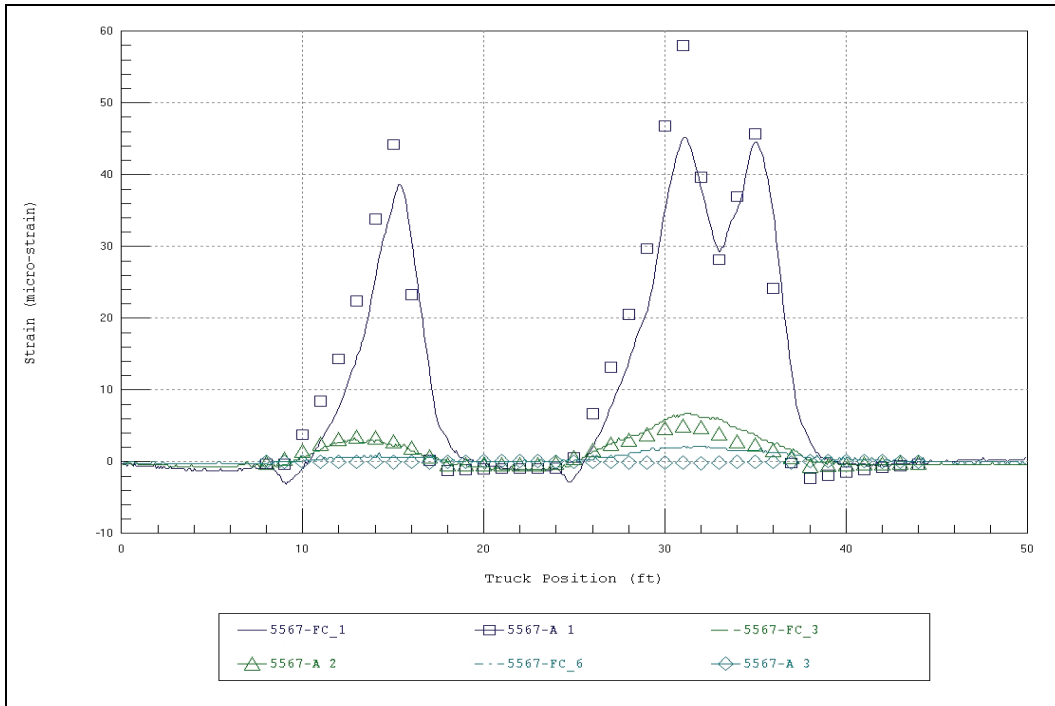


Figure 41. 3L/4 span strain comparisons-three truck passes-Beam 2W.

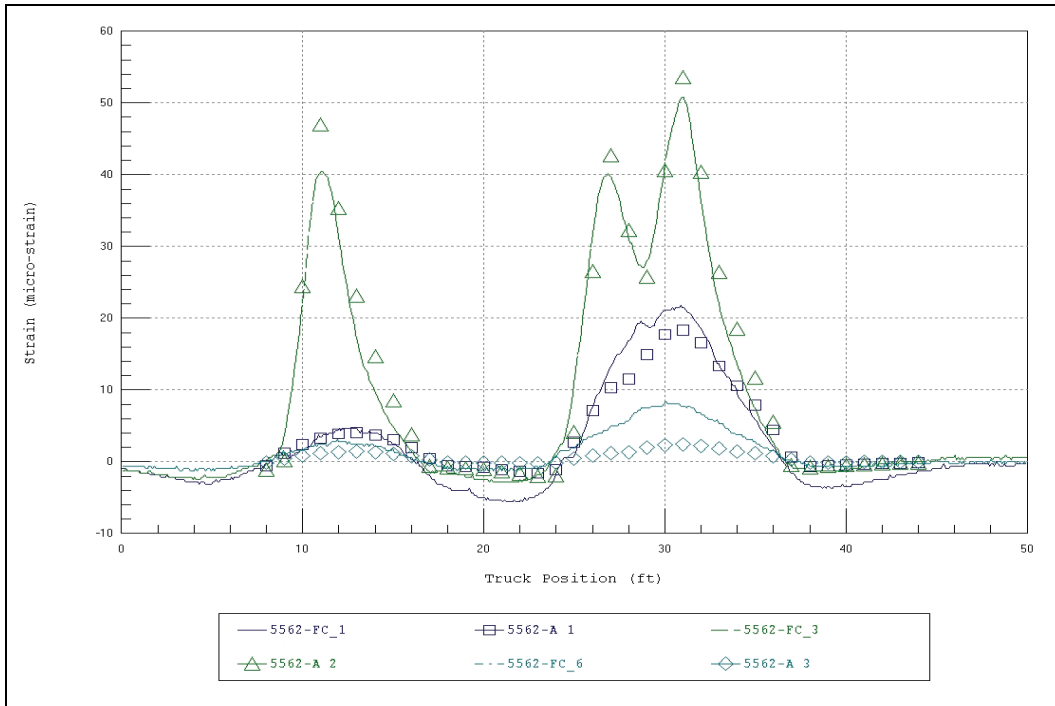


Figure 42. L/4 span strain comparisons-three truck passes-Beam 3E.

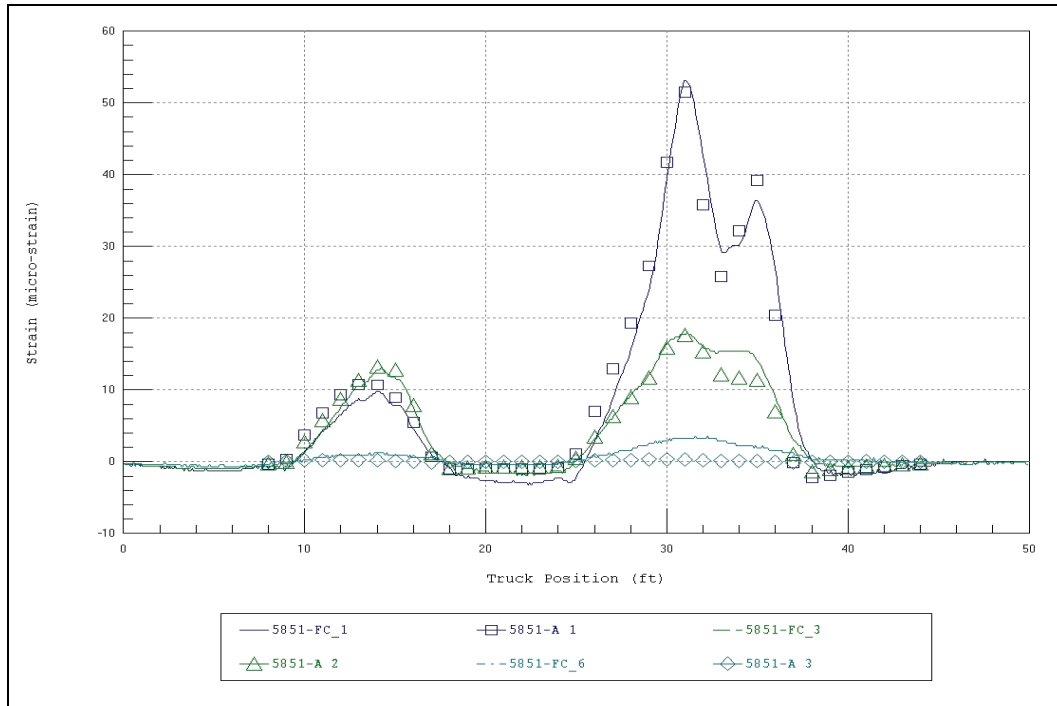


Figure 43. 3L/4 span strain comparisons-three truck passes-Beam 3E.

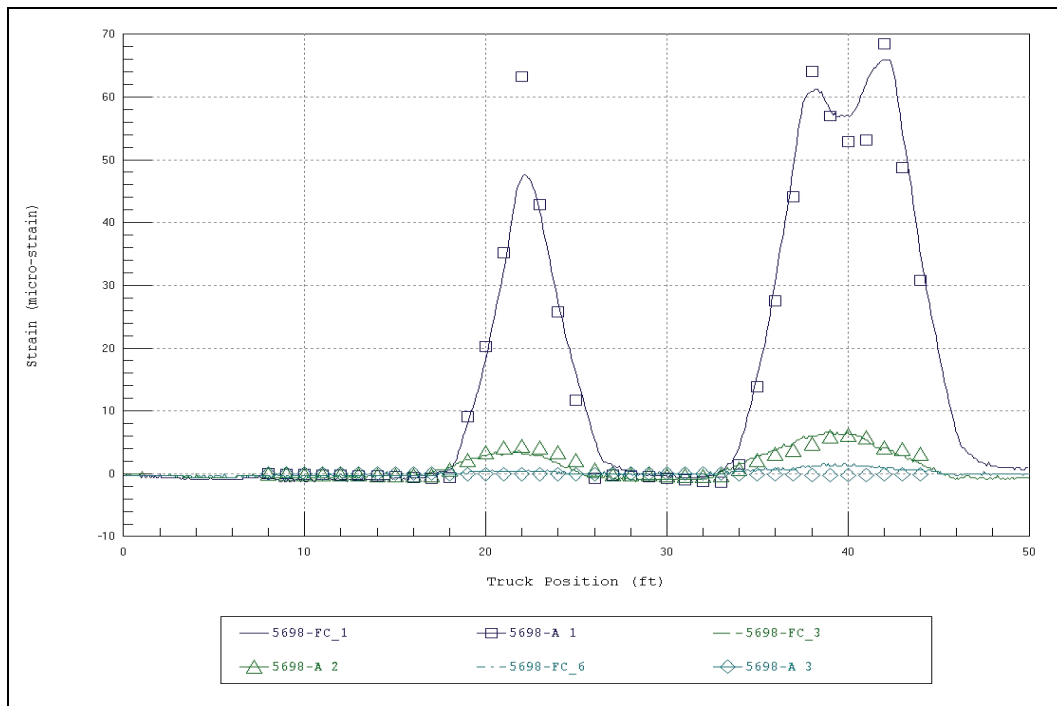


Figure 44. Midspan Span 4 strain comparisons-three truck passes-Beam 2W.

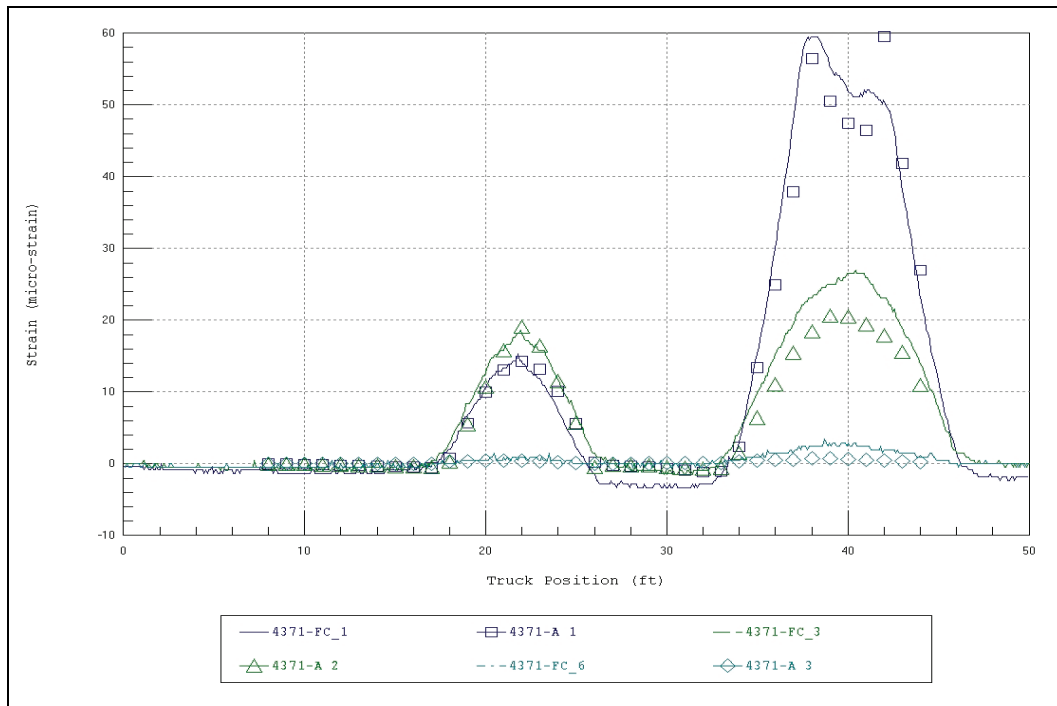


Figure 45. Midspan Span 4 strain comparisons-three truck passes-Beam 3E.

**RTCH DV43 cargo hauler test results**

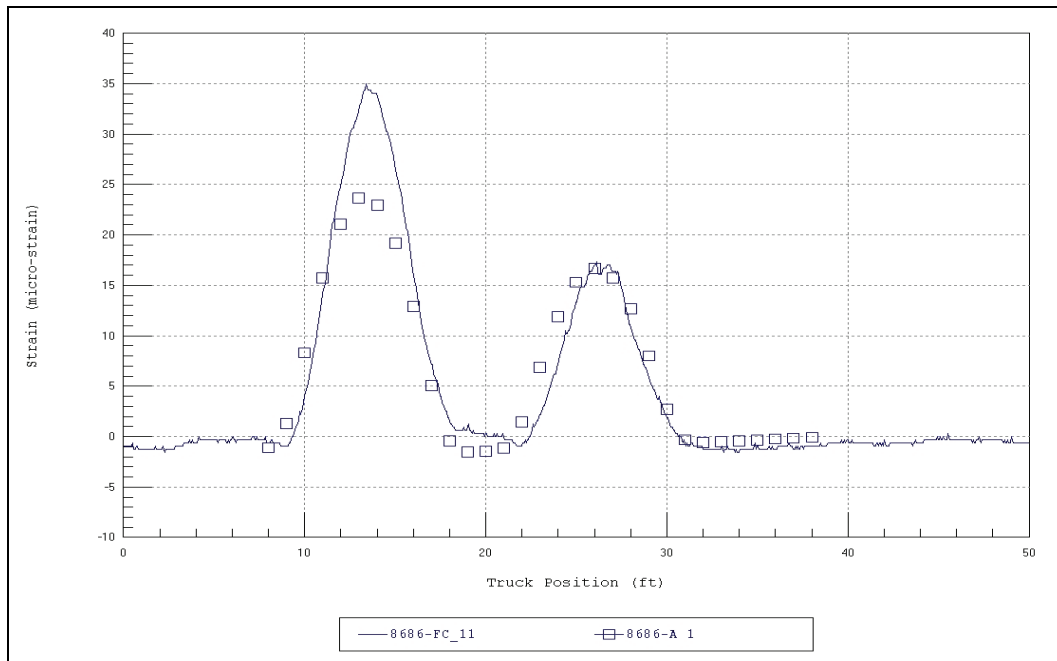


Figure 46. Midspan strain comparisons-RTCH DV43 crossing-Beam 2W.

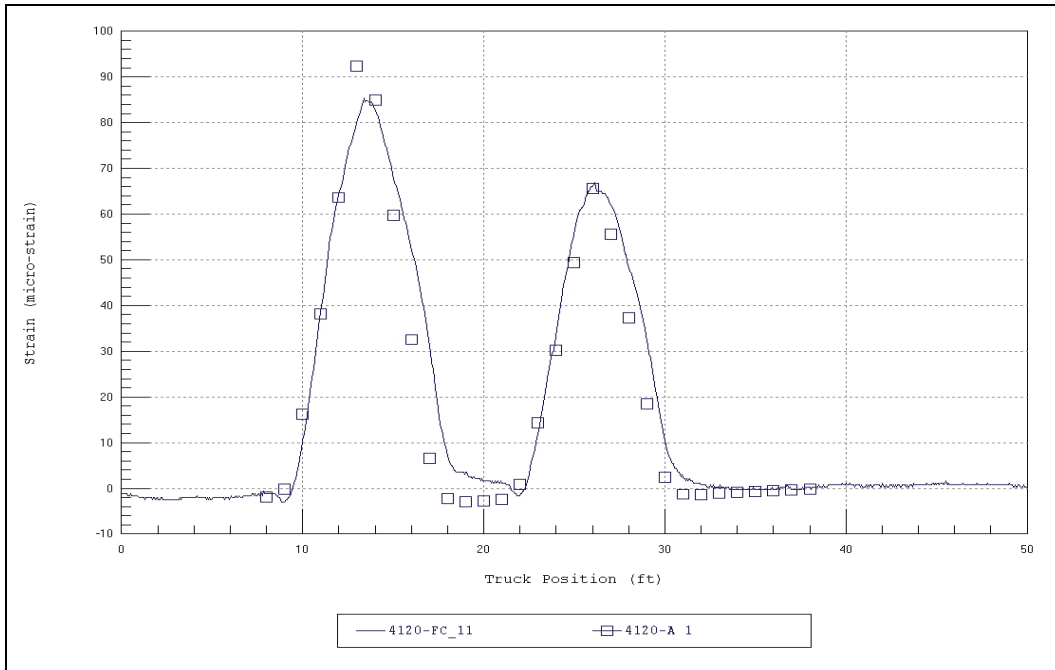


Figure 47. Midspan strain comparisons-RTCH DV43 crossing-Beam 3E.

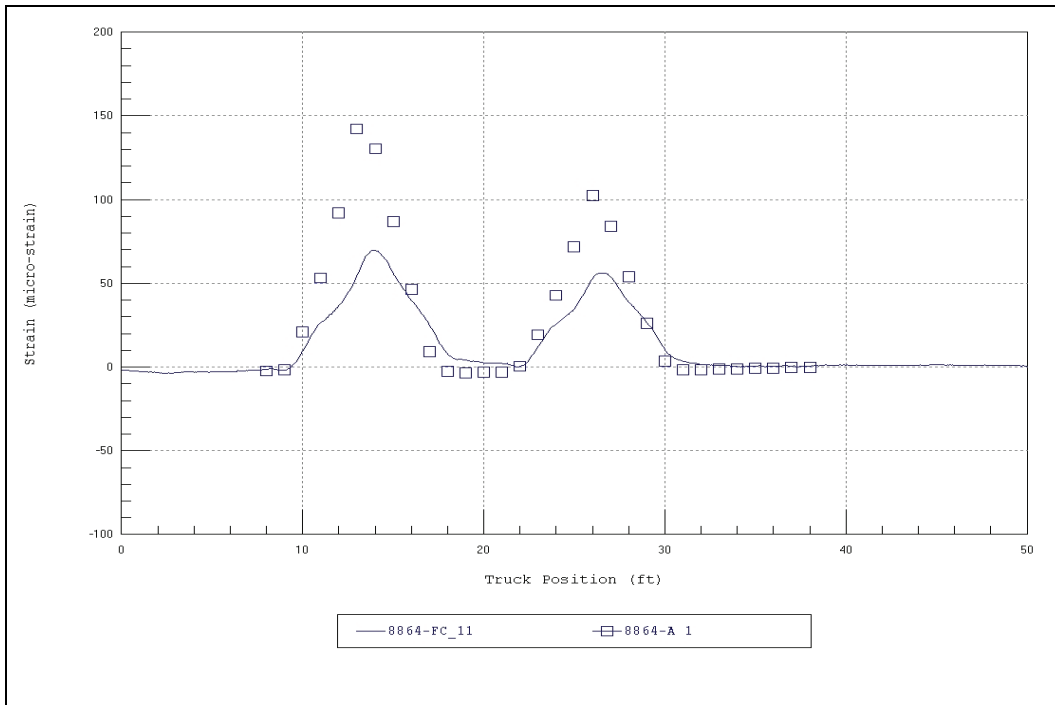


Figure 48. Midspan strain comparisons-RTCH DV43 crossing-Beam 3W.

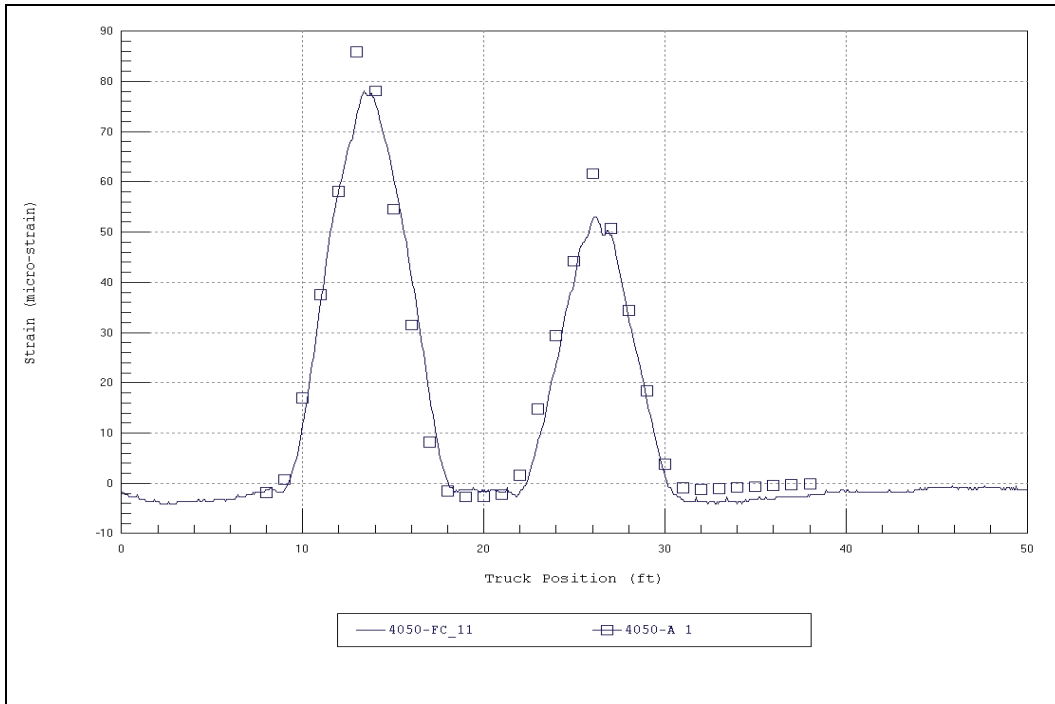


Figure 49. Midspan strain comparisons-RTCH DV43 crossing-Beam 4E.

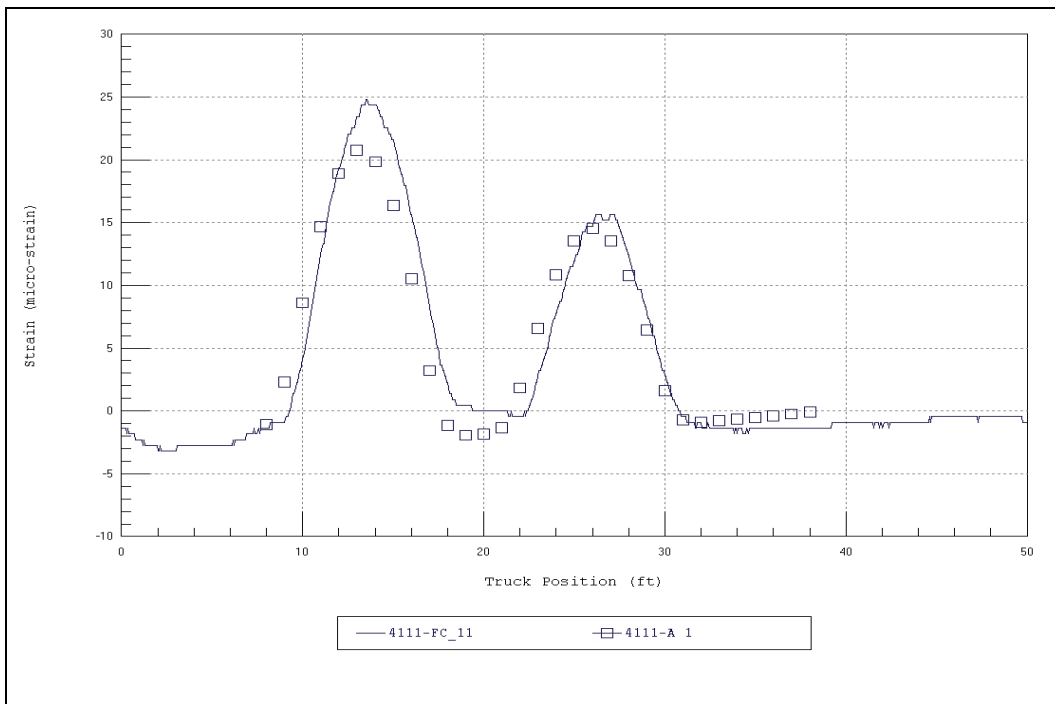


Figure 50. Midspan strain comparisons-RTCH DV43 crossing-Beam 4W.

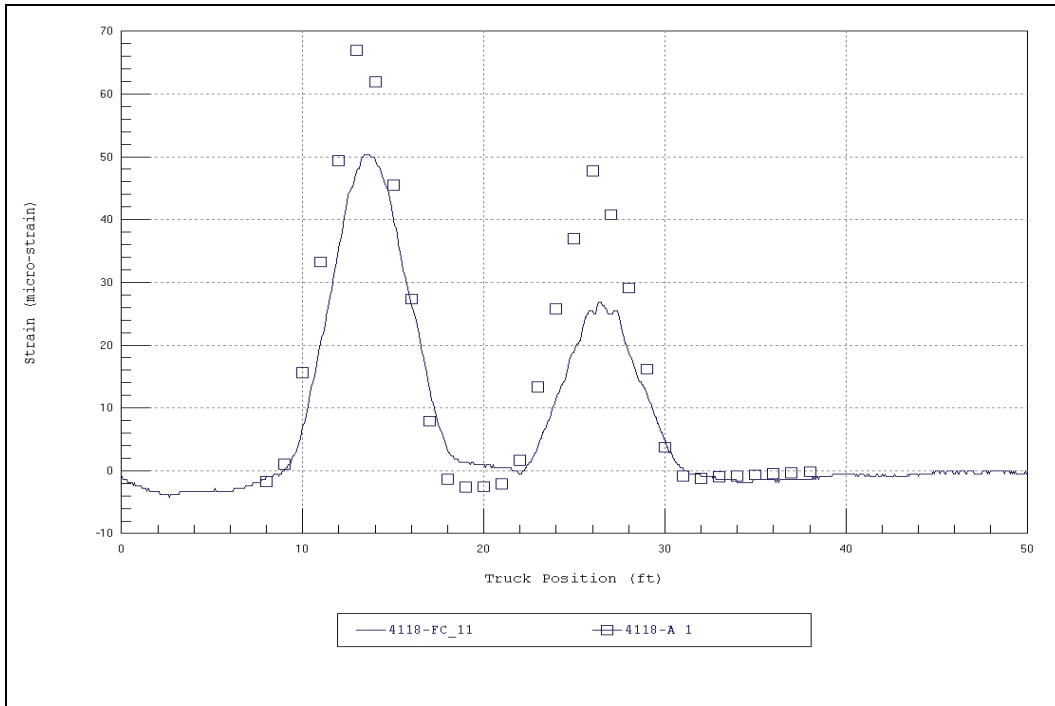


Figure 51. Midspan strain comparisons-RTCH DV43 crossing-Beam 5E.

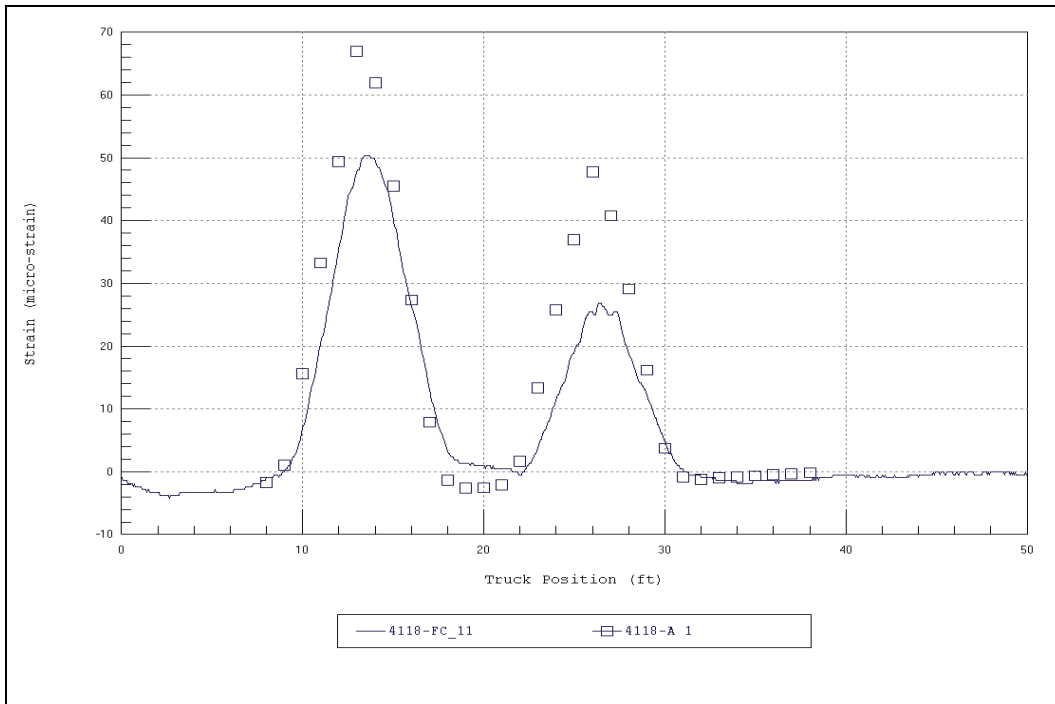


Figure 52. Midspan strain comparisons-RTCH DV43 crossing-Beam 5W.

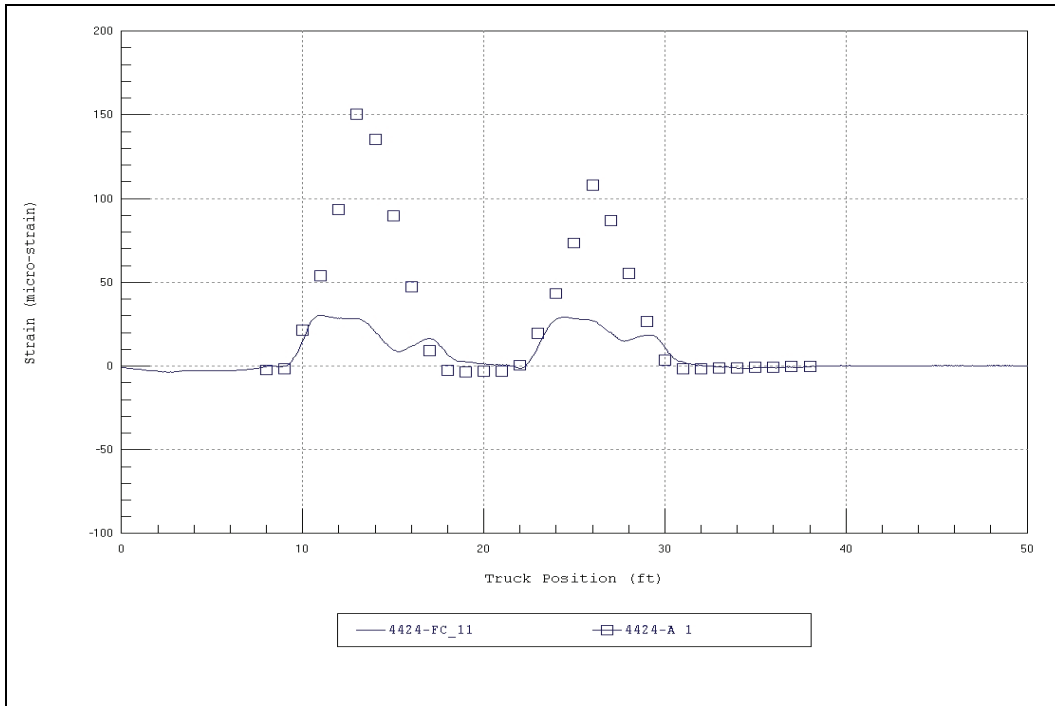


Figure 53. Midspan strain comparisons-RTCH DV43 crossing-Beam 6E.

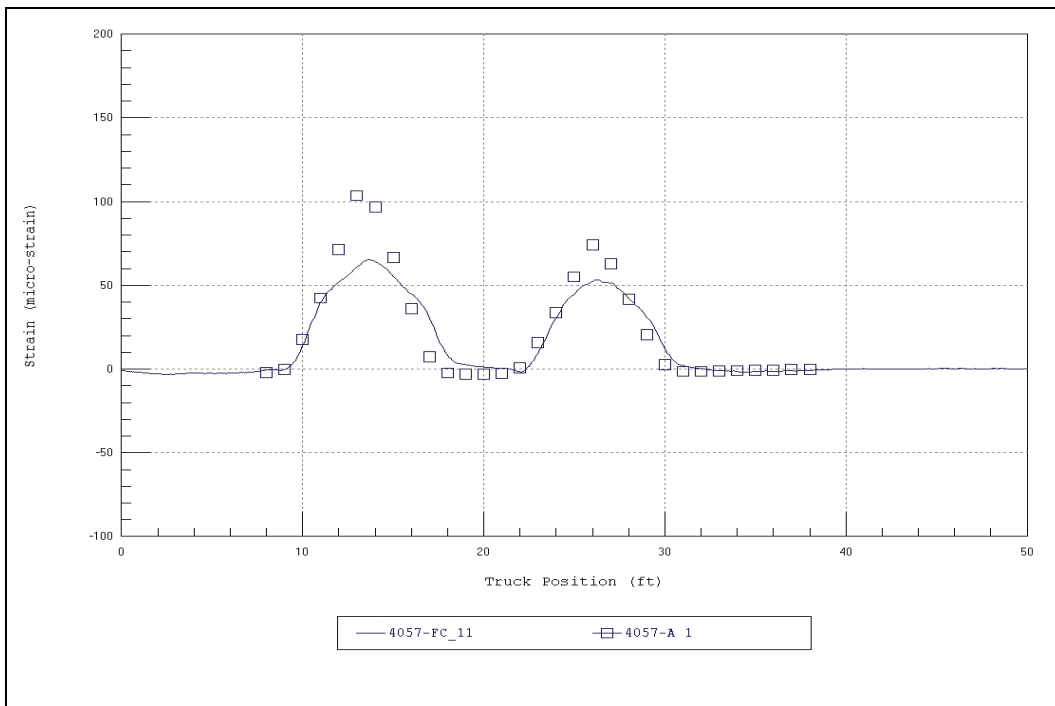


Figure 54. Midspan strain comparisons-RTCH DV43 crossing-Beam 6W.

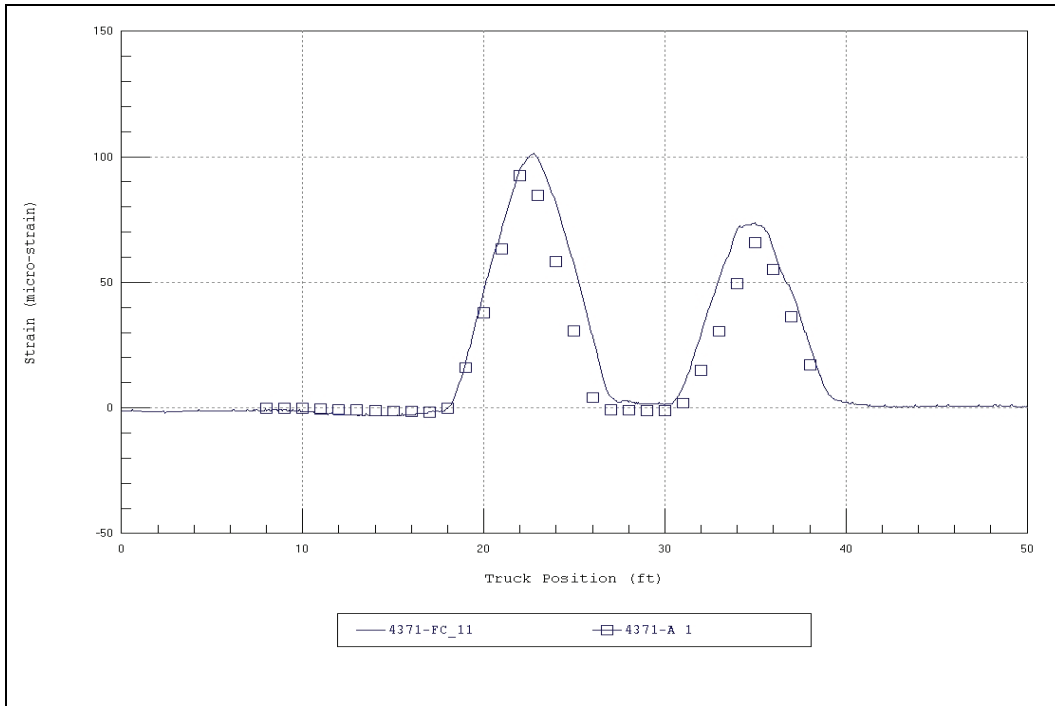


Figure 55. Midspan strain comparisons-RTCH DV43 crossing-Beam 3E.

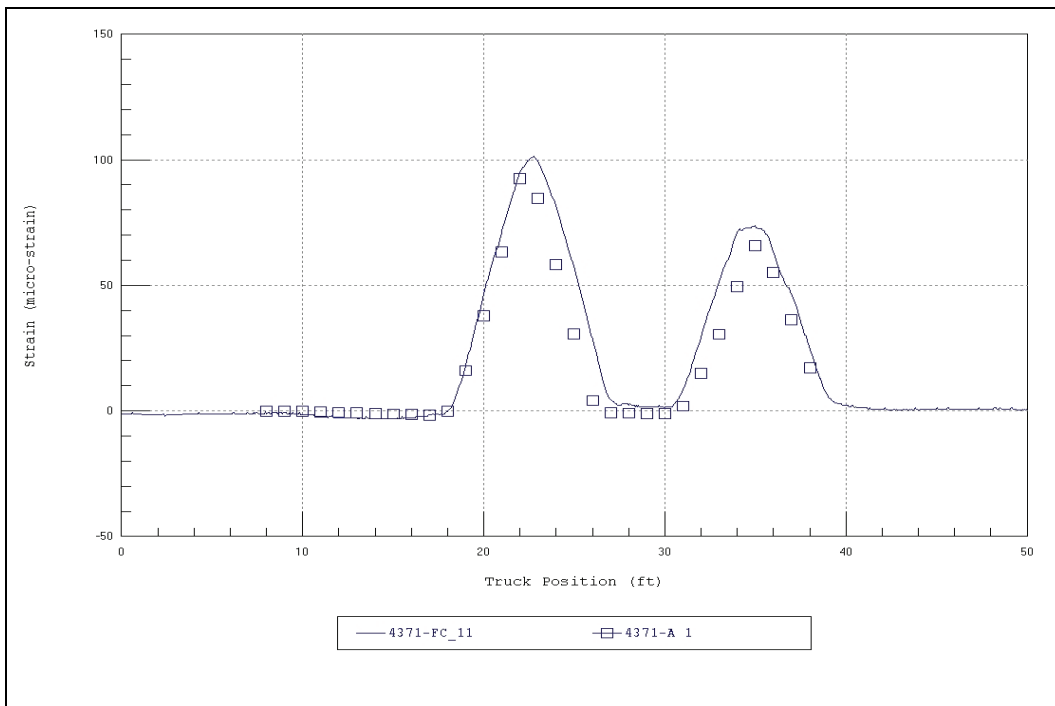


Figure 56. Midspan Span 4 strain comparisons-RTCH DV43 crossing-Beam 3E.



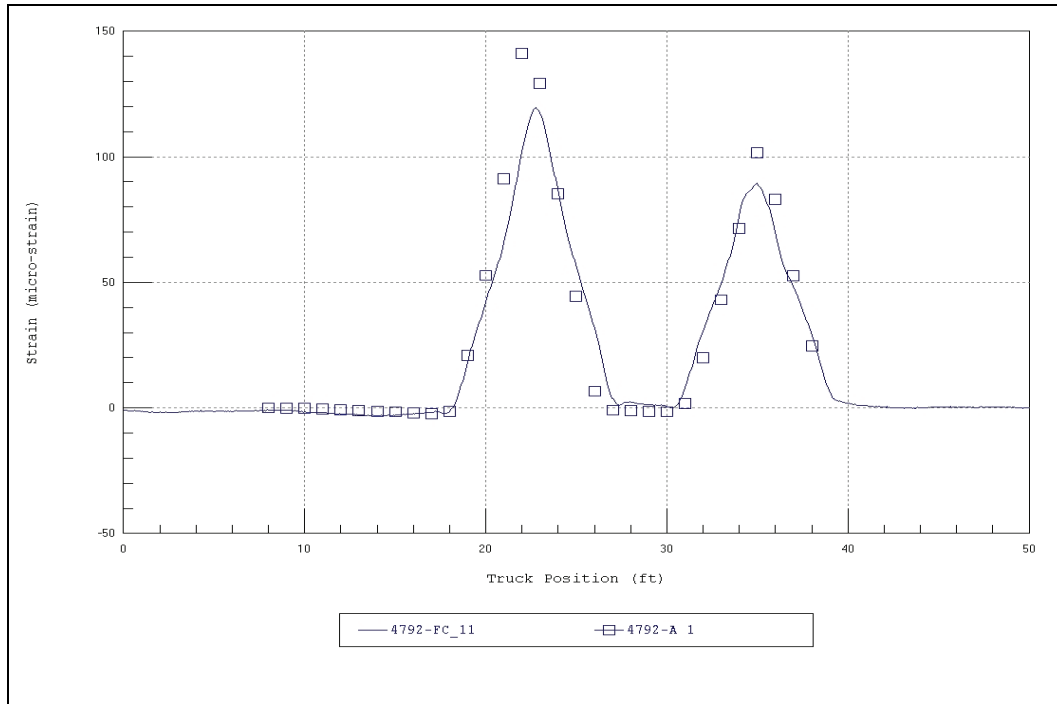


Figure 57. Midspan Span 4 strain comparisons-RTCH DV43 crossing-Beam 3W.

### HETS-M1A1 test results

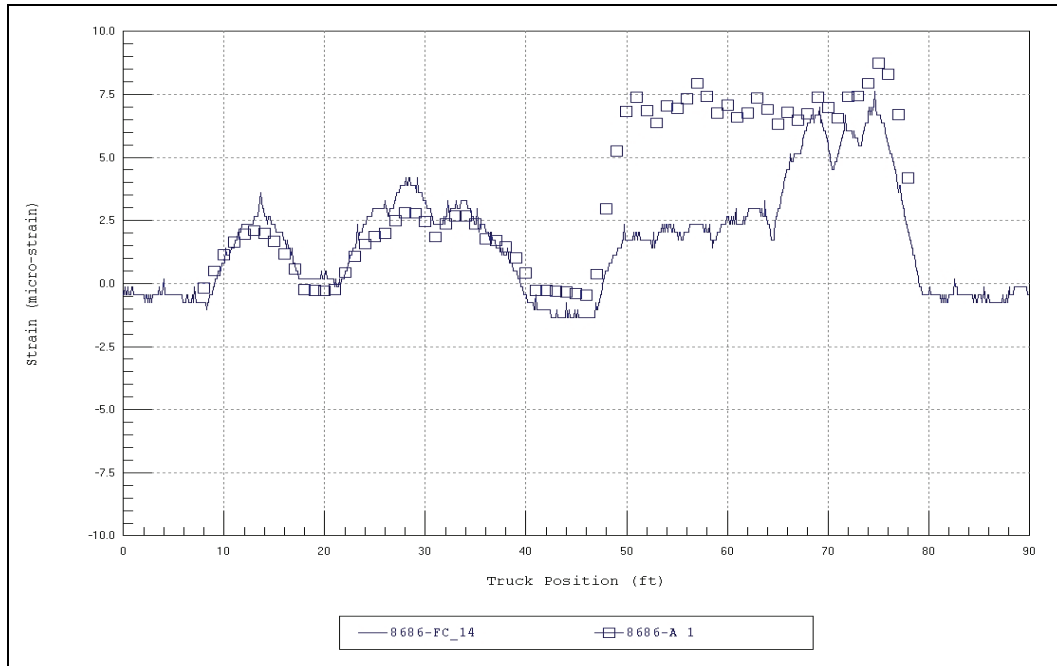


Figure 58. Midspan strain comparisons-HETS-M1A1 crossing-Beam 2W.

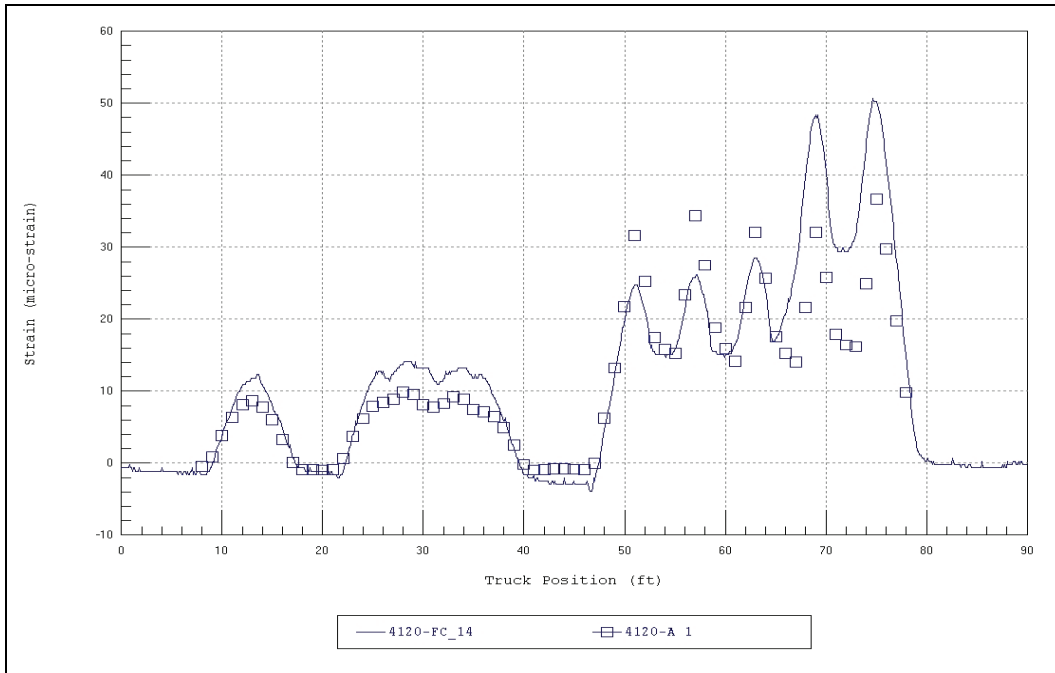


Figure 59. Midspan strain comparisons-HETS-M1A1 crossing-Beam 3E.

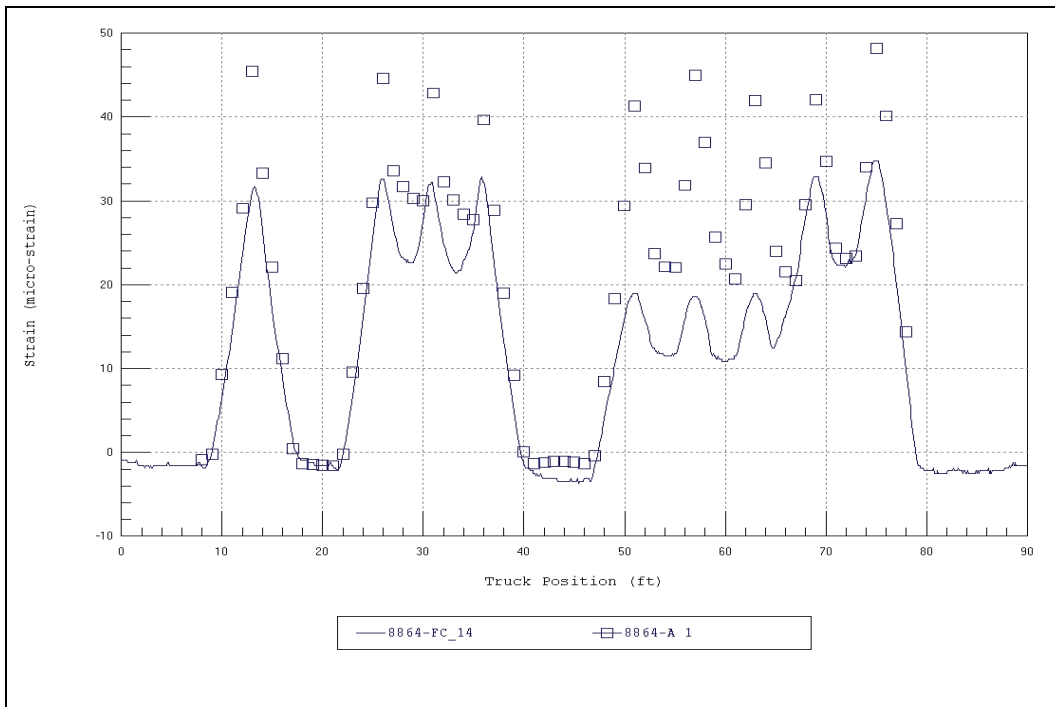


Figure 60. Midspan strain comparisons-HETS-M1A1 crossing-Beam 3W.

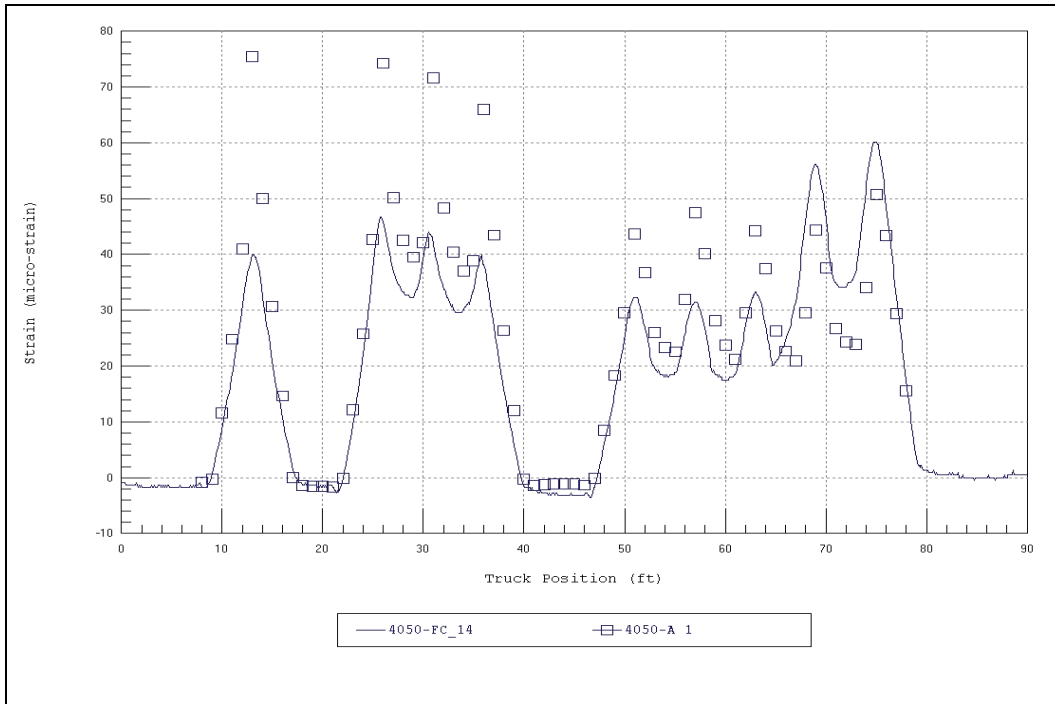


Figure 61. Midspan strain comparisons-HETS-M1A1 crossing-Beam 4E.

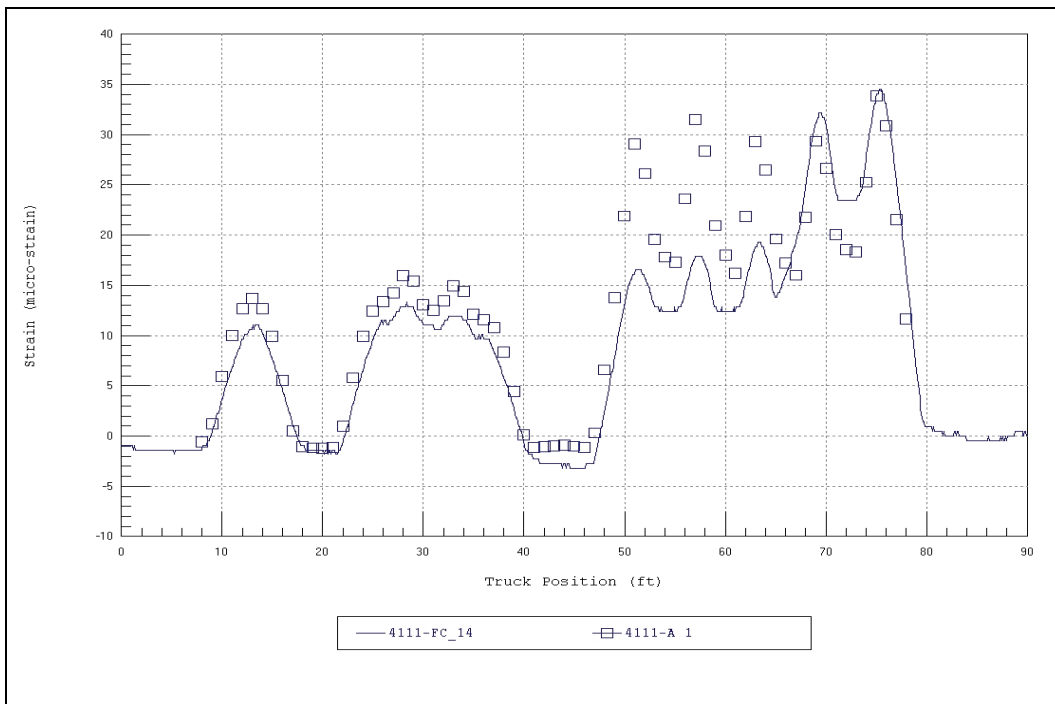


Figure 62. Midspan strain comparisons-HETS-M1A1 crossing-Beam 4W.

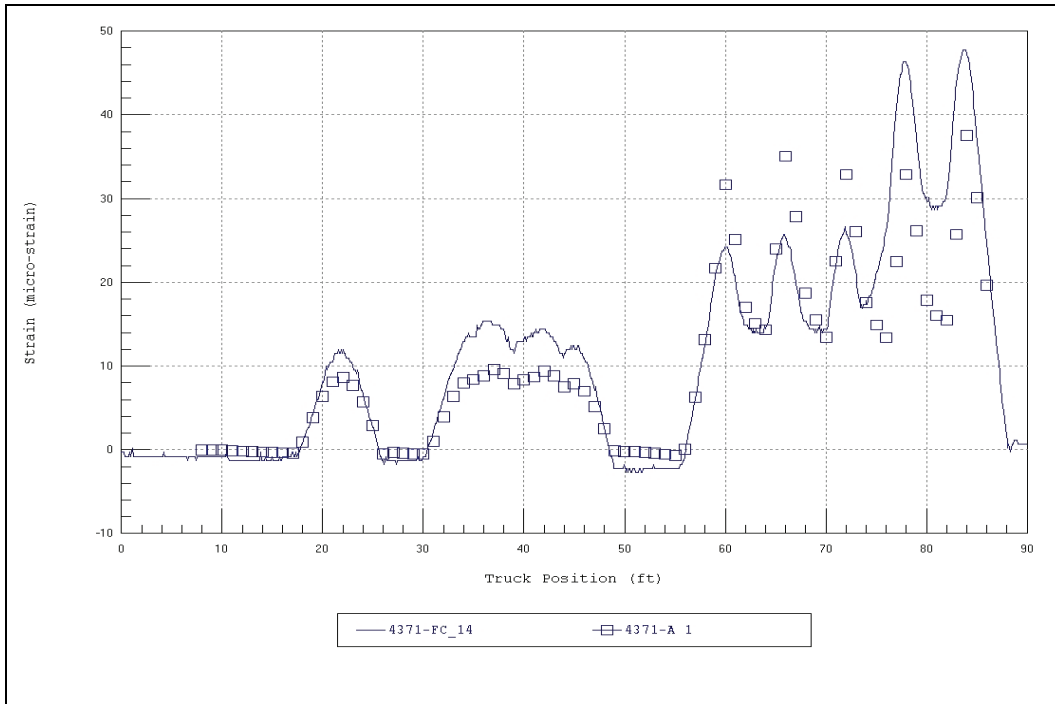


Figure 63. Midspan Span 4 strain comparisons–HETS-M1A1 crossing–Beam 3E.

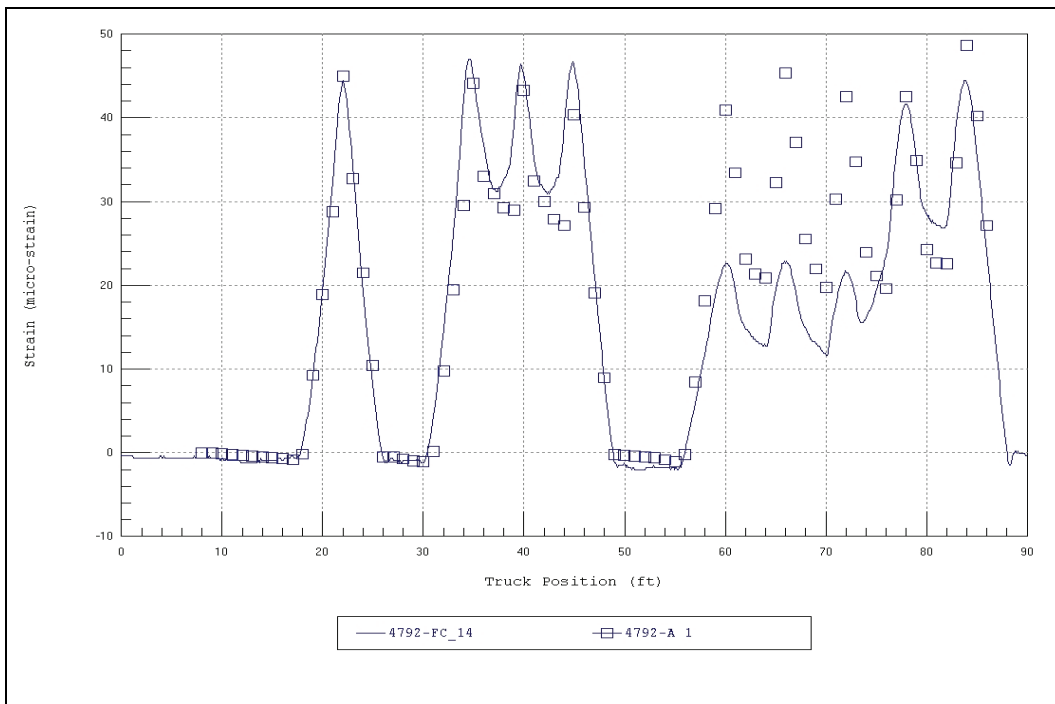


Figure 64. Midspan Span 4 strain comparisons–HETS-M1A1 crossing–Beam 3W.

## Appendix A: Field-Testing Procedures

The motivation for developing a relatively easy-to-implement field-testing system was to allow short and medium span bridges to be tested on a routine basis. Original development of the hardware was started in 1988 at the University of Colorado under a contract with the Pennsylvania Department of Transportation (PennDOT). Subsequent to that project, the Integrated Technique was refined on another study funded by the Federal Highway Administration (FHWA) in which 35 bridges located on the Interstate system throughout the country were tested and evaluated. Further refinement has been implemented over the last several years through testing and evaluating several more bridges, lock gates, and other structures.

The key to being able to complete the field-testing quickly is the use of strain transducers (rather than standard foil strain gages) that can be attached to the structural members in just a few minutes. These sensors were originally developed for monitoring dynamic strains on foundation piles during the driving process. They have been adapted for use in structural testing through special modifications, and have 3 to 4% accuracy, and are periodically recalibrated to NIST (National Institute of Standards and Technology) standards.

In addition to the strain sensors, the data acquisition hardware has been designed specifically for field use through the use of rugged cables and military-style connectors. This allows quick assembly of the system and keeps bookkeeping to a minimum. The analog-to-digital converter (A/D) is an off-the-shelf unit, but all signal conditioning, amplification, and balancing hardware have been specially designed for structural testing. The test software has been written to allow easy configuration (test length, etc.) and operation. The result is a system that can be used by people other than computer experts or electrical engineers. Other enhancements include the use of an automatic remote-control position indicator. The AutoClicker, a device that electronically counts wheel revolutions, is mounted on the test vehicle over one of the wheels. As the test vehicle crosses the structure along the preset path, a communication radio sends a signal to the strain measurement system that receives it and puts a mark

in the data. This allows the field strains to be compared to analytical strains as a function of vehicle position, not only as a function of time.

The use of a moving load as opposed to placing the truck at discrete locations has two major benefits. First, the testing can be completed much quicker, meaning there is less impact on traffic. Second, and more importantly, much more information can be obtained (both quantitative and qualitative). Also, normal operating conditions are better represented. Discontinuities or unusual responses in the strain histories, which are often signs of distress, can be easily detected. Since the load position is monitored as well, it is easy to determine what loading conditions cause the observed effects. If readings are recorded only at discrete truck locations, the risk of losing information between the points is great. The advantages of continuous readings have been proven repeatedly.

The following list of procedures has been reproduced from the BDI Structural Testing System (STS) Operation Manual. This outline is intended to describe the general procedures used for completing a successful field test on a highway bridge using the BDI-STS. Other types of structures can be tested as well with only slight deviations from the directions given here.

Once a tentative instrumentation plan has been developed for the structure in question, the strain transducers must be attached and the STS prepared for running the test.

### **Attaching strain transducers**

There are two methods for attaching the strain transducers to the structural members: C-clamping or using tabs and adhesive. For steel structures, quite often the transducers can be clamped directly to the steel flanges of rolled sections or plate girders. If significant lateral bending is assumed to be present, then one transducer may be clamped to each edge of the flange. If the transducer is to be clamped, ensure that the clamp is centered over the mounting holes. In general, the transducers can be clamped directly to painted surfaces. However, if the surface that is being clamped is rough or has very thick paint, it should first be cleaned with a grinder. The alternative to clamping is the tab attachment method outlined below.

1. Place two tabs in mounting jig. Place transducer over mounts and tighten the 1/4-20 nuts until they are snug (approximately 50 in.-lb.). This procedure allows the tabs to be mounted without putting stress on the transducer itself. When attaching transducers to R/C members, transducer extensions are used to obtain a longer gage length. In this case the extension is bolted to one end of the transducer, and the tabs are bolted to the free ends of the transducer and the extension.
2. Mark the center line of the transducer location on the structure. Place marks 1-1/2 in. on either side of the center line and using a hand grinder, remove paint or scale from these areas. If attaching to concrete, lightly grind the surface to remove any scale. If the paint is quite thick, use a chisel to remove most of it before grinding.
3. Very lightly grind the bottom of the transducer tabs to remove any oxidation or other contaminants.
4. Apply a thin line of adhesive to the bottom of each transducer tab.
5. Spray each tab and the contact area on the structural member with the adhesive accelerator.
6. Mount transducer in its proper location and apply a light force to the tabs (not the center of the transducer) for approximately 10 sec.

If the above steps are followed, it should be possible to mount each transducer in approximately 5 min. When the test is complete, carefully loosen the 1/4-20 nuts from the tabs and remove transducer. If one is not careful, the tab will pop loose from the structure and the transducer may be damaged. Use vice grips to remove the tabs from the structure.

### **Assembly of system**

Once the transducers have been mounted, they should be connected into an STS unit. The STS units should be placed near the transducer locations in such a manner to allow four transducers to be plugged in. Each STS unit can be easily clamped to the bridge girders. If the structure is concrete and no flanges are available to set the STS units on, transducer tabs glued to the structure and plastic zip-ties or small wire can be used to hold them up. Since the transducers will identify themselves to the system, there is no special order that they must follow. The only information that must be recorded is the transducer serial number and its location on the structure. Large cables are provided which can be connected between the STS units. The maximum length between STS units is 50 ft (15 m). If several gages are in close proximity to each other, then the STS units can be plugged

directly to each other without the use of a cable. All connectors will "click" when the connection has been completed properly.

Once all of the STS units have been connected in series, one cable must be run and connected to the power supply located near the PC. Connect the 9-pin serial cable between the computer and the power supply. The position indicator is then assembled and the system connected to a power source (either 12 volts DC or 120-240 volts AC). The system is now ready to acquire data.

## Performing load test

The general testing sequence is as follows:

1. Transducers are mounted, and the system is connected together and turned on.
2. The deck is marked out for each truck pass. Locate the point on the deck directly above the first bearing for one of the fascia beams. If the bridge is skewed, the first point encountered from the direction of travel is used and an imaginary line extended across and normal to the roadway. All tests are started from this line. In order to track the position of the loading vehicle on the bridge during the test, an X-Y coordinate system, with the origin at the selected reference point is laid out.

In addition to monitoring the longitudinal position, the vehicle's transverse position must be known. The transverse truck position is kept uniform by first aligning the truck in the center of the lane where it would normally travel at highway speed. Next, a chalk mark is made on the deck locating the transverse location of the driver's side front wheel. By making a measurement from this mark to the reference point, the transverse ("Y") position of the truck is always known. The truck is aligned on this mark for all subsequent tests in this lane. For two lane bridges with shoulders, tests are run on the shoulder (driver's side front wheel along the white line) and in the center of each lane. If the bridge has only two lanes and very little shoulder, tests are run in the center of each lane only. If the purpose of the test is to calibrate a computer model, it is sometimes more convenient to simply use the lane lines as guides because it is easier for the driver to maintain a constant lateral position. Responses due to critical truck positions are then obtained by the analysis.



The driver is instructed that the test vehicle must be kept in the proper location on the bridge. For example, the left front wheel needs to be kept on the white line for the shoulder tests. Another important item is that the vehicles maintain a relatively constant rate of speed during the entire test. The process of converting data to a function of truck position assumes constant speed between each click mark.

Two more pieces of information are then needed: the axle weights and dimensions of the test vehicle. The driver generally provides the axle weights, after stopping at a local scale. However, a weight enforcement team can use portable scales and weigh the truck at the bridge site. Wheelbase and axle width dimensions are made with a tape measure and recorded.

3. The program is started and the number of channels indicated is verified. If the number of channels indicated does not match the number of channels actually there, a malfunction has occurred and must be corrected before testing commences.
4. The transducers are initialized (zeroed out) with the Balance option. If a transducer cannot be initialized, it should be inspected to ensure that it has not been damaged.
5. The desired test length, sample rate, and output file name are selected. In general, a longer test time than the actual event is selected. For most bridge tests, a 1- or 2-minute test length will suffice because the test can be stopped as soon as the truck crosses completely over the structure.
6. To facilitate presenting data as a function of load position, rather than time, two items describing the Position Indicator (PI) information must be defined. The starting position and PI interval distance allow the data to be plotted using position coordinates that are consistent with a numeric analysis. The starting position refers to the longitudinal position of the load vehicle in the model coordinate system when the data recording is started. The interval distance is the circumference of the tire that is being used by the AutoClicker. It is important that this information be clearly defined in the field notes.
7. If desired, the Monitor option can be used to verify transducer output during a trial test. Also, it is useful to run a PI test while in Monitor to ensure that the clicks are being received properly.
8. When all parties are ready to commence the test, the Run Test option is selected which places the system in an activated state. The AutoClicker is positioned so that the first click occurs at the starting line. This first click starts the test. The AutoClicker puts one mark in the data for every wheel revolution. An effort should be made to get the truck across with no other

traffic on the bridge. There should be no talking over the radios during the test, as a "position" will be recorded each time the microphones are activated.

9. When the test has been completed, and the system is still recording data, hit "S" to stop collecting data and finish writing the recorded data to disk. If the data files are large, they can be compressed and copied to floppy disk.
10. It is important to record the field notes very carefully. Having data without knowing where they were recorded can be worse than having no data at all. Transducer location and serial numbers must be recorded accurately. All future data handling in BDI-GRF is accomplished by keying on the transducer number. This system has been designed to eliminate the need to track channel numbers by keeping this process in the background. However, the STS unit and the transducer's connector number are recorded in the data file if needed for future hardware evaluations.

## **Appendix B: Modeling and Analysis— The Integrated Approach**

### **Introduction**

In order for load testing to be a practical means of evaluating short- to medium-span bridges, it is apparent that testing procedures must be economical to implement in the field and the test results translatable into a load rating. A well-defined set of procedures must exist for the field applications as well as for the interpretation of results. An evaluation approach based on these requirements was first developed at the University of Colorado during a research project sponsored by the Pennsylvania Department of Transportation (PennDOT). Over several years, the techniques originating from this project have been refined and expanded into a complete bridge rating system.

The ultimate goal of the Integrated Approach is to obtain realistic rating values for highway bridges in a cost effective manner. This is accomplished by measuring the response behavior of the bridge due to a known load and determining the structural parameters that produce the measured responses. With the availability of field measurements, many structural parameters in the analytical model can be evaluated that are otherwise conservatively estimated or ignored entirely. Items that can be quantified through this procedure include the effects of structural geometry, effective beam stiffness, realistic support conditions, effects of parapets and other nonstructural components, lateral load transfer capabilities of the deck and transverse members, and the effects of damage or deterioration. Often, bridges are rated poorly because of inaccurate representations of the structural geometry or because the material and/or cross-sectional properties of main structural elements are not well defined. A realistic rating can be obtained, however, when all of the relevant structural parameters are defined and implemented in the analysis process.

One of the most important phases of this approach is a qualitative evaluation of the raw field data. Much is learned during this step to aid in the rapid development of a representative model.

## Initial data evaluation

The first step in structural evaluation consists of a visual inspection of the data in the form of graphic response histories. Graphic software was developed to display the raw strain data in various forms. Strain histories can be viewed in terms of time or truck position. Since strain transducers are typically placed in pairs, neutral axis measurements, curvature responses, and strain averages can also be viewed. Linearity between the responses and load magnitude can be indicated by the continuity in the strain histories. Consistency in the neutral axis measurements from beam to beam and as a function of load position provides great insight into the nature of the bridge condition. The direction and relative magnitudes of flexural responses along a beam line are useful in determining if end restraints play a significant role in the response behavior. In general, the initial data inspection provides the engineer with information concerning modeling requirements and can help locate damaged areas.

Having strain measurements at two depths on each beam cross section, flexural curvature and the location of the neutral axis can be computed directly from the field data. Figure B1 illustrates how curvature and neutral axis values are computed from the strain measurements.

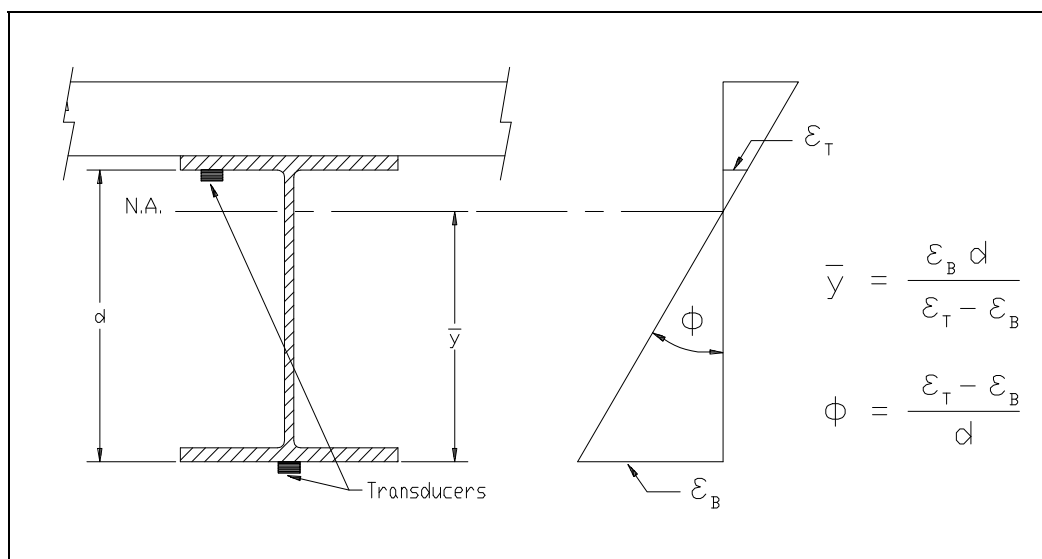


Figure B1. Illustration of neutral axis (NA) and curvature calculations.

The consistency in the NA values between beams indicates the degree of consistency in beam stiffness. Also, the consistency of the NA measurement on a single beam as a function of truck position provides a good quality check for that beam. If for some reason a beam's stiffness

changes with respect to the applied moment (i.e., loss of composite action or loss of effective flange width due to a deteriorated deck), it will be indicated by a shift in the NA history.

Since strain values are translated from a function of time into a function of vehicle position on the structure and the data acquisition channel and the truck position tracked, a considerable amount of bookkeeping is required to perform the strain comparisons. In the past, this required manipulation of result files and spreadsheets which was tedious and a major source of error. This process is now performed automatically by the software and all of the information can be verified visually.

### **Finite element modeling and analysis**

The primary function of the load test data is to aid in the development of an accurate finite element model of the bridge. Finite element analysis is used because it provides the most general tool for evaluating various types of structures. Since a comparison of measured and computed responses is performed, it is necessary that the analysis be able to represent the actual response behavior. This requires that actual geometry and boundary conditions be realistically represented. In maintaining reasonable modeling efforts and computer run times, a certain amount of simplicity is also required, so a planar grid model is generated for most structures and linear-elastic responses are assumed. A grid of frame elements is assembled in the same geometry as the actual structure. Frame elements represent the longitudinal and transverse members of the bridge. The load transfer characteristics of the deck are provided by attaching plate elements to the grid. When end restraints are determined to be present, elastic spring elements having both translational and rotational stiffness terms are inserted at the support locations.

Loads are applied in a manner similar to the actual load test. A model of the test truck, defined by a two-dimensional group of point loads, is placed on the structure model at discrete locations along the same path that the test truck followed during the load test. Gage locations identical to those in the field are also defined on the structure model so that strains can be computed at the same locations under the same loading conditions.

## Evaluation of rotational end restraint

A common requirement in structural identification is the need to determine effective spring stiffnesses that best represent in situ support conditions. It is generally simple to evaluate a spring constant in terms of moment per rotation, but the value generally has little meaning to the engineer. A more conceptual approach is to evaluate the spring stiffness as a percentage of a fully restrained condition—for example, 0% being a pinned condition and 100% being fixed. This is best accomplished by examining the ratio of the beam or slab stiffness to the rotational stiffness of the support.

As an illustration, a point load is applied to a simple beam with elastic supports (see Figure B2). By examining the moment diagram, it is apparent that the ratio of the end moment to the midspan moment ( $M_e/M_m$ ) equals 0.0 if the rotational stiffness ( $K_r$ ) of the springs is equal to 0.0. Conversely, if the value of  $K_r$  is set to infinity (rigid) the moment ratio will equal 1.0. If a fixity term is defined as the ratio ( $M_e/M_m$ ), which ranges from 0 to 100%, a more conceptual measure of end restraint can be obtained.

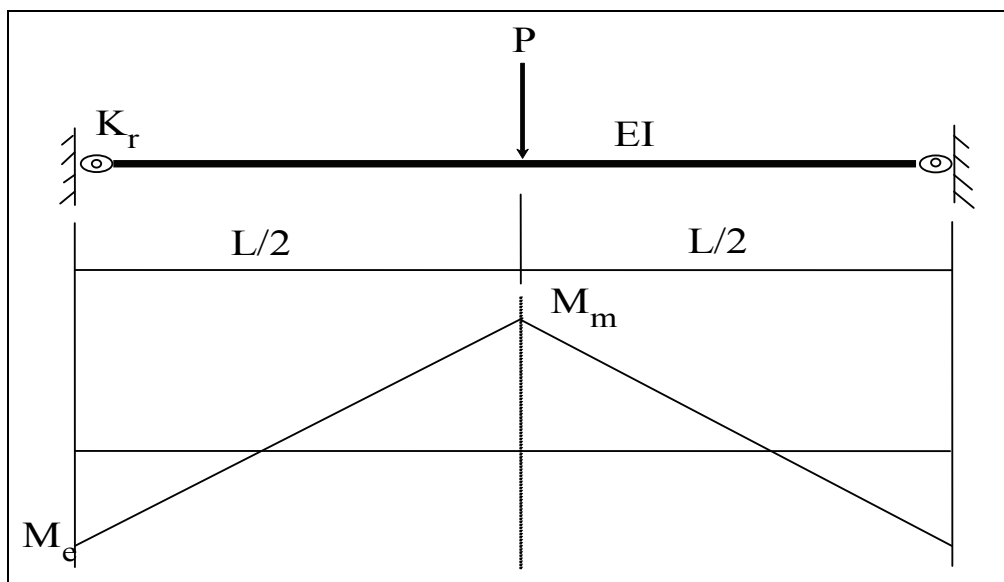


Figure B2. Moment diagram of beam with rotational end restraint.

The next step is to relate the fixity term to the actual spring stiffness ( $K_r$ ). The degree to which the  $K_r$  effects the fixity term depends on the beam or slab stiffness to which the spring is attached. Therefore the fixity term must be related to the ratio of the beam/spring stiffness. Figure B3

contains a graphical representation of the end restraint effect on a simple beam. Using the graph, a conceptual measure of end-restraint can be defined after the beam and spring constants are evaluated through structural identification techniques.

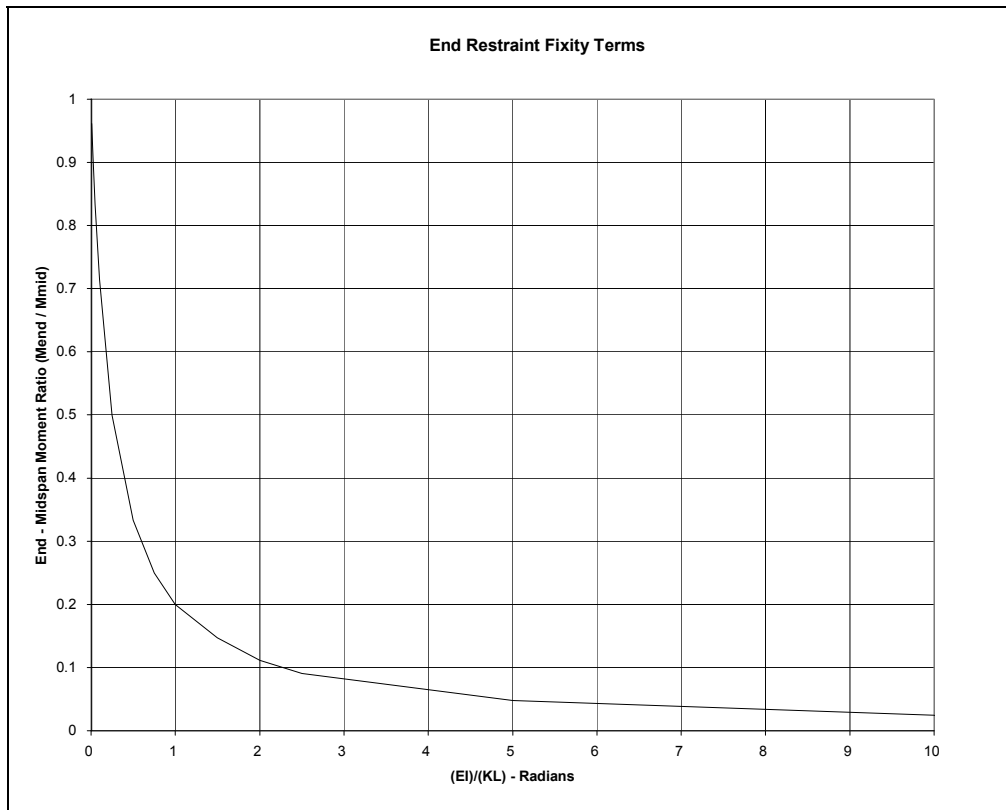


Figure B3. Relationship between spring stiffness and fixity ratio.

## Model correlation and parameter modification

The accuracy of the model is determined numerically by the analysis using several statistical relationships and through visual comparison of the strain histories. The numeric accuracy values are useful in evaluating the effect of any changes to the model, whereas the graphical representations provide the engineer with the best perception for why the model is responding differently than the measurements indicate. Member properties that cannot be accurately defined by conventional methods or directly from the field data are evaluated by comparing the computed strains with the measured strains. These properties are defined as variable and are evaluated such that the best correlation between the two sets of data is obtained. It is the engineer's responsibility to determine which parameters need to be refined and to assign realistic upper and lower limits to each

parameter. The evaluation of the member property is accomplished with the aid of a parameter identification process (optimizer) built into the analysis. The process consists of an iterative procedure of analysis, data comparison, and parameter modification. It is important to note that the optimization process is merely a tool to help evaluate various modeling parameters. As with any process, this works best when the number of parameters is minimized and reasonable initial values are used.

During the optimization process, various error values are computed by the analysis program that provides a quantitative measure of the model accuracy and improvement. The error is quantified in four different ways, each providing a different perspective of the model's ability to represent the actual structure: an absolute error, a percentage error, a scale error, and a correlation coefficient.

The **absolute error** is computed from the absolute sum of the strain differences. Algebraic differences between the measured and theoretical strains are computed at each gage location for each truck position used in the analysis; therefore, several hundred strain comparisons are generally used in this calculation. This quantity is typically used to determine the relative accuracy from one model to the next and to evaluate the effect of various structural parameters. It is used by the optimization algorithm as the objective function to minimize. Because the absolute error is in terms of micro-strain ( $\mu\epsilon$ ) the value can vary significantly depending on the magnitude of the strains, the number of gages, and the number of different loading scenarios. For this reason, absolute error has little conceptual value except for determining the relative improvement of a particular model.

A **percentage error** is calculated to provide a better qualitative measure of accuracy. It is computed as the sum of the strain differences squared divided by the sum of the measured strains squared times 100. The terms are squared so that error values of different sign will not cancel each other out, and to put more emphasis on the areas with higher strain magnitudes. A model with acceptable accuracy will usually have a percentage error of less than 10%.

The **scale error** is similar to the percentage error except that it is based on the maximum error from each gage divided by the maximum strain value from each gage. This number is useful because it is based only on



strain measurements recorded when the loading vehicle is in the vicinity of each gage. Depending on the geometry of the structure, the number of truck positions, and various other factors, many of the strain readings are practically negligible. This error function uses only the most relevant measurement from each gage.

Another useful quantity is the **correlation coefficient**, which is a measure of the linearity between the measured and computed data. This value determines how well the shapes of the computed response histories match the measured responses. The correlation coefficient can have a value between 1.0 (indicating a perfect linear relationship) and -1.0 (exact opposite linear relationship). Bridge Diagnostics, Inc., indicates that a good model will generally have a correlation coefficient greater than 0.90. A poor correlation coefficient is usually an indication that a major error in the modeling process has occurred. This is generally caused by poor representations of the boundary conditions or the loads were applied incorrectly (e.g., truck traveling in wrong direction).

Table B1 contains the equations used to compute each of the statistical error values:

Table B1. Error functions.

Error Function	Equation
Absolute Error	$\sum  \epsilon_m - \epsilon_c $
Percentage Error	$\sum (\epsilon_m - \epsilon_c)^2 / \sum (\epsilon_m)^2 \times 100$
Scale Error	$\frac{\sum \max  \epsilon_m - \epsilon_c _{gage}}{\sum \max  \epsilon_m _{gage}}$
Correlation Coefficient	$\frac{\sum (\epsilon_m - \bar{\epsilon}_m)(\epsilon_c - \bar{\epsilon}_c)}{\sum \sqrt{(\epsilon_m - \bar{\epsilon}_m)^2 (\epsilon_c - \bar{\epsilon}_c)^2}}$

In addition to the numerical comparisons made by the program, periodic visual comparisons of the response histories are made to obtain a conceptual measure of accuracy. Again, engineering judgment is essential in determining which parameters should be adjusted so as to obtain the most accurate model. The selection of adjustable parameters is performed by

determining what properties have a significant effect on the strain comparison and determining which values cannot be accurately estimated through conventional engineering procedures. Experience in examining the data comparisons is helpful; however, two general rules apply concerning model refinement. When the shapes of the computed response histories are similar to the measured strain records but the magnitudes are incorrect, this implies that member stiffness must be adjusted. When the shapes of the computed and measured response histories are not very similar, then the boundary conditions or the structural geometry are not well represented and must be refined.

In some cases, an accurate model cannot be obtained, particularly when the responses are observed to be non linear with load position. Even then, a great deal can be learned about the structure and intelligent evaluation decisions can be made.

## Appendix C: Load Rating Procedure

For borderline bridges (those that calculations indicate a posting is required), the primary drawback to conventional bridge rating is an oversimplified procedure for estimating the load applied to a given beam (i.e., wheel load distribution factors) and a poor representation of the beam itself. Due to lack of information and the need for conservatism, material and cross-section properties are generally over-estimated and beam end supports are assumed to be simple, when in fact even relatively simple beam bearings have a substantial effect on the midspan moments. Inaccuracies associated with conservative assumptions are compounded with complex framing geometries. From an analysis standpoint, the goal here is to generate a model of the structure that is capable of reproducing the measured strains. Decisions concerning load rating are based on the performance of the model, once it is proven to be accurate.

The main purpose for obtaining an accurate model is to evaluate how the bridge will respond when standard design loads, rating vehicles or permit loads are applied to the structure. Since load testing is generally not performed with all of the vehicles of interest, an analysis must be performed to determine load-rating factors for each truck type. Load rating is accomplished by applying the desired rating loads to the model and computing the stresses on the primary members. Rating factors are computed using the equation specified in the *AASHTO Manual for Condition Evaluation of Bridges* (2003)—see Equation C1.

It is important to understand that diagnostic load testing and the integrated approach are most applicable to obtaining Inventory (service load) rating values. This is because it is assumed that all of the measured and computed responses are linear with respect to load. The integrated approach is an excellent method for estimating service load stress values but it generally provides little additional information regarding the ultimate strength of particular structural members. Therefore, operating rating values must be computed using conventional assumptions regarding member capacity. This limitation of the integrated approach is not viewed as a serious concern, however, because load responses should never be permitted to reach the inelastic range.

Operating and/or Load Factor rating values must also be computed to ensure a factor of safety between the ultimate strength and the maximum allowed service loads. The safety to the public is of vital importance, but as long as load limits are imposed such that the structure is not damaged then safety is no longer an issue.

Following is an outline describing how field data are used to help in developing a load rating for the superstructure. These procedures will only complement the rating process and must be used with due consideration to the substructure and inspection reports.

1. **Preliminary Investigation:** Verification of linear and elastic behavior through continuity of strain histories, locate neutral axis of flexural members, detect moment resistance at beam supports, and qualitatively evaluate behavior.
2. **Develop representative model:** Use graphic preprocessors to represent the actual geometry of the structure, including span lengths, girder spacing, skew, transverse members, and deck. Identify gage locations on model identical to those applied in the field.
3. **Simulate load test on computer model:** Generate 2-D model of test vehicle and apply to structure model at discrete positions along same paths defined during field tests. Perform analysis and compute strains at gage location for each truck position.
4. **Compare measured and initial computed strain values:** Various global and local error values at each gage location are computed and visual comparisons made with postprocessor.
5. **Evaluate modeling parameters:** Improve model based on data comparisons. Engineering judgment and experience is required to determine which variables are to be modified. A combination of direct evaluation techniques and parameter optimization are used to obtain a realistic model. General rules have been defined to simplify this operation.
6. **Model evaluation:** In some cases it is not desirable to rely on secondary stiffening effects if it is likely they will not be effective at higher load levels. It is beneficial, though, to quantify their effects on the structural response so that a representative computer model can be obtained. The stiffening effects that are deemed unreliable can be eliminated from the model prior to the computation of rating factors. For instance, if a non-composite bridge is exhibiting composite behavior, then it can conservatively be ignored for rating purposes. However, if the bridge has been in service for 50 years and it is still behaving compositely, chances are that very heavy

loads have crossed over it and any bond-breaking would have already occurred. Therefore, probably some level of composite behavior can be relied upon. When unintended composite action is allowed in the rating, additional load limits should be computed based on an allowable shear stress

between the steel and concrete and an ultimate load of the non-composite structure.

7. **Perform load rating:** Apply HS-20 and/or other standard design, rating and permit loads to the calibrated model. Rating and posting load configuration recommended by AASHTO are shown in Figure C1 on the following page. The same rating equation specified by the AASHTO *Manual for the Condition Evaluation of Bridges* (2003) is applied:

LRFR equation:

$$RF = \frac{C - \gamma_{DC}(DC) - \gamma_{DW}(DW) \pm \gamma_P(P)}{\gamma_L(LL + IM)} \quad (C1)$$

where:

- $RF$  = Rating Factor for individual member
- $C$  = Member Capacity
- $\gamma_{DC}$  = LRFD load factor for structural components and attachments
- $DC$  = Dead-load effect due to structural components
- $\gamma_{DW}$  = LRFD load factor for wearing surfaces and utilities
- $DW$  = Dead-load effect due to wearing surface and utilities
- $\gamma_P$  = LRFD load factor for permanent loads other than dead loads = 1.0
- $P$  = Permanent loads other than dead loads
- $LL$  = Live-load effect
- $IM$  = Impact effect, either AASHTO or measured.

The only difference between this rating technique and standard beam rating programs is that a more realistic model is used to determine the dead-load and live-load effects. Two-dimensional loading techniques are applied because wheel load distribution factors are not applicable to a planar model. Stress envelopes are generated for several truck paths, envelopes for paths separated by normal lane widths are combined to determine multiple lane loading effects.

8. **Consider other factors:** Other factors such as the condition of the deck and/or substructure, traffic volume, and other information in the inspection report should be taken into consideration and the rating factors adjusted accordingly.

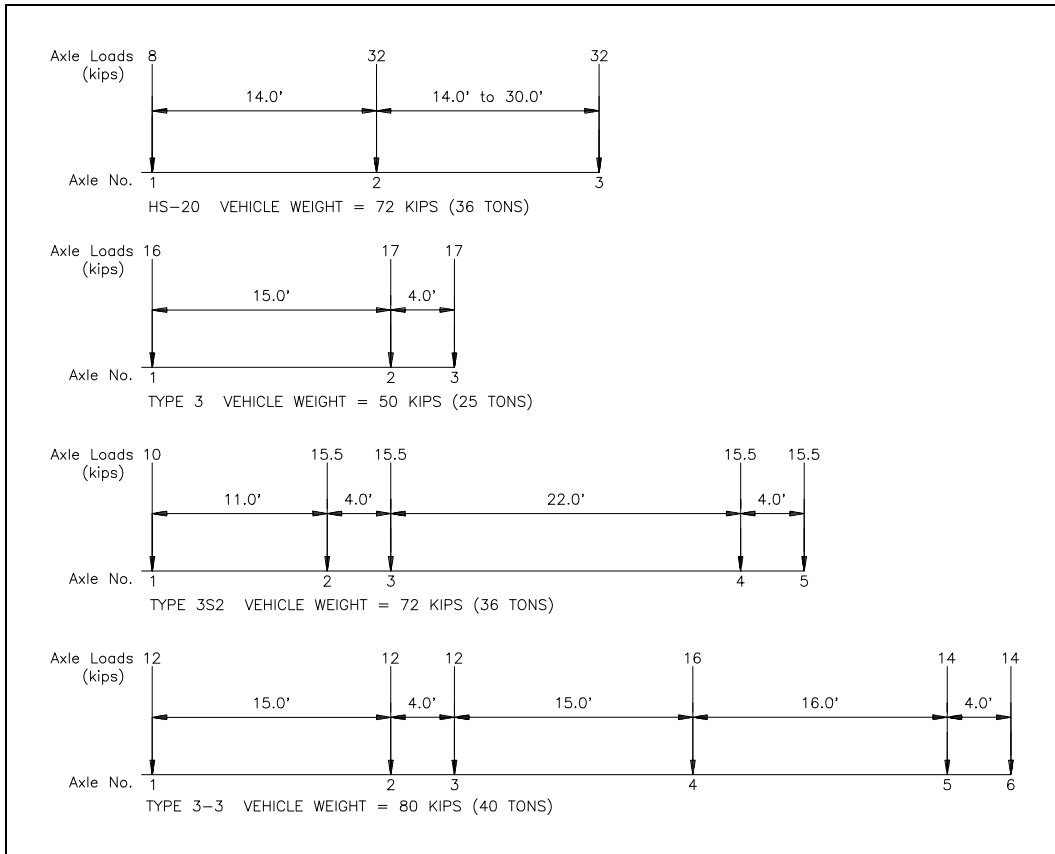


Figure C1. AASHTO rating and posting load configurations.

